# Advanced dispersive mirrors for ultrashort laser pulses from the near-UV to the mid-IR spectral range

**Florian Habel**


München 2016

# Advanced dispersive mirrors for ultrashort laser pulses from the near-UV to the mid-IR spectral range

**Florian Habel**

Dissertation
an der Fakultät für Physik
der Ludwig–Maximilians–Universität
München

vorgelegt von
Florian Habel
aus Bad Reichenhall

München, den 15.11.2016

Erstgutachter: Prof. Dr. Ferenc Krausz
Zweitgutachter: Prof. Dr. Detlev Ristau
Tag der mündlichen Prüfung: 16.02.2017

# Zusammenfassung

Dispersive Spiegel (auch bekannt als "gechirpte Spiegel") sind eine der Schlüsselkomponenten in Ultrakurzpulslasern. Solche Laser erzeugen Lichtblitze die nur aus wenigen Schwingungen des elektromagnetischen Feldes bestehen, und nur wenige Femtosekunden (fs) andauern ($1\,\mathrm{fs} = 10^{-15}$ Sekunden). Dispersive Spiegel sind unverzichtbar in der Dispersionskontrolle in solchen Femtosekundenlasern. Dispersion ist die wellenlängenabhängige Lichtgeschwindigkeit in einem Medium, und da Femtosekundenpulse aus einem breiten Spektrum an Wellenlängen bestehen, kann die Dispersion die zeitliche Form eines Pulses dermaßen verschlechtern, dass sich dessen Dauer um Größenordnungen erhöht. Dispersive Spiegel ermöglichen die Kompensation dieses Effekts, da sie so konstruiert werden können, dass verschiedene Wellenlängen zueinander gezielt zeitlich verzögert werden. Die Spiegel bestehen aus bis zu etwa 100 transparenten dünnen Schichten, die aus zwei Materialien mit verschiedenen Brechungsindizes bestehen. Hierbei wird die Reflexion eines Lichtstrahls durch die Interferenz aller Teilstrahlen bestimmt, welche an den Grenzflächen der dünnen Schichten reflektiert werden. Die relative Verzögerung zweier Wellenlängen wird erreicht, indem die Schichtdicken des Spiegels so angepasst werden, dass etwa eine Wellenlänge tiefer in die Schichtstruktur eindringen kann, und somit einen weiteren Weg bei der Reflexion zurücklegt. Somit erhält der Spiegel die gewünschte dispersive Eigenschaft.

Es gibt zahlreiche Anwendungen für Femtosekundenlaser, beispielsweise in den Materialwissenschaften, bei der medizinischen Diagnostik, der Attosekundenphysik und den Grundlagenwissenschaften. Bei zukünftigen Anwendungen steigt die Nachfrage für die zuverlässige und stabile Erzeugung von noch kürzeren Laserpulsen mit noch höheren Intensitäten, sowie die Erzeugung breitbandiger Laserquellen für unerforschte Bereiche des optischen Spektrums. Oft ist eine der nötigen Schlüsselentwicklungen der Fortschritt in der Technologie der dispersiven Spiegeln, welche erst die Realisierung der oben genannten neuartigen Laserquellen ermöglicht.

Im Rahmen dieser Arbeit werden die Eigenschaften derzeitiger dispersiver Spiegel in vielen Bereichen verbessert und deren Einsatzbereiche signifikant erweitert. Der spektrale Anwendungsbereich der Spiegeltechnologie wurde an beiden Enden des Spektrums erweitert. Es wird ein dispersiver Spiegel vorgestellt, dessen kürzeste Wellenlänge bei bisher unveröffentlichten 250 nm im nahen ultravioletten Spektralbereich liegt. Ein weiter dispersiver Spiegel wurde entwickelt, der die Grenze im mittleren infraroten Spektralbereich auf 11,500 nm schiebt. Um diesen extrem breiten Wellenlängenbereich abzudecken wurden mehrere verschiedene Beschichtungsmaterialien verwendet. Außerdem wurden drei verschieden Beschichtungstechnologien verwendet, um dünne Interferenzschichten mit diesen Materialien zu realisieren.

Ferner wurde ein neues Weißlichtinterferomter entwickelt, um die Dispersion der Beschichtungen für den mittleren infraroten Spektralbereich zu charakterisieren.

Des Weiteren wird gezeigt, dass die unvermeidbaren spektralen Oszillationen der Dispersion aktueller Spiegel, welche die Form ultrakurzer Pulse zerstören können, durch die neu erfundenen wedge-dispersiven Spiegel effizient unterdrückt werden können. Verglichen mit anderen Konzepten, die das gleiche Ziel verfolgen, werden diese neuartigen Spiegel in drei Schritten mit Hilfe nur eines Dünnschichtprozesses hergestellt. Auch ist der Einfluss des Einfallswinkels der wedge-dispersiven Spiegel nicht so empfindlich auf die Spektralen Eigenschaften als es bei aktuellen doppel-Winkel Spiegeln der Fall ist. Dadurch sind sie einfacher in Lasersystem zu integrieren. Überdies werden dispersive Spiegel vorgestellt, welche mit Hilfe der Ionenstrahlzerstäubung hergestellt wurden. Dabei wurden Spiegel mit extrem niedrigen optischen Verlusten von nur 3 Millionsteln demonstriert. Dies kommt einer Reflektion von 99.9997 % gleich. Außerdem wurde die prinzipielle Machbarkeit der Herstellung großer, hochmoderner dispersiver Spiegel mit einem Durchmesser von 300 mm gezeigt.

# Abstract

Dispersive mirrors (also known as "chirped mirrors") are one of the key components used in ultrafast lasers. Such lasers generate flashes of light consisting of only a few oscillations of the electromagnetic field which last only some femtoseconds ($1\,\mathrm{fs} = 10^{-15}$ seconds). In femtosecond lasers, dispersive mirrors are indispensable to control the dispersion within the system. Dispersion is the wavelength dependent speed of light in a medium, and since femtosecond pulses consist of a broad spectrum of wavelengths, it can degrade the temporal shape of an ultrashort laser pulse, such that it increases the pulse duration of orders of magnitudes. Dispersive mirrors enable the compensation of this effect, since thy can by constructed in such way, that different reflected wavelengths are delayed in respect to each other. The mirrors consist of up to around 100 transparent thin layers made with two materials with different refractive indices. Here, the reflection of a light ray is described by the interference of all partial light rays, which are reflected on the different interfaces of thin layers. The relative delay between two wavelengths is obtained by adjusting the thickness of the layers such, that for instance one wavelength penetrates deeper into the layer structure, and in this way, the path length on reflection is longer. Thus the mirror gains its desired dispersive properties.

The applications for femtosecond lasers are numerous for instance in material-science, medical diagnostics, attosecond-physics and fundamental research. For future applications the demand grows for the reliable and stable generation of ever shorter laser pulses with ever higher intensities, as well as the generation of broadband lasers sources for unexplored spectral ranges. Often one of the required key-developments is the progress made in dispersive mirror technology, which only enables the construction of new lasers with the desired properties just mentioned.

In the scope of this thesis, the properties of current dispersive mirrors were advanced in many aspects and its range of use was significantly extended. The applicable wavelength range of the current mirror technology is enhanced in both endings. Dispersive mirrors for femtosecond pulses are demonstrated with the lowest reported wavelength limit of 250 nm in the near-UV spectral range, and another dispersive mirror is shown with the highest ever reported wavelength limit of 11,500 nm in the mid-infrared spectral region. To cover this extreme spectral range, several different coating materials were employed. To deposit these materials, three different coating deposition techniques were employed. Besides, to characterize the mid-infrared dispersive coatings, a new white-light interferometer was developed, that enables the measurement of the dispersion introduced by a coating.

Moreover it is shown, that undesired spectral fluctuations of the group delay observed on current octave spanning mirrors, which can disrupt an ultrashort laser pulse, can be efficiently

suppressed by using the newly invented wedge dispersive mirrors. Compared to other concept pursuing the same goal, the novel mirrors are produced in three steps using only one thin-film process. Moreover they are not as sensitive on the angle of incident as current double angle mirrors, making them simpler to implement in laser systems.

Furthermore dispersive mirrors are introduced, which are manufactured using ion beam sputtering. Using this technique, a mirror coating is presented with ultra-low total losses of 3 parts per million (ppm), which implies a reflectance of 99.9997 %. Furthermore the capability of the manufacturing of large state-of-the-art dispersive mirrors with a diameter of up to 300 mm is shown.

# Contents

# Chapter 1

# Introduction

Dispersive mirrors [1–3] are one of the key components used in ultrafast laser systems. Such lasers generate flashes of light lasting only a few femtoseconds ($1\,\mathrm{fs} = 10^{-15}$ seconds). Dispersive mirrors are also known as chirped mirrors and were first introduced by Szipőcs et al. in 1994 [4]. The working principle of such a mirror is illustrated in Fig.1.1. Dispersive mirrors are indispensable to control the dispersion within a few-cycle laser [5]. For instance, such short flashes of light enable the time resolved observation of chemical reactions [6], whose discovery was awarded with the noble prize in 1999 to Ahmed Zewail. Furthermore, only powerful few-cycle pulses can generate the even shorter attosecond ($1\,\mathrm{as} = 10^{-18}$ seconds)

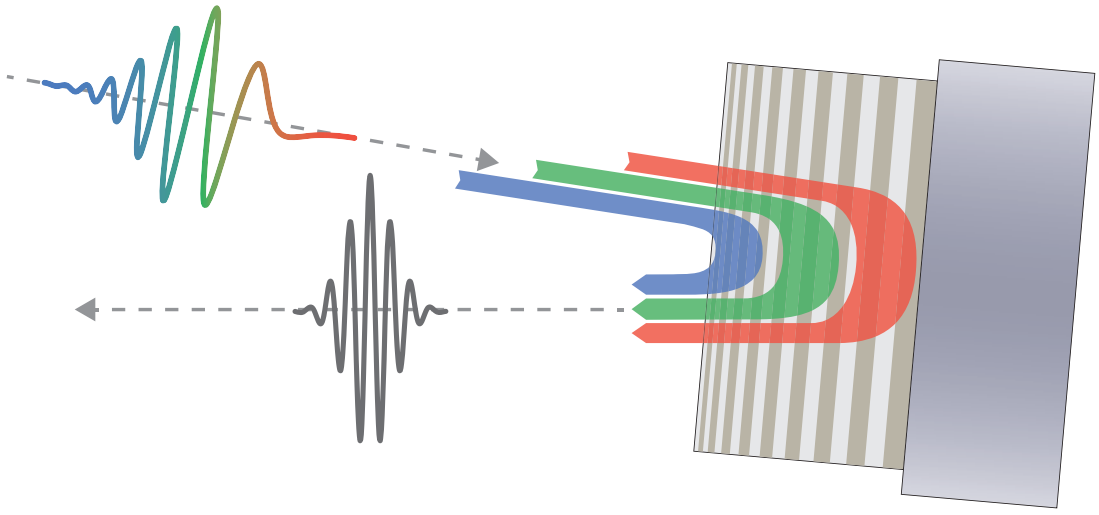

**Figure 1.1:** Working principle of a dispersive mirror: In this example the incident few-cycle pulse has a positive chirp, meaning that the shorter wavelengths are delayed to the longer wavelength. The dispersive mirror on the right, has a aperiodic layer structure, with thicker layers on the bottom, and thinner layers on top. Thus the longer wavelength penetrate deeper into the structure than the shorter wavelengths. The mirror delays the longer wavelength of the propagating pulse, which compresses it to a shorter pulse. Besides this penetration effect, also a Gires-Tournois interferometer (GTI) effect exists, which is introduced by cavity layers within the layer stack.

pulses of extreme ultraviolet light [7, 8], which were first observed [9] in 2001. Now, with attosecond time resolution, even the motion of electrons on the atomic length scale can be observed [10].

The generation of optical pulses in the few cycle regime relies on the precise compensation of dispersion introduced by material-dispersion and self-phase-modulation [7, 11]. Dispersion is simply the wavelengths dependent speed of light in a medium and it therefore modifies the temporal shape of a ultrashort laser pulses, which consists of the superposition of broad range of wavelengths. Dispersive mirrors can compensate this dispersion by delaying certain wavelength by letting them penetrate deeper into the multilayer coating. This wavelength dependent delay is called group delay (GD). Moreover a Gires-Tournois interferometer (GTI) can be implemented into a dispersive mirror structure using thicker cavity-layers. With this a higher group delay can be obtained, but only for a limited bandwidth. Since their invention, dispersive mirrors were steadily advanced. In 1997 the first so called double-chirped mirror was demonstrated, were it was analytically proven, that the undesired spectral oscillations in the group delay can be reduced by additionally chirping the high-index layers [12]. Since these oscillations can conventionally not be suppressed for dispersive mirrors with a very large bandwidth, a new kind of so called double-angle mirrors were introduced by Pervak et al. in 2009 [13]. Here, one dispersive coating design is applied at two different angle of incidences, at which the oscillations just cancel each other. In 2014, Shih-Hsuan et al. demonstrated [14] the first two-octave-spanning pair of mirrors, which supports sub-optical-cycle pulses as short as 1.9 fs. Recently in 2016, Hassan et al. [15], generated a even broader spectrum of light in the visible and nearby spectral ranges, and compressed the pulse even below 1 fs using a light-field synthesizer, were the more than two optical octave spectrum is split into four channels. The individual pulses in each channel are compressed using dispersive mirrors, and subsequently superimposed to obtain the sub-femtosecond pulse.

However, one shortcoming of such state-of-the-art broadband dispersive mirrors is, that they exhibit strong spectral oscillations in the group delay because of an impedance mismatch of the mirror and the ambient medium [16]. These modulations limit the minimal achievable pulse duration [11] and reduce the temporal contrast by generating satellite pulses [17]. Ways of optimizing the coating design were found to reduce the oscillations [16], but they are not successful enough for mirrors with an octave spanning bandwidth.

Besides, there are also applications for dispersive mirrors, were the coating should not introduce additional dispersion, since the incident pulse is already Fourier-transform-limited. For instance high power laser sources, such as regenerative amplifiers [18] and optical parametric amplifiers [19] are currently under development, which require broadband thin-film polarizers and broadband multilayer mirrors with low dispersion for separation, combination, power adjustment the steering of energetic pulses.

The mid-infrared between 2 to 20 μm spectral region gains more and more attraction by scientists, since there is the so called finger print region, were most molecules have fundamental vibrational modes. This makes mid-infrared spectroscopy an important tool for many fields

including quality control, food industry, forensic analysis, semiconductor electronics, biomedical applications and many others [20–23]. To increase the signal-to-noise ratio in optical spectroscopy, spatial coherent and high power light is desired. Recently, a source of coherent radiation with a spectrum spanning the range from 6.8 to 16.4 μm and an average power of 0.1 W was developed by Pupeza et al.[24]. This phase coherent source with a repetition rate of 100 MHz enables the resonant enhancement of radiation in a passive cavity and thus increases the interaction length with the examined medium. For instance, the phase of a pulse circulating in such an enhancement cavity must be well controlled by dispersive mirrors [25].

The key component, which often prevents the further power-scaling of state of the art ultrafast laser systems, is often a dielectric coating. Every interference coating absorbs light even if only in the lower parts per million (ppm) range. The absorbed energy transfers into heat, this deforms the optic and subsequently distorts the laser beam, which prevents the laser from a stable operation [25]. To reduce the heating of the optics, the further reduction of intrinsic absorption losses of coatings is mandatory. In the high energy femtosecond regime, a second absorption effect comes into place. The two photon absorption becomes dominant at high energies. Here the absorption is depends on the bandgap of the coating material [26–28]. Two photon absorption is the major damage mechanism for this regime, and it can be reduced within a limited range by using materials with a higher bandgap, which corresponds to a lower refractive index. Another approach to significantly reduce the absorption in optical coatings is to reduce the energy density of the incident radiation by increasing the beam diameter. This demands the development of large scale low loss multilayer optics.

## Outline of this thesis

**Chapter 2** contains a theoretical background on the influence of dispersion on ultrashort laser pulses, as well as some fundamentals of dispersive interference coatings and their deposition processes. **Chapter 3** provides an overview of the experimental basis employed for this thesis, like the coating machines and characterization devices. In **Chapter 4**, two low-dispersive optics are presented. The first optic is a mirror, which allows the steering of a UV-pulse. The second optic is a polarizer which allows the separation, combination and power adjustment of energetic 12 fs pulses. **Chapter 5** introduces a novel wedge dispersive mirror, which efficiently suppresses the spectral oscillations of the group delay. The manufacturing and the characterization of an octave spanning dispersive mirror is describes, as well as the prove of the successful compression of a pulse down to a duration of 3.8 fs. **Chapter 6** introduces the first dispersive mirrors for the mid-infrared range beyond 7 μm. Also a newly developed white-light interferometer, to measure the dispersion introduced by mid-infrared dispersive mirrors, is presented. In **Chapter 7** the implementation of the ion beam sputtering technique is described, and furthermore, the first results with the new coating process are given.

# Chapter 2

# Theory of ultrashort light pulses and multilayer coatings

In the following sections some theoretical aspects are highlighted, which are important for the experimental work presented in the following chapters. This chapter is divided into three sections, which deal with the different physical topics of ultrashort light pulses, interference coatings and thin-film deposition.

## 2.1 Ultrashort laser pulses and the influence of dispersion

A few-cycle optical pulse, like the two illustrated in Fig. 1.1 on page 1, can be described with the following complex electric field given in the time-domain [29, 30]

$$E(t) = A(t)e^{i\varphi_0}e^{i\varphi_a(t)}e^{i\omega_0 t} \tag{2.1}$$

where $A(t)$ is the field envelope function. $e^{i\omega_0 t}$ describes the rapid oscillating field with the carrier frequency $\omega_0$. $\varphi_0$ is the carrier to envelope phase CEP and $\varphi_a(t)$ is an additional phase function, which describes time dependent frequency changes, called a chirp. All contributions can be joined in a the time dependent phase

$$\varphi(t) = \varphi_0 + \varphi_a(t) + \omega_0 t. \tag{2.2}$$

To better understand the influence of dispersion on short pulses, it is useful to represent the electric filed in the frequency-domain by a Fourier transformation:

$$\tilde{E}(\omega) = |\tilde{E}(\omega)|e^{i\varphi(\omega)} \tag{2.3}$$

Here $|\tilde{E}(\omega)|$ is the spectral amplitude, which is proportional to the spectral intensity measured with a spectrometer. $\varphi(\omega)$ is the spectral phase, which is usually manipulated is the experiment. Its change directly alters the real electric field $E(t)$. The spectral phase can be separated into different contribution when expanded into a Taylor series

$$\varphi(\omega) = \varphi(\omega_0) + \left.\frac{\partial\varphi}{\partial\omega}\right|_{\omega_0}\cdot(\omega-\omega_0) + \frac{1}{2}\left.\frac{\partial^2\varphi}{\partial\omega^2}\right|_{\omega_0}\cdot(\omega-\omega_0)^2 + \ldots \tag{2.4}$$

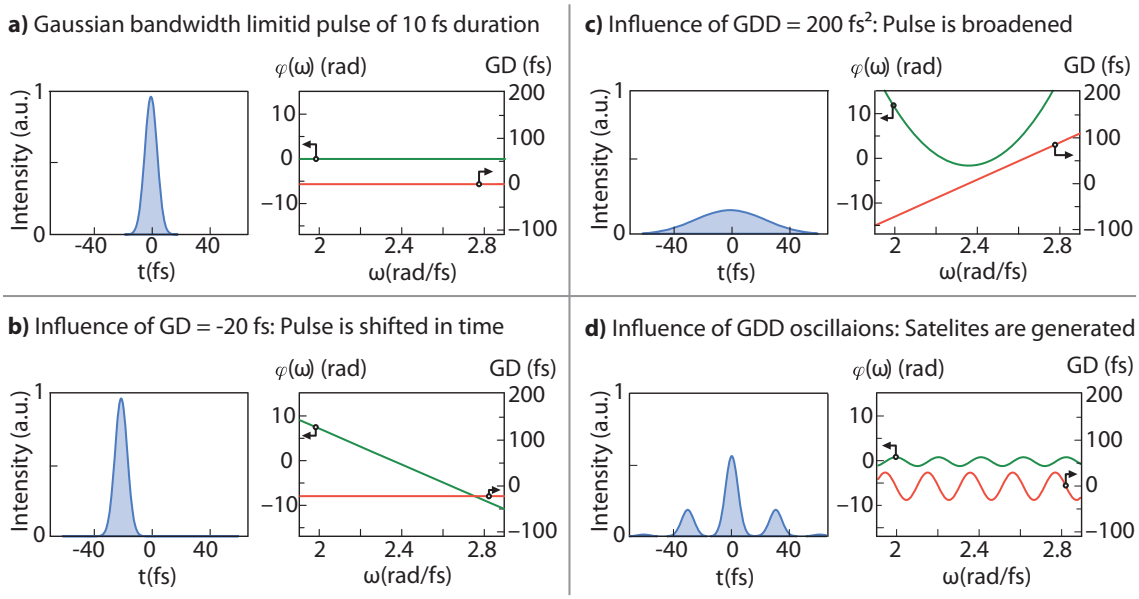


**Figure 2.1:** In the figure, four cases **(a)**-**(d)** are shown. For each case the intensity of the pulse in the time-domain is shown on the left, where-else the phase and the GD in the frequency space is shown on the right. **(a)** shows the bandwidth-limited Gaussian laser pulse with the duration of 10 fs. **(b)** The introduction of GD $= -20$ fs shifts the whole pulse back in time. **(c)** The introduction of GDD $= 200\,\mathrm{fs}^2$ broadens the pulse significantly while the peak-intensity drops. **(d)** Demonstrates the influence of GD-oscillations (also GDD-oscillations), which can be introduces by dispersive mirrors. Pre- and post-pulses are generated (also called satellites). The peak-intensity drops. After [29].

The zero order term $\varphi(\omega_0)$ is in the time-domain again the CEP. The first-order term contains the group delay GD, which is defined as:

$$\mathrm{GD}(\omega) = \frac{\partial \varphi}{\partial \omega}(\omega) \qquad [\mathrm{fs}] \tag{2.5}$$

The second order term contains the group delay dispersion GDD:

$$\mathrm{GDD}(\omega) = \frac{\partial^2 \varphi}{\partial \omega^2}(\omega) \qquad [\mathrm{fs}^2] \tag{2.6}$$

For instance the influence of different contributions from the GD and GDD on the spectral shape of a Gaussian pulse, with the duration of $\Delta$t=10 fs (full width of half maximum FWHM), is illustrated in Fig. 2.1.

In Fig. 2.1**(c)** one can clearly see that a frequency dependent GD, meaning a non-zero GDD, leads to pulse broadening. In Fig. 2.1**(d)** the influence of GDD-oscillations is illustrated. These ripples considerably modify the temporal spectrum, they lead to satellite-generation and drop

the peak intensity. Such oscillations are unavoidably caused by conventional broadband dispersive mirrors, but are highly suppressed by double-angle dispersive mirrors or by the novel wedge dispersive mirrors presented in section 5.

A pulse gains the spectral phase $\varphi_m(\omega)$ when traveling through a transparent medium with the thickness $d$ [29]

$$\varphi_m(\omega) = k(\omega)d = \frac{\omega}{c} n(\omega)d \tag{2.7}$$

with the wave-number $k$, the speed of light $c$ and the frequency dependent refractive index $n(\omega)$. By taking the second derivative of $\varphi_m(\omega)$, and then converting it to the wavelength-space, one becomes the material specific expression for the GDD depending on the wavelength $\lambda$:

$$\mathrm{GDD}(\lambda) = \frac{\lambda^3 d}{2\pi c^2} \frac{d^2 n}{d\lambda^2} \qquad [\mathrm{fs}^2] \tag{2.8}$$

The GDD in units of thickness or length is often called the group velocity dispersion GVD, in units of typically [fs²/mm]. In formula 2.8 the second derivative of the refractive index is contained. For experimental data for $n(\lambda)$ this derivation is possible, when the refractive index is expressed for instance in the Sellmeier equation, which describes its wavelength dependency empirical:

$$n^2(\lambda) = A_0 + \frac{A_1\lambda^2}{(\lambda^2 - A_2)} + \frac{A_3\lambda^2}{(\lambda^2 - A_4)} + \ldots \tag{2.9}$$

The Coefficients $A_i$ are the Sellmeier coefficients and are determined experimentally. By inserting formula 2.9 in 2.8 the GDD of any material with know dispersion $n(\lambda)$ can be calculated. For instance, the GDD at the wavelength of 800 nm for a fused silica (amorphous silicon dioxide $SiO_2$) substrate, with the thickness of 5 mm, is 200 $\mathrm{fs}^2$. The duration of a Gaussian pulse after traveling through this glass can be calculated by:

$$\Delta t_{\mathrm{GDD}} = \sqrt{\Delta t^2 + \left(4\ln 2 \frac{\mathrm{GDD}(\lambda_0)}{\Delta t}\right)^2} \tag{2.10}$$

When following the example above, the GDD introduced by 5 mm fused silica will broaden a 10 fs pulse to 56 fs, which is also illustrated in Fig. 2.1**(c)**.

## 2.2 Interference coatings for ultrashort light pulses

Interference coatings consist of multiple transparent thin layers with different refractive indices. The reflectance, transmittance and the phase shift induced by a multilayer coating can be exactly calculated, when the refractive index $n$ and the thickness of the layers are known [31]. With the refractive index $n$ the characteristic optical admittance $\tilde{n}$ is calculated by $\tilde{n} = nY$, were $Y$=1.654,4 × $10^{-3}$ S, which is the admittance of free space (Note: In Gaussian units, $Y$ is 1 and then $\tilde{n} = n$.). For a non-absorbing incidence medium, its admittance $\tilde{n}_0 = n_0 Y$ is real. The admittance of the substrate is $\tilde{n}_s = n_s Y$. Now the reflectance $R$, the

transmittance $T$ and the phase shift $\varphi$ is given for one wavelength by:

$$R = \left(\frac{\tilde{n}_0\acute{E} - \acute{B}}{\tilde{n}_0\acute{E} + \acute{B}}\right)\left(\frac{\tilde{n}_0\acute{E} - \acute{B}}{\tilde{n}_0\acute{E} + \acute{B}}\right)^* \tag{2.11}$$

$$T = \frac{4\tilde{n}_0 \mathrm{Re}(\tilde{n}_s)}{(\tilde{n}_0\acute{E} + \acute{B})(\tilde{n}_0\acute{E} + \acute{B})^*} \tag{2.12}$$

$$\varphi = \arctan\left(\frac{\mathrm{Im}\left[\tilde{n}_s(\acute{E}\acute{B}^* - \acute{B}\acute{E}^*\right]}{(\tilde{n}_s^2\acute{E}\acute{E}^* - \acute{B}\acute{B}^*)}\right) \tag{2.13}$$

Here $\acute{E}$ and $\acute{B}$ are the tangential electric and magnetic fields at the front interface of a multilayer stack consisting of $q$ layers. The fields are calculated by the following product containing all characteristic matrices for each layer $i$:

$$\begin{bmatrix}\acute{E}\\ \acute{B}\end{bmatrix} = \left\{\prod_{i=1}^{q}\begin{bmatrix}\cos\delta_i & (\mathrm{i}\sin\delta_i)/\tilde{n}_i\\ \mathrm{i}\tilde{n}_i\sin\delta_i & \cos\delta_i\end{bmatrix}\right\}\begin{bmatrix}1\\ \tilde{n}_s\end{bmatrix} \tag{2.14}$$

$$\text{with} \quad \delta_i = \frac{2\pi}{\lambda} nd\cos(\alpha) \tag{2.15}$$

$\delta_i$ is referred to as the phase thickness of the i-th layer. The phase thickness contains the wavelength of the incident light, the angle of incidence and the refractive index of the layer.

If the wavelength dependent phase shift $\varphi(\lambda)$ (Eq. 2.13) is calculated, the GD and GDD (see definitions 2.5 and 2.6) introduced by a multilayer stack are obtained by its first and second derivation with respect to the angular frequency $\omega = 2\pi c/\lambda$:

$$\mathrm{GD} = \frac{\partial\varphi}{\partial\omega} \tag{2.16}$$

$$\mathrm{GDD} = \frac{\partial^2\varphi}{\partial\omega^2} \tag{2.17}$$

These two formulas connect the theory of dispersive mirrors with the theory of few-cycle laser pulses (see formula (2.5) and (2.6)).

### 2.2.1 Optimization of multilayer designs

Every coating design optimization needs a target-design function, which represents the desired values for the spectral properties of the coating as a function of wavelength. For instance the target function can be the group delay dispersion for a discrete number $L$ of wavelengths $\lambda_i$, giving $\mathrm{GDD}_T(\lambda_i)$ ($i \in \{1,..,L\}$). Of course also the reflectance $R$, the transmittance $T$ or the group delay GD can be a target value. The variables of the actual coating design are the layer thicknesses $d_i$ for each of the $q$ layers. With the $q$ layer thicknesses expressed with the vector $\vec{d}$,

the group delay dispersion and the reflectance are expressed by $\mathrm{GDD}(\vec{d},\lambda)$ and $\mathrm{R}(\vec{d},\lambda)$. Now a weighted mean square deviation for the target function and the coating design is defined, which is commonly called merit function MF [32]:

$$\mathrm{MF} = \left\{ \frac{1}{N} \sum_{i=1}^{N} \left[ \left( \frac{\mathrm{GDD}(\vec{d},\lambda_i) - \mathrm{GDD}_T(\lambda_i)}{\Delta \mathrm{GDD}_i} \right)^2 + \left( \frac{\mathrm{R}(\vec{d},\lambda_i) - \mathrm{R}_T(\lambda_i)}{\Delta \mathrm{R}_i} \right)^2 \right] \right\}^{\frac{1}{2}} \tag{2.18}$$

Here $\Delta\mathrm{GDD}_i$ and $\Delta\mathrm{R}_i$ are the tolerances for each target point. The merit function decreases when the coating design gets closer to the target, which is the aim of optimization. The only variables here are the layer thicknesses $d_i$. The optimization is now a mathematical problem and can be carried out by using for instance the well-known Newton's method. The method of optimizing multilayer-designs is also referred to as refinement. With Newton's method one needs to have a good starting design, which is usually not available especially for advanced dispersive mirrors. For such complex designs, the optimization of the merit function is extended by the so called needle optimization technique, combined with the gradual evolution technique. The needle technique introduces a thin layers (needles) into a well-chosen position in the multilayer structure [33], and executes a refining step afterward, which should result in a lower merit function as before the needle step. The gradual evolution rather forces the increase of the total thickness of the design by for instance adding layers on top of the structure [34].

### 2.2.2 Bandwidth of highly reflective interference coatings

Since ultrashort pulses cover a broad spectral range, the bandwidth of interference coatings becomes important. For a quarter-wave stack, a compact formula exists to calculate this bandwidth. Such a multilayer stack consists of alternating layers of high ($n_H$) and low ($n_L$) refractive index materials. For each layer, the optical layer thickness $d_o = nd$ is the quarter of the central wavelength $\lambda_0$. Here the physical thickness is $d$ and is not equal for the two materials. A relative wavelength $g$ can be defined as $g = \lambda_0/\lambda$, and the total relative bandwidth $2\Delta g$ for a quarter-wave stack can be estimated with [31]:

$$\Delta g = \frac{2}{\pi} \arcsin\left( \frac{n_H - n_L}{n_H + n_L} \right) \tag{2.19}$$

The bandwidth of a quarter-wave stack only depends on the ratio of the refractive indices $n_L$ and $n_H$ of the two layer materials. The relative bandwidth is plotted versus the ratio $n_H/n_L$ in Fig. 2.2. Also included in the graph are points for most material combinations used for this work. One can see, that the combination often used for the UV, that is hafnium-dioxide ($n_H = 1.9$) and silicon-dioxide ($n_H = 1.46$) has the lowest bandwidth. The highest bandwidth is obtained by the infrared materials germanium ($n_H = 4.1$) and zinc sulfide ($n_L = 2.2$), which was one reason to select them for the mid-infrared dispersive mirrors presented in chapter 6.

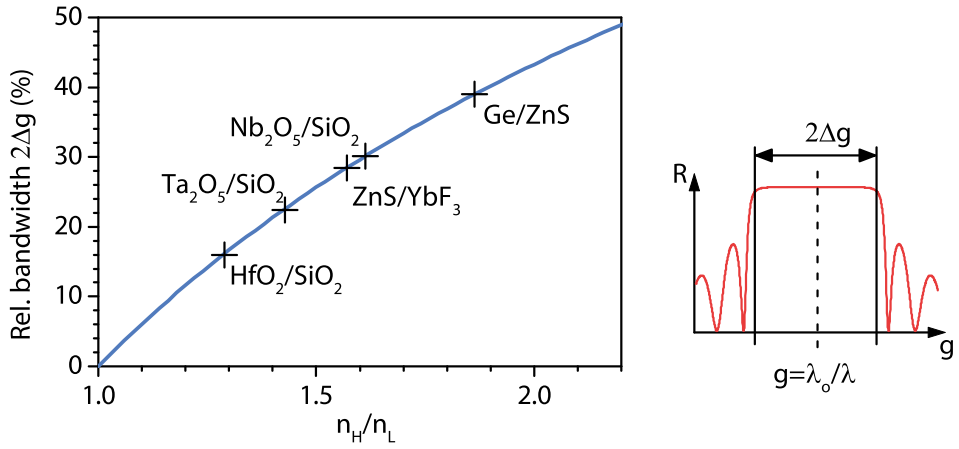


**Figure 2.2:** The bandwidth of the high-reflectance range of a quarter-wave stack versus the ratio of the refractive indices. (After [31])

### 2.2.3 Interference coatings at oblique incidence

When deriving the characteristic matrices for a layer at oblique incidence, the following expressions appear, and it's a convention to call them "effective index" is made [35]:

$$n_s = n\cos\alpha \tag{2.20}$$

$$n_p = \frac{n}{\cos\alpha} \tag{2.21}$$

Here $n$ is the refractive index of the medium. With increasing angle of incidence, the effective index for s-polarized light decreased, while it increases for p-polarized light. The effective index is plotted for the two materials niobium pentoxide and silicon dioxide in Fig. 2.3. Note that the polarization splitting is less for the high index material. Also arrows are added to explain the spectrum of a quarter-wave stack at oblique incidence on the right in Fig. 2.3. As shown in the previous section, the bandwidth of a reflector depend only on the contrast in refractive index. Since the contrast becomes more for the s-polarization, and less for p-polarization, also the bandwidths for their reflectance zones is different. The zone were s-polarized light is reflected and p-polarized light is transmitted is exploited by thin-film polarizers, like the one shown in section 4.2.

## 2.3 Layer deposition processes

For laser applications, mainly physical vapor deposition (PVD) processes are employed. Hereby the material to coat is brought to the gas-phase by physical process. The material then condenses on the substrates and form a layer. It is crucial that the gaseous atoms or molecules do not collide with other unwanted atoms during their flight to the substrate, to have enough energy to form a compact layer. A too high pressures lead to thin-films with poor quality.

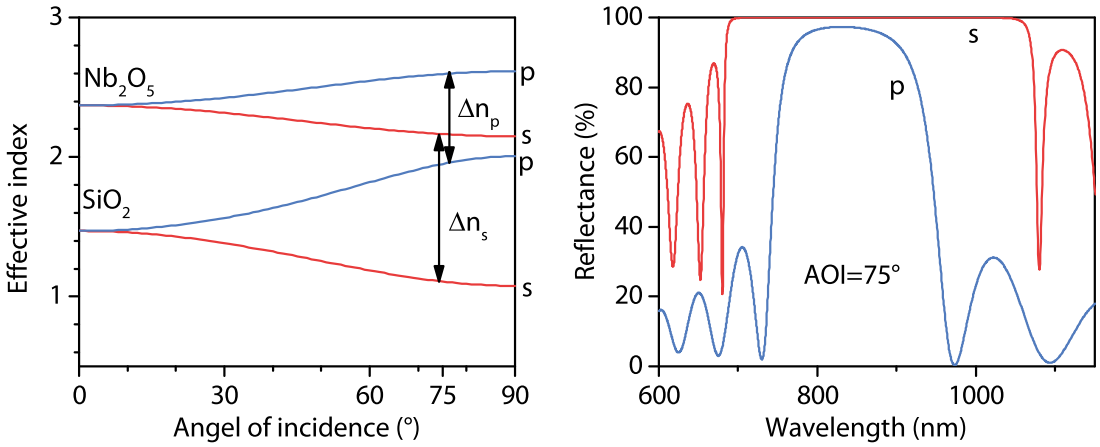


**Figure 2.3:** Left: Effective index for niobium pentoxide and silicon dioxide as a function of angle of incidence for the two polarizations s and p. Right: The reflectance spectra for the two polarizations of a quarter-wave stack at 75°. The bandwidth for s-pol is much higher than for p-pol, being the fundamental principle of a thin-film polarizer, like the one described in section 4.2.

Therefore coating processes are made in high-vacuum. The mean free path of the coating material should be at least of the distance between source and substrates [31]. In this work, mainly reactive coating processes for oxide-materials were employed. Here the coating material is the pure element like for example tantalum. The material is only oxidized within the coating process, by adding the process gas oxygen. Then on the substrate a film of pure tantalum pentoxide $Ta_2O_5$ is deposited. Thereby the mean free path is less, since fully oxidized films are desired. To find the ideal press-pressure can be a demanding task. For this work, different PVD coating processes have been employed. They can be separated in two different groups. First there is thermal evaporation, were the coating material is heated by supplying energy until it vaporizes. The second group are sputtering processes, were high energetic ions directly eject atoms or molecules from the coating material.

**Thermal evaporation:** The heating of the material can be realized by restive crucibles or commonly called 'boats'. They have a low electrical resistance and therefore become hot when an electric current flows through it. With the heat, the coating material is evaporated. Another method of applying heat is with an electron beam source. Here electrons are extracted from a hot filament by applying a high voltage. The electron beam is formed by a Wehnelt cylinder and steered onto the coating material by a magnetic field. The current is increased until the material evaporates. This method has several advantages over the resistive heating and is therefor the mostly desired way of evaporation. For example materials with a high melting point like metals can be heated directly by a focused e-beam. The melting point is reached fast where the electron beam hits the material. This is an advantage especially when a large amount of material is used. With a resistive boat, the whole crucible and all the coating material must be heated up to the melting point and this takes longer, as it also takes longer to

cool down. The kinetic energy of the evaporated material is usually not high enough to form dense and compact layers, since the atoms or molecules immediately 'freeze' when they arrive at the substrate. They don't have enough energy to move on the surface to fill voids. Therefore the substrates are heated by infrared radiators inside the vacuum chamber to temperatures of 80 to 300°. Instead of heating the substrates, also a plasma source can be used. Charged atoms are accelerated and hit the substrates. They transfer their momentum and thus compact and dense layers can be built. Such a plasma ion assisted deposition (PIAD) process was developed for this work (see appendix A).

**Magnetron sputtering:** Next to thermal evaporation are sputter processes, which are mostly applied for the production of dispersive mirrors for the UV-NIR spectral range. Here the coating material is called target. Accelerated atoms from a plasma hit the target with high kinetic energy and eject one or more atoms or molecules. The coating material has now a higher energy when it hits the substrates, compared to thermal processes. As a consequence the layers grow more compact in a sputter process. Two completely different approaches to sputtering have evolved during the last decades. First there is magnetron sputtering which is widely used for complex optical coating-designs. For this work, plasma assisted reactive magnetron sputtering (PARMS) is employed [36–38]. Here the name magnetron means that the plasma is confined close to the targets by magnetic fields for higher deposition rates. Only metallic target materials can be used and therefore the metal atoms must react with oxygen to form dielectric oxide layers. Oxygen is introduced using an additional plasma source. The undesired arcing events known from other magnetron concepts, were dielectric layers isolate the target, are avoided by using dual-magnetrons were each target is connected to a mid-frequency power supply. Even though magnetron sputtering is the most sophisticated sputtering process, there is a drawback concerning the realization of low-loss coatings. The pressure directly at the substrate is relatively high during the growth of a layer, since the argon plasma is close. This fact reduces the film quality and introduces higher scattering losses [39]. The magnetron sputter process is used for all coatings in chapter 4

**Ion beam sputtering:** The second sputtering process is called ion beam sputtering (IBS). In comparison to magnetron sputtering the IBS [40, 41] concept spatially separates the plasma generation from the coating material and from the substrates. Especially for low loss coatings, this concept combines the advantages of thermal evaporation and magnetron sputtering. As with thermal evaporation, the particle contamination of the coatings is reduced by coating the substrates facing downwards, and the lower working pressure increases the film quality, resulting in lower scattering losses. And as with magnetron sputtering the coating material has a high kinetic energy to be able to form dense and compact layers. In the Kaufman-type ion source, a plasma is generated in a discharge chamber and the ions are extracted using a ion-optic. The accelerated ions hit the coating material and sputter one or more atoms or molecules. Like in magnetron sputtering the coating material now condenses on the substrate surfaces. This process is used for ultra-low loss coatings for large substrates (see chapter 7).

# Chapter 3

# Experimental basis and methods

In this chapter all coating plants and characterization devices used for this work are described. Further the key ingredients for the coating processes are described. Also some transmission spectra of the employed optical materials are shown.

## 3.1 Coating plants

Some theoretical aspects of the different coating methods are described before in section 2.3. In the following the specific coating machines used for this work are shown below. All machines are installed in clean rooms, to reduce the particle contamination of coatings.

**Thermal evaporating plant:** The SyrusPro 710 from Leybold Optics (Bühler Alzenau GmbH, Germany) implements thermal evaporation using two electron guns and one optional restive evaporation source (see Fig. 3.1). On this machine the coatings for the mid-infrared spectral range were deposited (see chapter 6). With the use of the plasma source, a process for dispersive mirrors was developed, which is shortly described in appendix A.

**Magnetron sputtering plant:** The magnetron sputter process is implemented using the Helios machine, also from Leybold Optics GmbH. All coatings for the UV up to the NIR range shown in chapter 4 were manufactured with this machine. Also the wedge dispersive mirror is manufactured using Helios (chapter 5). Because of the proximity of the target to the substrate, the highly wedged layer can be produced by just tilting the substrate, so that one side is closer, and the other side is farther away from the target. See Fig. 5.4 on page 37 for illustration.

**Ion beam sputtering plant:** A tender for a IBS coating machine was carried out and the plant was after all acquired from Cutting Edge Coatings GmbH, which is a spin-off company of the Laser Zentrum Hannover. More details of the machine are given in chapter 7, and a sketch can be seen on page 61. Ion beam sputtering (IBS) more or less combines the advantages of the two methods described above. It uses plasma sputtering for dense and precise layers combined with the advantageous geometry of thermal evaporation, where the substrates are coated upside-down and are separated from the coating source, which leads to less contamination of the coatings. This is the main reason for the development of the IBS process, the manufacturing of low loss coatings [40].

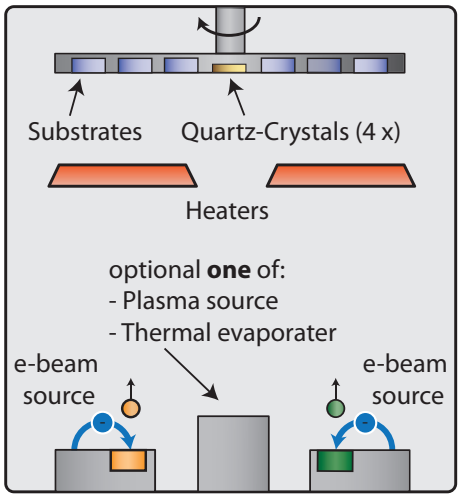


**Figure 3.1:** Sketch of the thermal evaporation coating (Syrus) plant showing all parts important for this work. The substrates are mounted in fixtures and face downward. Two electron beam sources and an optional restive evaporation source is available. The latter can be replaced by a plasma source, for ion assisted deposition (IAD).

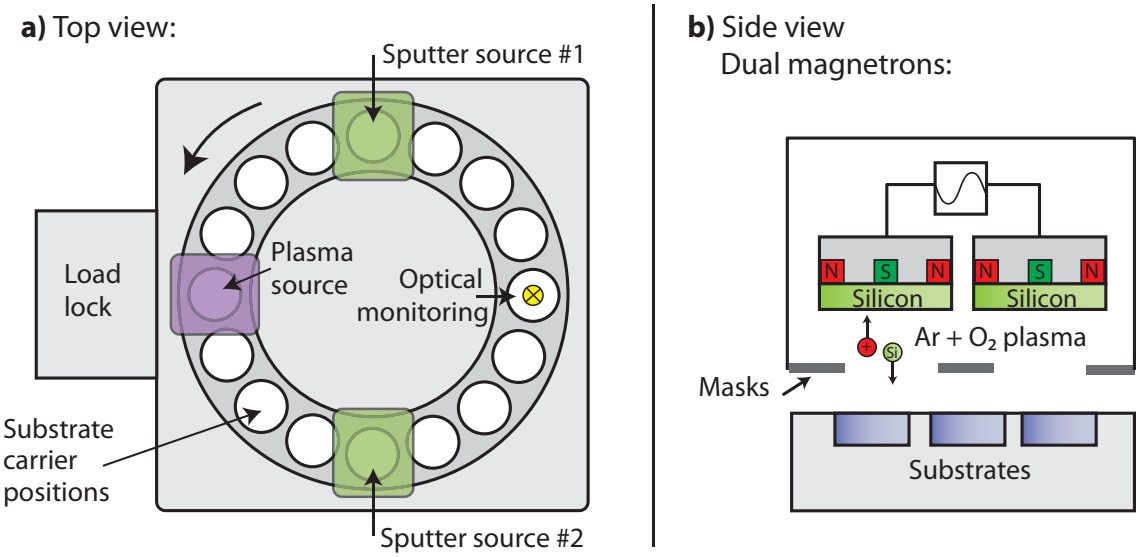


**Figure 3.2:** Sketch of the magnetron sputtering machine (Helios). The top view (left) shows the turn table including 16 positions for substrate carriers. Each carrier can be loaded, for instance with seven 1" substrates. Above the substrates the two dual magnetrons and the assist plasma source are distributed. The machine is equipped with a broad band optical monitoring system (BBOM). The substrates are coated with the surface to coat facing up (right). The target (dual magnetrons), and thus the sputtering plasma, are close to the substrates. The layer uniformity is controlled by masks.

## 3.2 Thickness monitoring

The precise thickness-control for each individual layer of a dispersive mirror is of highest importance. With state of the art monitoring techniques explained below, layer-thickness can be controlled with sub-nanometer precision.

**Quartz-crystal monitoring:** A quartz crystal for thickness monitoring has the geometry of a flat disc. It sits inside the chamber and is ideally coated with the same layers as the substrates. Both surfaces of the disc are contacted with a metal layer, so that is can be connected to an oscillating circuit. The resonant frequency of a uncoated disc is about 5.9 MHz and is permanently measured with an accuracy of 0.3 Hz. Due to the change of mass, when the crystal is coated, the thickness of the film with known density is calculated. The advantage of this method is, that nearly any kind of material, whether its dielectric or metallic, can be monitored, independent of its optical properties. For this work germanium for mid-infrared applications (see chapter 6) was deposited with quartz crystals, because there was no optical monitor available in our labs for the range of transparency. This advantage is also a disadvantage for high precision optical coating, because this monitoring technique doesn't take the optical properties into account. Another disadvantage is that the frequency measurement is strongly temperature dependent, and the measurement is not always exactly linear with the mass.

**Broad band optical monitoring (BBOM):** This is an in situ optical monitoring technique, where a broad-band transmission spectrum is measured directly on the substrate, during the coating process [42, 43]. Therefore the coatings have to be transparent in the monitoring range. Commonly a separate monitoring substrate is used, which is kept and stored for later reference. A evaluation software, which has the design and dispersion data of the coating materials, can calculate the thickness of the current layer from the measured spectrum. For each measurement, the software iteratively changes the thickness of the current layer, calculates the transmittance-spectrum and compares it with the measurement, until the mean squared error (MSE) of the two curves is minimized. Of course this method is only reliable if the transmission measurement is very accurate and the refractive indices are known with high precision. The later is usually very challenging during process development. The method is very powerful for most kind of optical coatings, since it is very robust when it is correctly optimized. It enables fully automated process without the need of intervention. The disadvantage of BBOM is, that the thickness errors increase with the layer numbers. The reason is, that even small measurement errors and dispersion deviations lead to small errors of the layer thickness calculation. These small errors accumulate layer by layer. Depending on the design, the errors become too high after 30 to 50 layers. For coatings with a high number of layers, which is mostly the case for dispersive mirrors, this method comes to its limit. There is also the possibility of changing the monitoring glass during the process and continue with an uncoated glass. But the increasing and also unpredictable thickness errors make BBOM not the first choice for the monitoring of dispersive mirrors.

**Calibrated time monitoring:** Layer thicknesses can be determined during the coating process by just measuring the deposition time. To reach a high precision, the deposition rate must

be very stable and known with high accuracy. Sputter processes are known to be very stable and therefore this method is only employed for the magnetron and the IBS machines described before. A coating process starts with time control with the deposition rates from the previous run. Slowly changing process conditions can lead to altered deposition rates, that create errors when using only time control. These variations may are caused by target-erosion or the degree of contamination of the recipient. For a high accuracy in layer thicknesses required for chirped mirrors, the deposition rate is monitored by the broad band monitoring system described above, with the difference, that the BBOM is in passive mode, meaning that it does not determine the moment when the layer has reached its target-thickness. The BBOM only acquires a spectrum after its finished by time control. This spectrum, and all spectra of the previous layers, are now processed with specialized software like OptiRE (Optilayer GmbH) or SPEKTRUM (Laser Zentrum Hannover e.V.). The algorithms calculate now the MSE for all layers simultaneously while trying to reach a global minimum by changing all layer thicknesses. The evaluation yields the thickness error for each layer. With this result, the time control can be calibrated. This method was integrated and optimized for the IBS coater.

## 3.3 Materials for laser optics

The selection of the right material for the desired application is crucial and mainly decides if the designed optic will successfully work in the laser, or if it fails. This choice has always to be made before a new optic is designed. For this work a wide range of materials were employed. Fig 3.3 gives an overview of the transmission spectra in the range of 250 nm to 20 µm for different types of substrates. This data is helpful for choosing the right material for an application.

## 3.4 Characterization

**Spectrophotometers for UV-VIS-NIR:** Transmittance and reflectance are carried out using two Lambda 950 spectrophotometers from PerkinElmer Inc. One device is equipped with an universal reflectance accessory (URA) which allows absolute reflectance-measurements from 185 to 3,100 nm at angle of incidences of 8 to 65°. The accuracy is estimated to be better than 1 %, depending in the circumstances of the measurement and the properties of the sample. The second spectrophotometer is used for transmittance measurements and has two detector-modules to choose from. The 3D-module has three detectors to cover the range of 175 to 3,300 nm. The second module is using an integration sphere to collect all light transmitted by the sample. This is essential for precise transmittance measurements on samples at oblique incidence, because here the beam is displaced. For example, the ultrabroadband-polarizer in section 4.2 is measured at an angle of incidence of 75° using this integrating sphere.

**FTIR spectrophotometer for NIR-MIR:** To extend the measuring capabilities to the mid-infrared range and thus enabling the development of dispersive mirrors for these wavelengths,

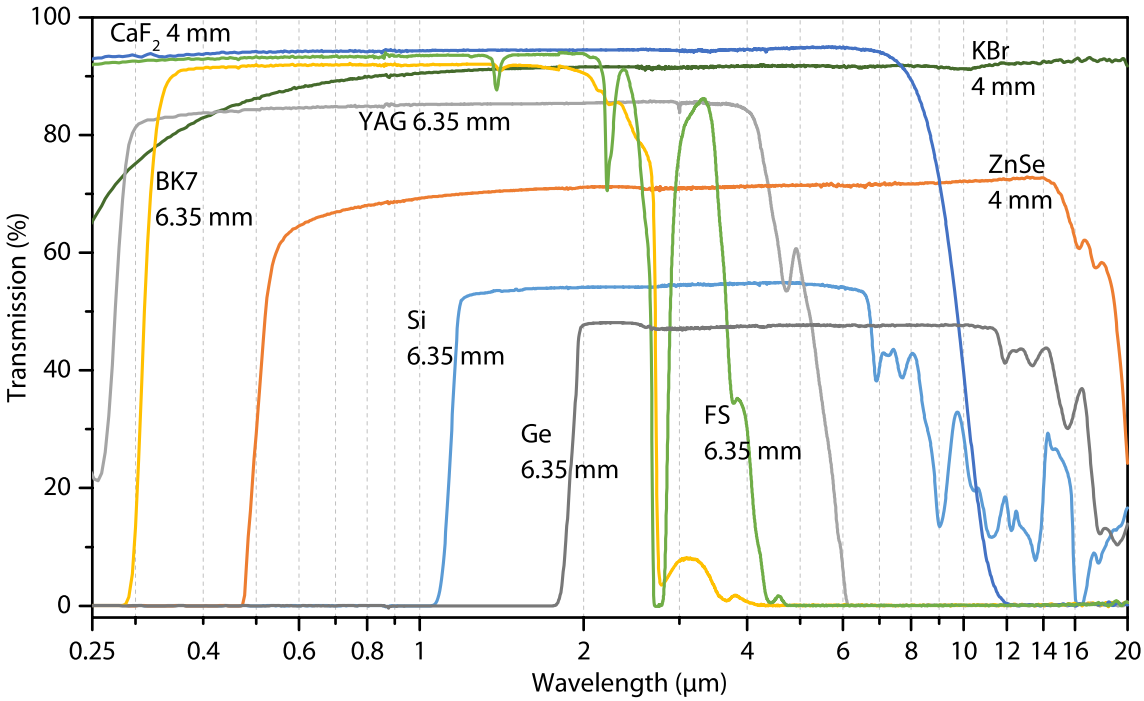


**Figure 3.3:** Transmission spectra of common substrate materials used for laser optics. The measurement was carried out using two spectrometers, the Lambda 950 for the shorter, and the FTIR spectrometer (see section 3.4) for the longer wavelength.

as demonstrated in chapter 6, a Fourier transform infrared (FTIR) spectrometer Vertex 70 from Bruker Optics GmbH was acquired. Since such devices are mainly deployed in chemical labs, the spectral specifications are given in inverse centimeters $cm^{-1}$. The bandwidth of the device is 8,000 to 350 $cm^{-1}$. One can simply convert these numbers to wavelengths in µm by dividing 10,000 by the wavelength in $cm^{-1}$. Then the range is 1.25 to 28.5 µm. The maximal resolution is specified as 0.4 $cm^{-1}$. The spectral range is limited by the combination of the MIR light source, the KBr beam splitter and the DLaTGS detector. For transmittance measurements the accessory A480 from Bruker is used, which collimates the beam at the sample position for precise absolute results. The absolute reflectance measurements are conducted using the V-W accessory A519. One key element of the spectrometer is the external input. This option, and an additional sensitive MCT detector enabled the development of the mid-infrared white light interferometer (see section 6.1).

**Dispersion measurements for UV-VIS-NIR:** Most of the GD and GDD measurements for this work were carried out using our home built white light interferometer (WLI). The working principle was at first proposed by Knox et al. [44] and our setup is described in the diploma thesis of Grupe [45]. Next to the right hardware setup, a sophisticated and reliable algorithm is required to evaluate the interferograms measured by the WLI. We use the algorithm proposed by Amotchkina et al. [46]. For the mid-infrared WLI (section 6.1), I developed another algorithm with more options and customized for the FTIR spectrometer. This new software is also capable to evaluate the data of the existing WLI (see appendix A).

**Measurement of the total optical losses:** The Total optical losses (TOL) are measured by using the cavity ring down (CRD) technique [47, 48]. With this method the decay time of a cavity containing the mirror of interest is measured. Two devices covering the wavelengths 808 nm, 1,030 nm and 1,550 nm are available. They are commercial devices with the name LossPro from NovaWave Technologies. At first, the losses of a linear reference cavity $L_{\mathrm{ref}}$ with the length $l_1$ consisting of two mirrors is determined by measuring the decay time $\tau_1$. At this measurement it is crucial, to have the exactly the same conditions as for the later measurement with the sample, to avoid systematic errors. If the losses $\mathrm{Loss}_{\mathrm{ref}}$ are known, the sample is now added as a third mirror to the cavity as a folding mirror, now having the length $l_2$ (here 62.5 cm). Again the decay time $\tau_{\mathrm{sample}}$ is measured and the losses of the sample $\mathrm{Loss}_{\mathrm{sample}}$ can now be calculated taking the losses of the linear cavity into account:

$$\mathrm{Loss}_{\mathrm{sample}} = \frac{l_2}{c \cdot \tau_{\mathrm{sample}}} - \mathrm{Loss}_{\mathrm{ref}} \tag{3.1}$$

Here c is the speed of light. One typical decay curve is given in Fig. 3.4. One loss measurement is usually averaged over 1000 cavity decays.

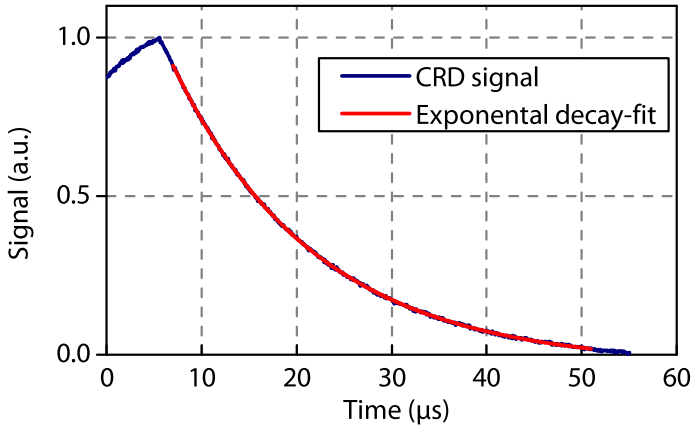


**Figure 3.4:** Typical measurement of the decay time of a cavity used to determine the total optical losses of a highly reflecting mirror. Of the exponential decay-fit, the decay time $\tau$ is determined.

# Chapter 4

# UV and NIR coatings with low dispersion

In the following two sections the experimental results of two low-dispersive coatings are presented. Both coatings are designed to manipulate the phase of the incident pulse as less as possible. In section 4.1, a highly reflective UV turning mirror with low dispersion is shown, which substantially increases the sensitivity of a UV pump-probe spectrometer. In section 4.2, a ultra-broadband polarizer is described whose bandwidth is sufficient to support pulses as short as 12 fs, which enables for instance the development of regenerative amplifiers in this time domain.

## 4.1 High reflective UV turning mirror with low dispersion

Many fundamental phenomena in biology and chemistry can only be observed in the UV spectral bandwidth. At the chair of biomolecular optics[1] of the Ludwig-Maximilians-University, a novel transient UV spectrometer is under development. Within this project, they also found a novel method of measuring the GD directly with their setup. The measurement is shown below. The device has several metal mirrors for beam steering, especially in the delay line, and therefore it suffers from huge optical losses, since metal mirrors have a poor reflectance in the UV. Therefore a dielectric mirror was developed with high reflectance and low dispersion to replace the metal mirrors and thus dramatically increasing the sensitivity of the spectrometer. Its designed bandwidth for s-polarized light ranges from 250 to 370 nm for an angle of incidence of 45°. The dispersion shall be as low as possible. For physical reasons, the group delay cannot be zero for all wavelengths, because that would mean, that all wavelengths are reflected at one infinitesimal thin layer. This may be the case for metal mirrors, but for interference coatings, light has always a wavelength dependent penetration depth. One can compensate this behavior by using two different mirrors, one having negative GDD and the other one with a positive GDD of the same amount. The effective GDD can then be close to zero. For the presented application below, one single mirror design having a low and smooth dispersion is sufficient, since the residual linear chirp can be corrected by a prism compressor already incorporated in the setup. The coating materials are carefully selected for the UV region, since the usual employed high-index materials for dispersive mirrors in the VIS-NIR

[1] The work was done in collaboration with Prof. Riedle and Bastian Baudisch, within the framework of the cluster of excellence: Munich center of advanced photonics (MAP)

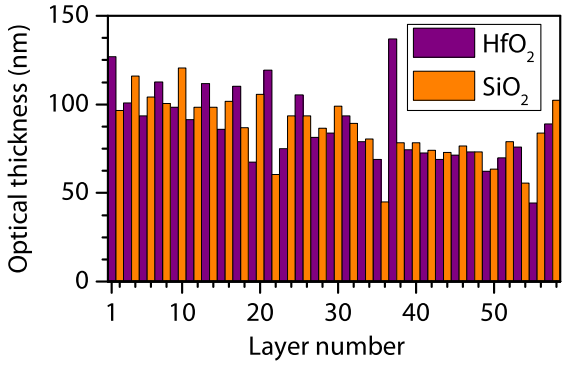


**Figure 4.1:** Optical thicknesses of the coating design consisting of 58 layers. The total physical thickness is 2.8 µm. Hafnium dioxide and silicon dioxide are used for this UV-mirror.

region like niobium pentoxide ($Nb_2O_5$) or tantalum pentoxide ($Ta_2O_5$), have a fundamental absorption band below 400 nm and 350 nm respectively. The combination of hafnium dioxide (n(400 nm)=2.1) and silicon dioxide (n(400 nm)=1.48) has still a high contrast in refractive index, are well known materials for UV applications [49] and are therefore chosen for this application. The coating process is magnetron sputtering (see section 3.1), because it creates dense layers with a high precision in thickness, which is especially important for UV coatings, since their average layer-thicknesses are low. The layer-thickness of the coating design are given in Fig. 4.1. The design consists of 58 layers and has a total physical thickness of 2.8 µm.

A low GDD of 10 $fs^2$ on average for the defined bandwidth is achieved. The calculated reflectance spectrum and the dispersion data are given in Fig. 4.2 and 4.3 together with their measurements. The absolute reflectance of the manufactured mirror is measured at the angle of incidence of 45° with s-polarized light using the URA (universal reflectance accessory) from Perkin Elmer (Section 3.4). The measurement is seen in Fig. 4.2. A value greater than 98.0 % is measured. The absolute uncertainty for this measurement is estimated to be 1 %, meaning that there could be some low absorption in the coating. Interesting to note, that the absorption is less at shorter wavelength, because the shorter waves are reflected at the first few layers of the coating-stack, while the longer wave penetrate deeper. For comparison the reflectance measurement of a uncoated aluminum mirror is included in the Graph, demonstrating the high efficiency of the new dielectric mirror.

Furthermore, to alternatively characterize the dispersion of the new mirrors, Prof. Riedle and B. Baudisch found a novel technique to measure the group delay of the mirror directly within their setup. The method is based on an existing pump probe spectrometer [50]. The new technique and first measurements were presented on the international conference on ultrafast phenomena in Santa Fe (USA, 2016) [51]. The technique makes use of the so called coherent artifact [52], that can be observed in a pump probe spectrometer, when the pump

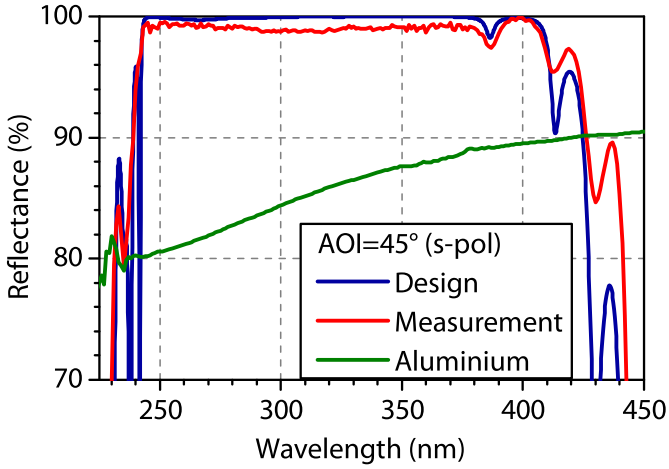


**Figure 4.2:** Absolute Reflectance measured at an AOI of 45° with s-polarized light. Our spectrophotometer with the universal reflectance accessory (URA) enabled this measurement. The reflectance is slightly dropped by 2 % caused by absorption, which is common for UV-coatings with hafnium dioxide.

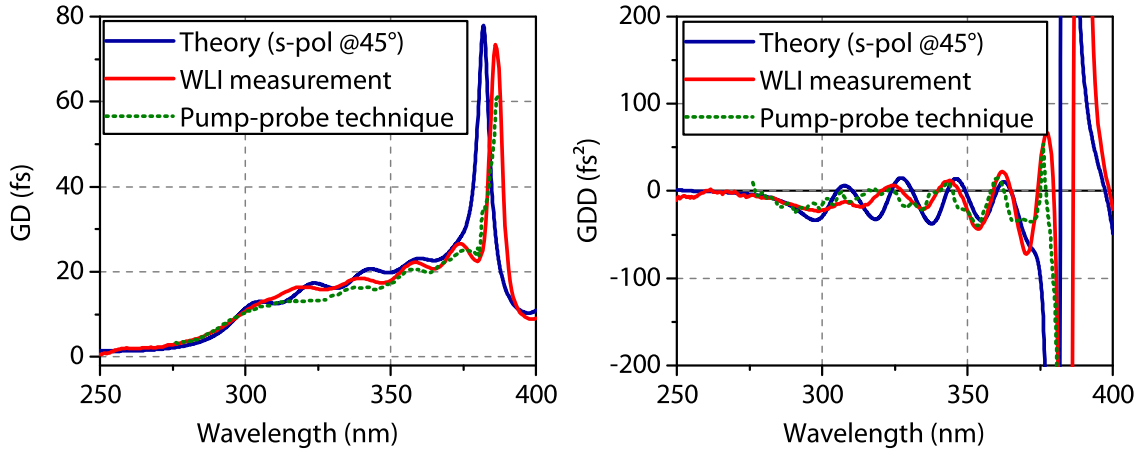


**Figure 4.3:** Dispersion measurements at an AOI of 45° using s-polarized light. Left is the GD and on the right is the GDD. One measurement (red) was carried out using our home-built white-light interferometer. The second measurement (dots) is made with the pump-probe technique described in the text.

pulse and the probe pulse interact in a non-linear way in the sample-medium. In the developed pump probe spectrometer, a pulse as short as 150 fs is split into two parts. One part is compressed to 25 fs and will then be the pump pulse. The second part of the beam is spectral broadened using white light generation in a calcium fluoride crystal. The two beams then interact with each other in a BBO crystal, generating the coherent artifact, which is measured with an spectrometer.

After measuring the intrinsic chirp of the white light as a reference, one or more metal mirrors from the white light path are exchanged to the dielectric mirrors to test. After the reference is subtracted, the measurement with the dielectric mirrors represent directly their introduced group delay. The result is shown Fig. 4.3. Here, also the data from our UV extended white light interferometer (WLI, see section 3.4) is plotted. One can see, that both measurements agree well with the theoretical values, but the WLI reproduces the GD-oscillations slightly better. The advantage of the pump-probe setup is, that researchers having access to such a device can directly characterize their dispersive mirrors with the same ultrashort pulses used as in the actual experiment, with only minor changes to the setup.

## 4.2 Ultra-broadband thin-film polarizer

Parts of this chapter are reproduced from my publication [53]. A broadband non-dispersive thin-film polarizer for ultrafast applications is presented. The polarizer has a controlled flat-phase and a high extinction ratio of 23:1 in the working bandwidth from 680 to 900 nm. This bandwidth allows supporting laser pulses as short as 12 fs. The unavoidable mechanical stress of the interference coating is completely compensated by a specially designed antireflection coating on the second side of the substrate, allowing the use of a thin substrate, which reduces the dispersion gained by the transmitted pulse. Broadband thin-film optical coatings are an indispensable tool to advance the progress in ultra-short laser science. The technology plays a key-role in the generation and manipulation of few-femtosecond pulses. High power laser sources, such as regenerative amplifiers [18] and optical parametric amplifiers [19] are currently under development. This novel trend will require broadband thin-film polarizers for separation, combination and power adjustment of high-power laser beams.

Here, the design and production of a ultra-broadband thin-film polarizer is shown, which allows manipulating and controlling the polarization of the transmitted and reflected light. At the same time, the coating doesn't introduce additional GDD to the laser-pulse. The extinction ratio of the non-dispersive broadband polarizer is at least 23. To my knowledge, in combination with the unprecedented bandwidth of 220 nm, this is the best result reported so far. To achieve the high bandwidth and good extinction ratio of the dielectric coating, an angle of incidence (AOI) of 75° was chosen.

In the following section 4.2.1, the design and production of the polarizer is described in detail. In Section 4.2.2, the results for transmission, GDD and flatness measurements are presented. Also a pulse simulation is performed, to demonstrate that the coating introduces

no distortion to the phase of the pulse. In addition, the unavoidable bending of the substrate, caused by the sputter deposition processes, is compensated. The deposited layers have strong intrinsic stress. This mechanical stress bends the substrate and therefore the beam profile of a reflected and transmitted laser beam is distorted. The fused silica substrate has a diameter of 25.4 mm and a thickness of 3 mm. For the polarizer the bending is compensated by depositing a very thick antireflection coating on the back side. The latter allows to deposit the coating on even thinner substrates, that helps to avoid the significant and unavoidable group velocity dispersion of substrates for transmitted beams.

After two bounces on such a polarizer the extinction ratio is more than 530, and four bounces exceed a extinction ratio of 280,000 with a total reflection of the main beam of at least 74 %. The polarizer provides the possibility to improve the polarization or to split s- and p- polarized femtosecond pulses. In combination with a rotatable half-wave plate the polarizer can be used as a variable attenuator that allows continuous power control of ultrashort pulses. A thin-film polarizer is also used in regenerative amplifiers [18]. The pulse circulating in the cavity is coupled out after a defined number of roundtrips by a polarizer, a quarter-wave plate and a Pockels cell. The combination of a polarizer and a Pockels cell can be used to interleave two pulse trains of two regenerative amplifiers used in a multi-kilowatt, joule-class picosecond laser setup [19].

### 4.2.1 Design and realization of the polarizer

A thin-film polarizer might be designed for the Brewster angle, which is about 56° for fused silica. At the Brewster angle, the p-polarized light has no reflection from the surface and therefore 100 % of it is transmitted through an uncoated substrate, while the s-component is still reflecting. The ratio of the transmitted p-polarized $T_p$ and s-polarized light $T_s$ gives the extinction ratio. A thin-film polarizer coating increases this extinction ratio. A standard thin-film polarizer has a limited bandwidth. To increase the bandwidth of the coating, which doesn't introduce noticeable dispersion to an ultrashort pulse, the coating design must be optimized with sophisticated methods. Also some fundamental properties of interference coatings at oblique incidence are described in detail in section 2.2.3 of the theory part. Besides the coating design two more details are important for a large bandwidth. The angle of incidence is increased to 75°. And we chose two coating materials with a high contrast in refractive index. The materials are niobium pentoxide ($Nb_2O_5$, n=2.37 at 500 nm) and silicon dioxide ($SiO_2$, n=1.47 at 500 nm).

The software OptiLayer was used to design the multilayer coating. Gradual evolution and needle optimization were employed [33, 34, 54]. The polarizing coating on the front side has 74 layers with a total physical thickness of 12.7 µm (Fig. 4.4, left). The thickest layer is made of $SiO_2$ with 1.19 µm and the thinnest layer is of $Nb_2O_5$ with only 17.2 nm.

The antireflection coating for the back side of the substrate (Fig. 4.4, right) has 45 layers. To compensate the mechanical stress of the front side coating, the total thickness of the antireflection coating was designed to be the same as of the front side coating [55]. Also the ratio

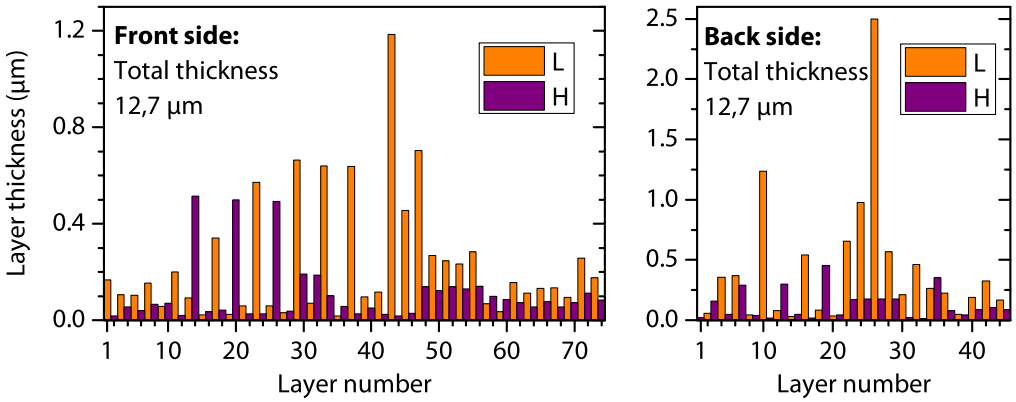


**Figure 4.4:** Physical layer thicknesses for the polarizing coating on the front side (left) and the stress compensating antireflection coating on the back side (right).

of $Nb_2O_5$ and $SiO_2$ was chosen to be about the same, since the two materials have different stress tensors. Magnetron sputtering was used for coating deposition because it produces high quality layers with high precision of the layer thicknesses. Well calibrated time monitoring combined with an optical broad band monitoring system for in-situ transmission measurements was used to control the layer thickness. The model of the magnetron sputtering coating plant was Helios by Leybold Optics (Bühler AG, Switzerland).

### 4.2.2 Characterization of the polarizer

The polarization dependent transmission measurements for an angle of incidence of 75° is performed using a Lambda 950 spectrophotometer from PerkinElmer Corporation. A Glan-Thompson polarizer is used to select s- and p-polarized light. For light detection of wavelengths below 860 nm a Photomultiplier tube and a slit of 2 nm is used. For wavelengths above that wavelength, a lead sulfide (PbS) photoconductive detector and a slit of 10 nm is selected. The light for the detector is collected by an integrating sphere (Fig. 4.5), which is mandatory in order to get precise results for non-normal incidence measurements on plane optics. This kind of light detection is insensitive to beam displacements caused by the thickness of a substrate. A standard detector suffers from the inhomogeneous sensitivity of the active area. To compensate the residual inhomogeneity of the integrating sphere, two measurements for each polarization are conducted and averaged: one at AOI = 75° and another with AOI = −75°. The measurement is in good agreement with the theoretical coating design (Fig. 4.6). The transition between the two doctors at 860 nm is smooth, which is typically not the case if a standard detector is used. The measured transmittance for s-polarization Ts is less than 4 % and for p-polarization $T_p$ more than 93 %, on average. Therefore, the extinction ratio $T_p/T_s$ is about 23:1.

The dispersion measurement was made using a home-built white light interferometer (see section 3.4). The measured group delay dispersion (GDD) is shown in Fig. 4.8. The mea-

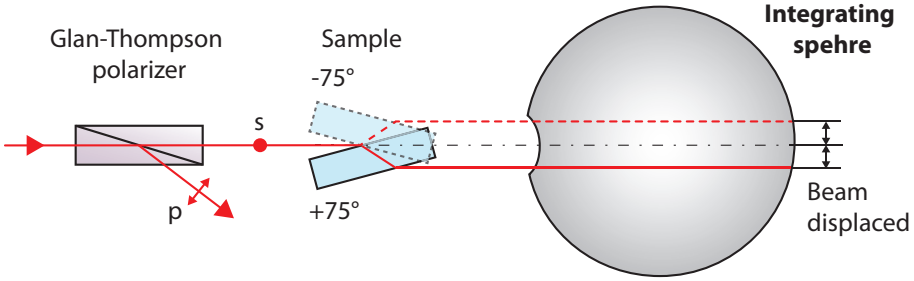


**Figure 4.5:** Optical path for the transmission measurement. An integrating sphere was used to avoid measurement error caused by the displaced beam. Also the sample was measured at a positive and negative AOI to the residual inhomogeneity of the integrating sphere.

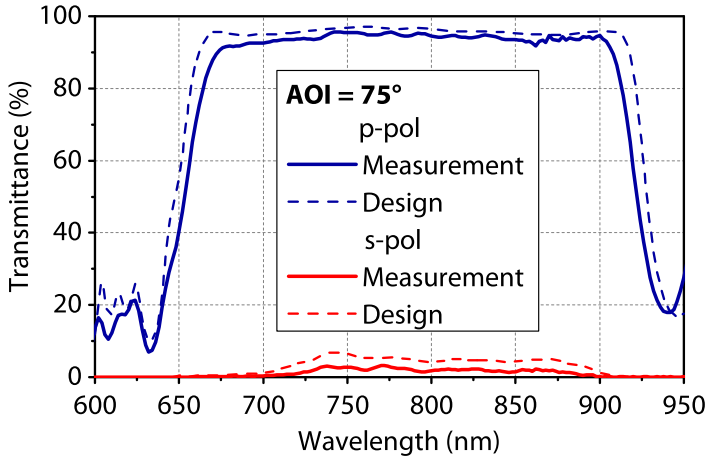


**Figure 4.6:** Absolute transmission measurements at AOI=75° (solid). Calculated Design including the antireflection coating on the back side (dashed).

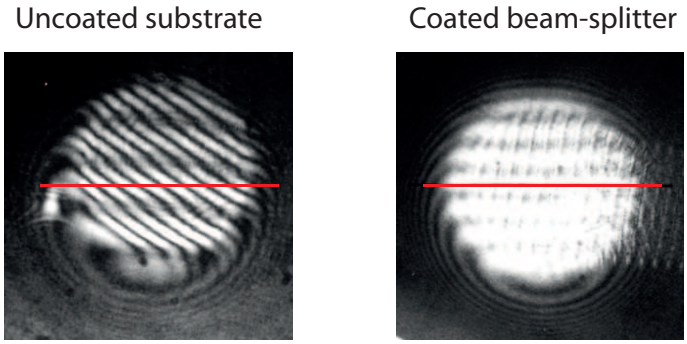


**Figure 4.7:** Flatness-measurement made with a homemade Fizeau-interferometer. The red line is drawn to indicate the flat interference fringes from the front-side. The signal is overlaid by the reflected light off the back-side.

surement shows excellent agreement with the theoretical data. The GDD of the reflected s-polarized pulse is nearly zero for the whole bandwidth. Therefore, the temporal profile of a reflected pulse is almost unchanged. The AR coating itself has also zero GDD but the dispersion of the 3 mm thick fused silica substrate leads to the non-zero GDD in the measurement. This dispersion cannot be compensated by the transparent antireflection coating but it could be compensated by additional dispersive mirrors with negative dispersion.

The surface flatness of the polarizer is measured (Fig. 4.7) using a homebuilt Fizeau interferometer. The uncoated substrate, the substrate and the polarizer with two coatings is measured. The flatness of the uncoated substrate and that of a substrate with two coatings were $\lambda/10$ each, meaning that the stress was successfully compensated.

With the data from the coating design a simulation for the temporal profile of a Gaussian pulse of 11 fs (FWHM) centered at 780 nm was made (Fig. 4.9). One can see that the reflected and the transmitted pulses are almost unchanged. There is no pulse broadening and no satellite pulse generation. Only a small drop in intensity is observed. For the transmitted pulse the dispersion of the fused silica substrate was not taken into account to illustrate the capability of the coating.

## Summary of the chapter about low-dispersive coatings

Two new low-dispersive optics were developed. At first a UV turning mirror with its high reflectance of more than 98 % outperforms metallic mirrors by far. Besides the temporal profile of the reflected pulse is nearly unchanged, since the GDD is low. The second low-dispersive optic is a ultra-broadband polarizer, with an unprecedented bandwidth which supports sub-12 fs pulses. The stress of the coating and the resulting deformation of the substrate are compensated by a specially adapted antireflection coating on the second side of the substrate, keeping the spatial beam-profile unchanged for both, the reflected and the transmitted pulses.

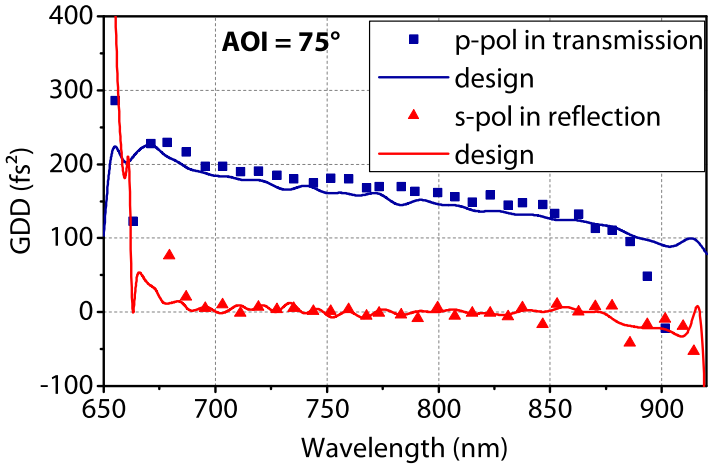


**Figure 4.8:** GDD measurement at AOI=75° (symbols). The calculated design includes the dispersion of the substrate with a thickness of 3 mm and the antireflection coating (solid).

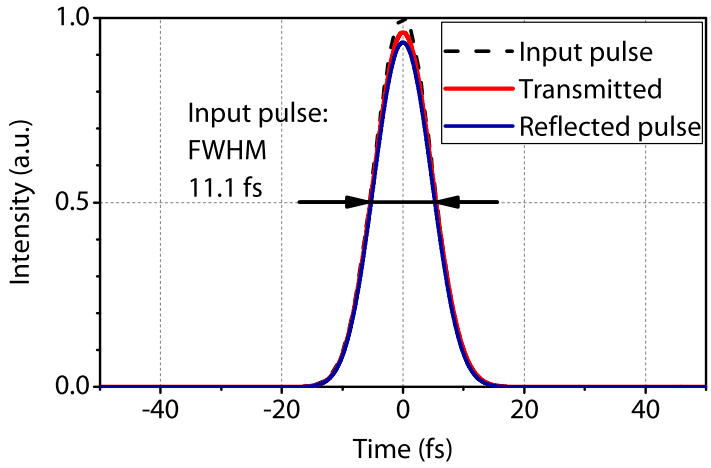


**Figure 4.9:** Simulations for the interaction of a Gaussian pulse with duration of 11.1 fs with the polarizer-coating. The shapes of the reflected and transmitted pulses is not changed by the coating. The dispersion of the substrate was not included to demonstrate the capability of the coating

This ultra-broadband polarizer paves the way for novel laser systems, wherein energetic few-femtosecond pulses are separated, combined or attenuated.

# Chapter 5

# Novel wedge dispersive mirror with low GDD-oscillations

This chapter deals with a novel octave spanning dispersive mirror with low oscillations in the GDD. The so called wedge dispersive mirror can dramatically simplify optical setups and allows the development of dispersive mirrors with even more bandwidth. Parts of this section are reproduced from my publication [56].

The generation of optical pulses in the sub-5-fs regime relies on the precise compensation of dispersion introduced by material-dispersion and self-phase-modulation [11]. Specially designed dispersive mirrors are capable to compensate this dispersion enabling pulses with durations shorter than 3 fs [57]. But such octave spanning dispersive mirrors exhibit strong spectral oscillations in the group delay dispersion (GDD), because of an impedance mismatch of the mirror-stack and the ambient medium [16]. The explanation is the following: There is a reflection on the interface layer between air and the layer-stack. In case the layer material is silicon dioxide, roughly 4 % of the incident pulse is directly reflected and does not penetrate into the stack. The main reflection of the dispersive mirror then interferes with the slight reflection from the front interface, and thus generates the GDD oscillations, as in a Gires-Tournois interferometer. These modulations limit the minimal achievable pulse duration [11] and reduce the temporal contrast by generating satellite pulses [17] (see also Fig. 2.1 on page 6). Ways of optimizing the coating design were found to reduce the oscillations [16], but they are not successful enough for mirrors with an octave spanning bandwidth.

## 5.1 Discussion of existing mirror concepts for low GDD-oscillations

Two general mirror design approaches exist to avoid GDD-oscillations. There are methods were one single mirror has already low oscillations and there are methods using pairs of mirrors which compensate the oscillations of each other. Both design approaches are explained in detail below.

### 5.1.1 Single mirror approach

In the single mirror approach the generation of the oscillations is prevented by avoiding the Fresnel-reflection from the surface of the top layer, which is the interface to the ambient medium [16, 58]. The reflected light from the surface interferes with the main beam and causes the dispersion ripples. One method to avoid this interference is to tilt the interface with respect to the coating-stack [59]. The tilted surface causes a separation of the reflected light from the top-layer and the main beam leading to an oscillation-free GDD. For manufacturing, a thin substrate is fixed on top of the coated mirror by optical contacting. Then the contacted substrate is polished down to a thickness of less than 100 um. Simultaneously, the contacted substrate must have the necessary wedge angle. The realization is technically difficult. The yield of usable mirrors is low, because the polishing process is not well controlled. Even for the good mirrors only about half of the aperture can be used. Another method is to provide ideal impedance matching between the coating and the incident medium by applying the dispersive coating on the back side of a substrate [60]. Also here the substrate must be very thin to avoid unwanted additional group velocity dispersion (GVD). The GVD of the substrate must be compensated by the coating. For example, an octave spanning dispersive coating can roughly compensate the GVD of only 1 mm fused silica. Then there is no way to introduce additional negative GDD, which is usually desired. Additionally a substrate with a thickness of 1 mm does not fulfill the requirement in flatness after being coated, since the intrinsic stress of the coating deforms the substrate too much. A stress-compensating antireflection coating [53] can be deposited on the front side. One more way to provide ideal impedance matching is to use p-polarized light for the mirror at Brewster angle [17, 61]. This concept suffers from the relatively low reflectance obtained for p-polarized light and the high angle of incidence (AOI) which makes the mirror unsuitable for many optical setups.

### 5.1.2 Mirror pair approach

There are concepts where the oscillations are not avoided at one mirror but they are heavily reduced by employing alternating mirror pairs. The first mirror pair concept is based on a complementary pair of mirrors [57, 62, 63]. The oscillations still exist after reflection at the first mirror, but they are compensated by a second mirror which has similar oscillations which are spectrally shifted to be in anti-phase. The result after an even number of bounces on these mirrors is a relatively smooth dispersion. A disadvantage of this method is that two different coatings are necessary which must be perfectly matched. The precision of the total thickness should be within 0.1 % from one coating run to another. Higher deviations result in an increased amplitude of the residual oscillations. Another way to get such a complementary pair from one single coating run are so called double angle mirrors [64]. Since the GDD-spectrum shifts to shorter wavelength when the AOI increases, there is an angle where the oscillations of two mirrors used under two different angles have an opposite phase. Since the mirrors are from one coating run, they don't need to be matched to be used in double-angle configura-

tion. But when many mirrors are made in one coating run, the mirrors still must be matched because of the inhomogeneity in layer thicknesses caused by the coating plants. Another disadvantage of these mirrors is that they must be accurately aligned in order to meet the AOI of the coating design. Small deviations of the AOI lead to increasing GDD-oscillations. Below the novel wedge dispersive mirrors are explained and compared with conventional double angle mirrors, because nowadays they are one of the most common types of mirrors used for broadband pulse compression. The design target was the same for both mirror concepts in order to make the comparison feasible.

## 5.2 Concept of the wedge dispersive mirror

In a wedge dispersive mirror, the compensation of spectral GDD oscillations is realized in one single multilayer stack. It is thus a single mirror approach. The key element of the new mirror is a wedged layer which is coated onto a specially optimized dispersive multilayer stack (Fig. 5.1). During the design process, fused silica was used as incidence medium, and not air as for conventional dispersive mirrors. The wedged layer has a thickness of about 8 µm on one side of the mirror and 6 µm on the other side. In Fig. 5.1a the coating stack thickness is about in scale with the wedge thickness. But the lateral dimension is not in scale, it is 25 mm in reality. Therefore this very flat wedge should be considered as a wedge shaped layer. This thick layer introduces high frequent GDD oscillations which are shifted spectrally along the gradient of the wedge. This is illustrated by the two rays shown in Fig. 5.1a. In this picture, the two rays A and B interact with the coating at two different positions $x_A$ and $x_B$. The GDD curves for these two individual positions are given in Fig. 5.1b. In this idealized case the oscillations are in anti-phase and therefore cancel each other. It's important to note, that the pulse has a slight spatial chirp after being reflected of a wedge mirror, meaning that one side of the pulse has a different phase as the other side. This is compensated by putting the next mirror anti-parallel to the first one as illustrated in Fig. 5.1c.

Generally, the phase and its derivatives are not additive values, but the main contribution to the result is provided by focal plane zones of constructive interference, where phases are rather close. Zones of destructive interference have small contribution and can be neglected in this approximation. Therefore, the effective GDD a laser pulse with a beam profile $I(\mathbf{r})$ has obtained from a mirror can be considered as an integration of the GDD values along the diameter of the beam. In the focal spot, were all GDD components are superimposed, the effective $\overline{\text{GDD}}$ can be expressed as:

$$\overline{\text{GDD}}(\lambda) = \int \text{GDD}(\lambda, \mathbf{r}) \cdot I(\mathbf{r}) d\mathbf{r} \tag{5.1}$$

Here $\lambda$ is the wavelength and $\mathbf{r}$ is the radius of the beam. The averaged $\overline{\text{GDD}}$ for the wedge mirror design is shown in Fig. 5.2b. For comparison the GDD of a state-of-the-art double angle mirror system is shown for both AOIs and the resulting effective values in Fig. 5.2a. Both con-

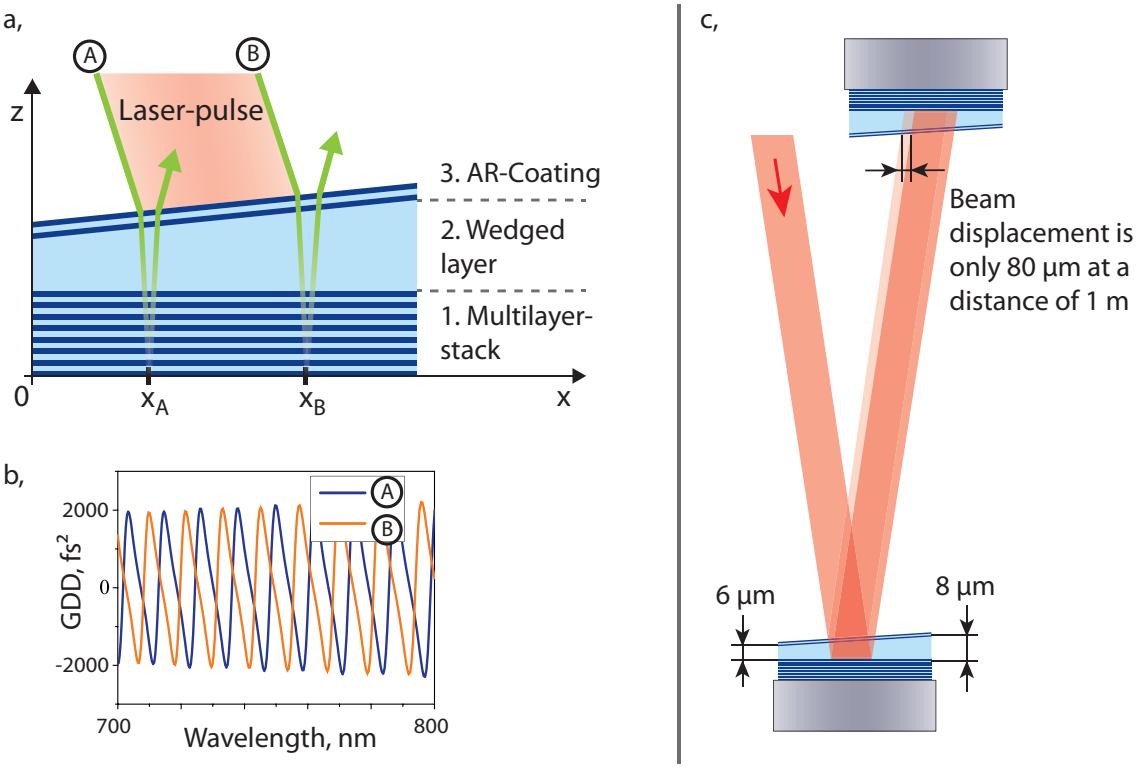


**Figure 5.1:** Concept of a wedge dispersive mirror (a). It consists of three major parts: The multilayer stack, the wedged layer and the antireflection coating to suppress interference fringes in the reflected beam. For illustrating the principle of operation the two rays A and B are drawn. They hit the coating on two different spots with a different thickness of the wedged layer. The GDD spectral phases of the two rays differ and cancel each other (b). The slope of the wedge is very small (c). The reflected light from the wedge surface is still overlapped with the main beam from the dispersive mirror structure. Therefor the antireflection coating is indispensable.

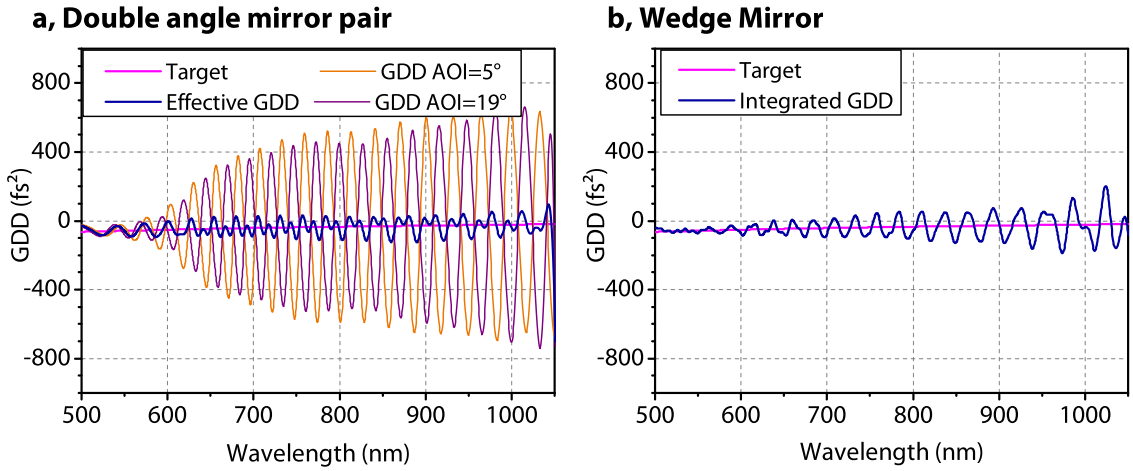


**Figure 5.2:** Calculated group delay dispersion: The target (magenta line) was chosen to be the same for both mirror concepts. a, Double angle mirrors: The red and the black line show the GDD of one reflection at an angle of incidence of 5° and respectively 19°. Blue is the effective GDD.

cepts have similar characteristics with the important difference that the novel wedge mirrors achieve this result after only one reflection. Also wedge dispersive mirrors are more convenient to use in an optical setup, because the angle of incidence must not be aligned with high precision. Also the number of bounces, thus the number of mirrors, can also be odd, resulting in more freedom in the design phase of an optical setup. Another advantage is that the new mirrors don't need to be matched as it is the case for double angle mirrors.

The antireflection coating on the wedged layer effectively reduces front surface reflections and avoids interference fringes in the reflected beam without affecting the effective dispersion of the mirror.

The multilayer-stack and the antireflection coating are designed independent from each other using OptiLayer. The dispersive multilayer mirror is optimized using the same target GDD-values as used for the double angle mirror. For the calculations fused silica is used as the incidence medium, taking into account that the silicon dioxide layer is deposited onto the stack. After fabrication of the mirrors discussed here, we found that in future optimizations the amplitude of the GDD oscillations can be further reduced by using $SiO_2$ as incidence layer for the design calculations.

The obtained design with the optical layer thicknesses is shown in Fig. 5.3. For the production three coating runs are necessary. At first the actual dispersive layer stack is coated. Then the wedged layer is deposited, followed by the AR coating.

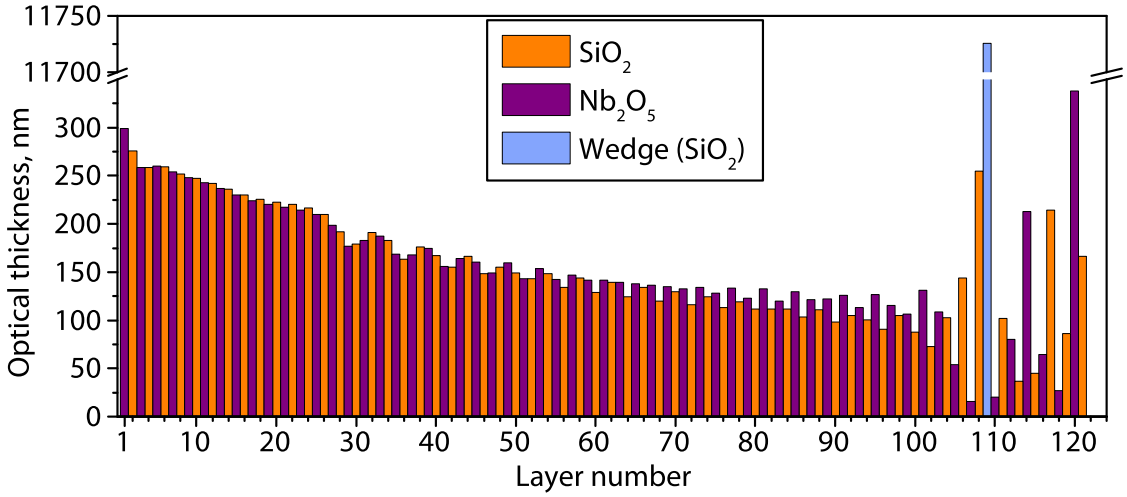


**Figure 5.3:** Design of the wedge dispersive mirror with optical layer thicknesses plotted. The first layer is on the substrate, the last layer number 121 is exposed to air. Notify that the y-axis is discontinued for the thick wedged layer. The blue color was chosen for highlighting the wedged layer, but the same $SiO_2$ was also used for the other low index layers. The layers of the basic dispersive mirror stack are almost perfectly chirped. The double angle design deviates significantly from being chirped. For comparison see the similar design shown in the IBS chapter in Fig. 7.6 on page 66.

## 5.3 Manufacturing of the wedge dispersive mirror

The thin film design was deposited on fused silica substrates with 1 inch diameter using the magnetron sputtering plant Helios (section 3.1). Well calibrated time monitoring combined with an optical broad-band monitor for in-situ transmission measurements was used to control the layer thickness. Niobium pentoxide $Nb_2O_5$ and silicon dioxide $SiO_2$ are the layer materials. The wedge dispersive mirror is realized in three different coating runs. In the first run, the basic dispersive mirror structure is deposited having a homogeneous thickness all over the substrate. The fabrication of the wedged layer is the key step of the process. A simple technique was developed to apply the wedged layer using the same standard magnetron sputtering process as used for the multilayer structure. The samples are mounted in in a tilted position (Fig. 5.4). Thus one part of the surface is closer to the magnetron and one part is farther away. The coating is then deposited inhomogeneously along one axis of the surface of the substrate resulting in a wedge-shaped layer. Here the advantage of using magnetron sputtering is that the sputtering target is very close to substrates and therefor the gradient of the wedge becomes very large. The orientation of the wedge gradient is marked on the substrate for later reference. After the wedged layer is finished the coated substrates are put in the standard fixtures to apply the antireflection coating homogeneously.

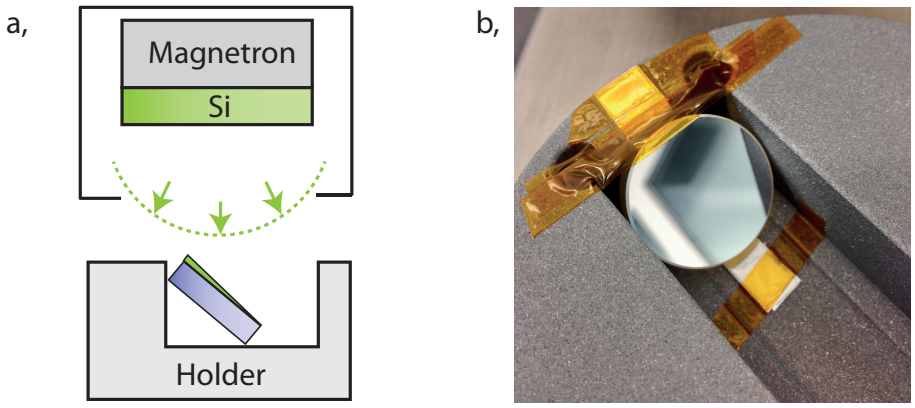


**Figure 5.4:** Concept of the deposition of the wedge shaped layer (a). The substrate with the dispersive multilayer structure is mounted tilted in a large and deep fixture, which is usually used for large rectangular substrates (b). The substrate has to be fixed tightly because the turn-table of the Helios sputter machine rotates with 4 rounds per second.

## 5.4 Characterization of the wedge dispersive mirror

The new wedge dispersive mirrors is extensively characterized to proof its reliable operation. GDD-measurements were conducted using a WLI. Also the new mirrors were used in a compression stage of a high power Ti:Sa laser system and here they again were compared with conventional PC70 double angle mirrors. FROG measurements are conducted and beam-profiles were measured.

### 5.4.1 GDD measurement using a WLI

To measure the GDD of the mirrors the white light interferometer described in section 3.4 was used. The results are shown in Fig. 5.5. The wedge dispersive mirrors are measured at an AOI of 8°. For comparison the two double angle dispersive mirrors were measured simultaneously at an AOI of 5° and respectively 19°. The result was then divided by a factor of 2 to get the so-called effective GDD, which embodies the value of one single mirror.

### 5.4.2 FROG measurements

The new mirrors were also tested in a Ti:Sa based laser system whose pulses are spectrally broadened to one octave in a nonlinear hollow core fiber [65] (Fig. 5.6). The emitted pulses are compressed by six of the wedge dispersive mirrors. For comparison six double angle mirrors (PC70) aligned at an AOI of 5° and 19° are employed. The power was 1.6 W. The pulse duration after the compressor is measured with FROG [66]. The traces for both types of mirrors are shown in Fig. 5.7 and are similar. The pulse duration is 3.8 fs for both types of mirrors. In case of the wedge mirrors we observe slightly less satellite pulse generation which means

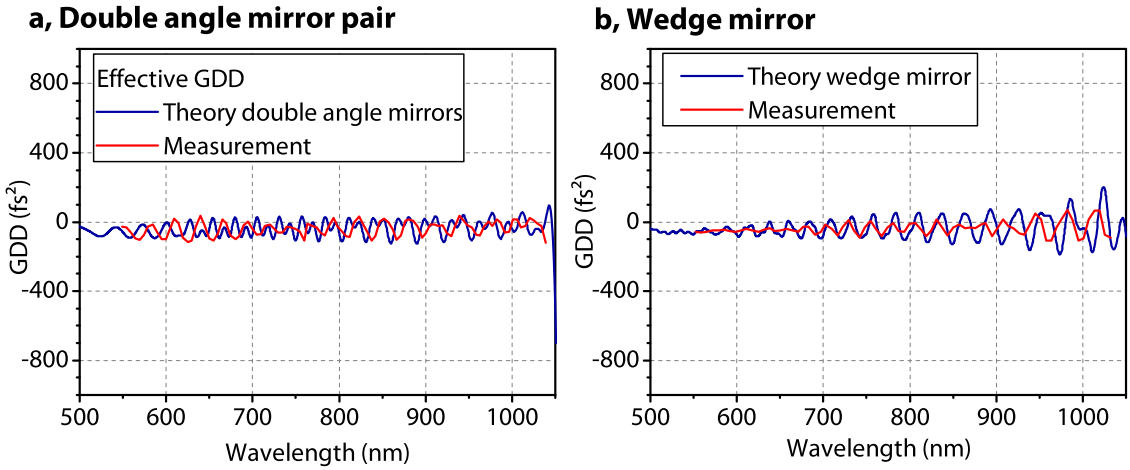


**Figure 5.5:** Dispersion measurements using a white light interferometer: Measurement and Theory of the group delay dispersion (GDD) for one pair of double angle mirrors (a) and wedge dispersive mirror (b).

that more energy is concentrated in main pulse.
The FROG measurements prove that a pulse compressor consisting of the novel wedge dispersive mirrors generates pulses as short as using a compressor consisting of conventional double angle mirrors.

### 5.4.3 Beam profiles

Also the beam profiles are measured at the focal spot with and without the wedge mirrors. One can observe changes in the beam profile when using the wedge mirrors (see Fig. 5.8b,). The reason is a lensing effect generated by the wedged layer, which is not uniformly produced yet. The wedge has perpendicular to the wedge-gradient a slight cylindrical concave shape. By rotating the six mirrors in respect to the wedge-gradient by 30 degrees, that means the rotation angles are [0° 30° 60° 90° 120° 150°], the lensing effect was sufficiently compensated (see Fig. 5.8c,). The coating process of the wedge shaped layer (Fig. 5.4) could be further optimized to get a more planar wedge, to avoid this lensing effect. Masks can be mounted onto the fixture during coating process to modify and improve the shape of the wedged layer.

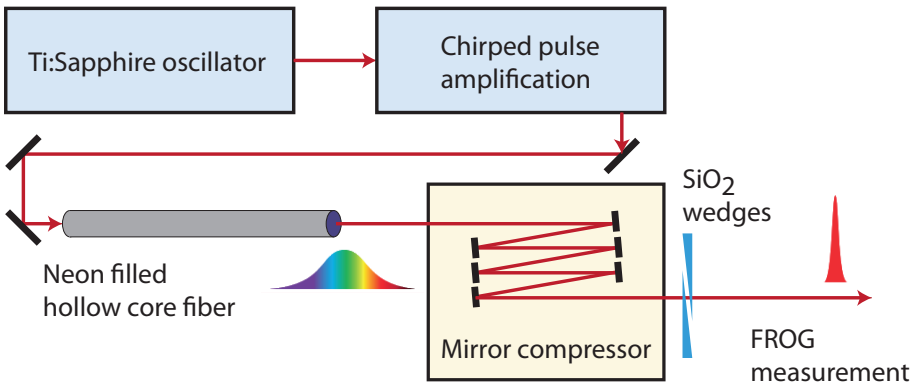


**Figure 5.6:** Simplified layout of the FP2 laser system at the Max-Planck Institute of Quantum Optics, where the wedge mirrors were tested. The pulse of a Ti:Sapphire laser is amplified and spectral broadened using a neon-filled hollow core fiber. The pulses are then compressed in time using the new wedge mirrors. The pulse duration is measured using FROG. Also the beam profile of the pulse after the compressor was measured (see Fig. 5.8).

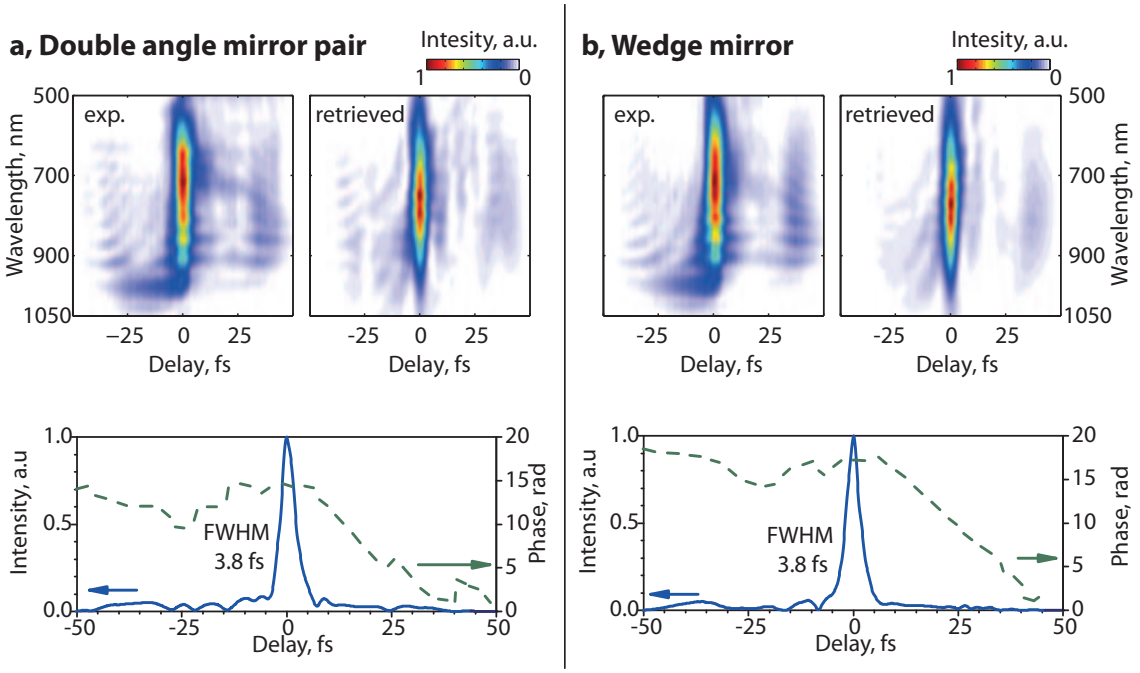


**Figure 5.7:** Experimental FROG traces taken after the compression with six mirrors of conventional double angle mirrors (a) and wedge dispersive mirrors (b). Also the retrieved FROG traces are shown. The retrieved temporal profiles and the phases are below.

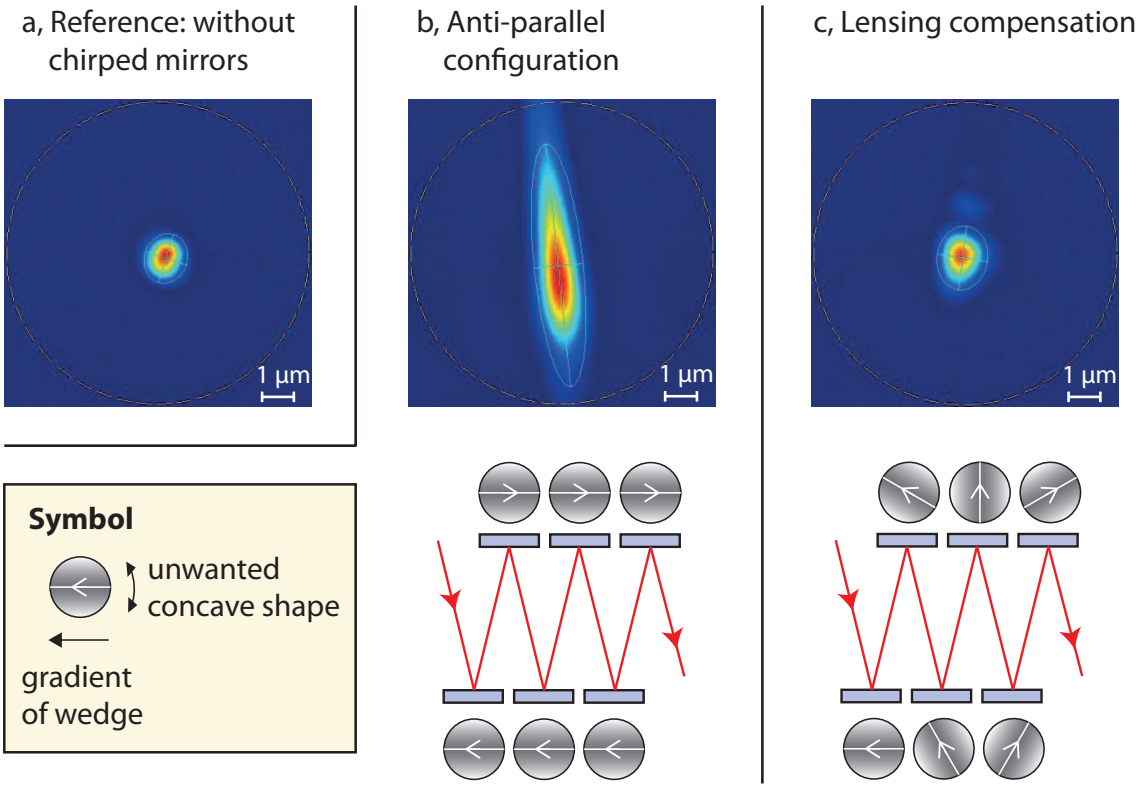


**Figure 5.8:** The beam profile of the unaltered pulse at the focus before the mirror compressor (a). The beam is focused with a concave metal mirror. A change of the beam profile is observed, when the mirrors are arranged anti-parallel, to avoid a spatial chirp (b). The distortion is caused by the not flat surface of the wedge. The wedge has a slightly cylindrically convex shape, defocusing the beam in the vertical plane. This problem can be solved by optimizing the coating process of the wedge. A successful work around is shown in (c). The mirrors are rotated by 30° relative to each other, resulting in a good focus without major distortions.

## Conclusion of wedge dispersive mirrors

The novel wedge dispersive mirror was invented, designed, produced and characterized. For one application, wedge dispersive mirrors were manufactured, which compress an energetic octave spanning near-infrared laser pulse down to a duration of 3.8 fs. The mirrors exploit a newly discovered averaging effect of oscillations in the group delay dispersion by introducing a wedged layer. The new wedge dispersive mirrors combine the advantages of the two existing approaches of oscillation-free dispersive mirrors. Since the wedged layer can be realized by a standard thin-film coating process, the new mirrors are simpler to produce than mirrors basing on the conventional single mirror approach. Furthermore the wedge dispersive mirrors are much easier to implement in optical setups than double angle mirrors, since the angle of incidence has a wide working range.

# Chapter 6

# Mid-infrared dispersive mirrors

In the so called finger print region between 2 to 20 μm, most molecules have fundamental vibrational modes, making mid-infrared (MIR) spectroscopy an important tool, which attracts more and more scientists around the world. A laser source suitable for this application was developed recently by Pupeza et al. [24]. It generates high power ultrashort light pulses in the mid-infrared spectral region of 6.8 to 16.4 μm with an average power of 0.1 W. A key-role for advancing this new technology plays the availability of suitable dispersive mirrors which allow the efficient generation and manipulation of broadband few-femtosecond mid-infrared pulses.

This chapter presents pioneer work for dispersive mirror coatings for the mid-infrared spectral range up to a wavelength of 11.5 μm. The limits are determined by fundamental absorptions of the employed coating materials. As can be seen in Fig. 3.3 on page 17, bulk germanium has already minor absorption at 12 μm. Bulk zinc sulfide has a similar low absorption in this range [67]. For the development of these novel dispersive coatings, the equipment for GD and GDD measurements are indispensable. Two devices making the dispersion of optics accessible up to a wavelength of 20 μm are described in section 6.1. These results are published [68].

In section 6.2 the high-vacuum coating process for fabrication of the multilayer coatings is shown. In the last section 6.3 of this chapter two dispersive mirrors are shown including dispersion measurements. The results for the first mid-infrared dispersive mirror are to be published. The submitted article is accepted at Applied Optics for the feature edition: "Optical Interference Coatings 2016".

## 6.1 Development of GDD measuring devices for mid-infrared optics

Some of the content of this chapter is reproduced from my publication mentioned above [68]. Two measurement devices are presented, which both allow the direct measurement of the group delay (GD) and group delay dispersion (GDD) of interference coatings, covering the near- and mid-infrared spectral range of 2 to 20 μm (500 to 5,000 $cm^{-1}$). One of the devices is a resonant scanning interferometer (RSI) and the other is a white light interferometer (WLI). The WLI is also capable of measuring the GDD in transmission, for instance of bulk material.

GDD measurements of a high dispersive mirror for wavelengths from 2.0 to 2.15 µm and one of a multilayer mirror from 8.5 to 12.0 µm are presented. A measurement of a zinc selenide (ZnSe) substrate in transmission was made with the WLI demonstrating the full bandwidth of the device from 1.9 to 20 µm. The comparison of all measurements with their related theoretical values shows a remarkable correspondence.

Recently, GDD measurements in the UV-vis-NIR optical region using a home-made WLI [46] and a RSI [69] were published. In my thesis, these techniques were advanced to enable the development of the new devices for the mid-infrared range. Unfortunately, none of the optical components of the existing setups for the UV-vis-NIR optical region are suitable for MIR radiation. In the previous devices the spectrometer, light source, beam splitter and partial reflectors were selected for a spectral region up to only 2 µm. In the MIR wavelength range typically Fourier transform infrared spectrometers (FTIR) are used, but they are less sensitive than VIS-NIR spectrometers. As a result the MIR interferograms measured with the WLI are more noisy and require more acquisition time. That makes it impossible to use the old evaluation algorithms. Extending the previously known working principles to the MIR wavelength region required the search for new optical components, light source, spectrometer and a new evaluation software, resulting in the development of completely new devices.

All optical components, the light source and the spectrometer, must be designed to work in the MIR spectral range. The dominating type of spectrometers for the MIR are typically FTIR spectrometers. Besides also dispersive grating spectral photometers exist, but they are too insensitive for the new applications. For the measurement setups showed below, a FTIR spectrometer Vertex 70 from Bruker Opik GmbH is used (see section 3.4 for more details). The device is a stand-alone FTIR spectrophotometer which allows transmittance and reflectance measurements of optical components, but it also has an external input to measure the light from the interferometers described below. For the high acquisition rates needed for the WLI, the FTIR spectrometer is equipped with a sensitive mercury cadmium telluride (MCT) detector, which is cooled with liquid nitrogen and has a working range of 1.25 to 20 µm (8,000 to 500 $cm^{-1}$). For the incoherent MIR light source a silicon carbide globar (Newport Corp.) is used which emits radiation from 1.7 to 25 µm. Most of the optical components were coated in-house with an electron beam deposition system described in section 3.2. The alignment of a MIR-optical path was found to be very challenging, since I couldn't find a way to make the MIR light visible. Therefore, gold mirrors were produced which have some residual transmittance of about 1 % in the visible range. Due to this one can see the glowing filament of the globar by eye, looking through the backside of the gold mirrors. This method was found to be most practical for aligning the optical setups. Two different approaches to measure the GDD of optics were realized. The first approach is based on a resonant scanning interferometer (RSI) [69]. The second measurement setup is a scanning white light interferometer [44, 46, 70, 71].

### 6.1.1 Resonant scanning interferometer (RSI)

An RSI is basically a Fabry-Perot interferometer consisting of two semitransparent mirrors and is operated with a white light source. The two mirrors are separated by a thin air spacer. The spectrum of the light transmitted by the end mirror exhibits sharp resonance peaks. From the spectral distance of the resonant peaks to each other, the group delay can be calculated when the thickness of the air spacer is known [72]. By having multiple spectrums at different thicknesses of the air spacer, the group delay can be calculated with a high spectral resolution, without knowing the distance of the two mirrors, using an advanced algorithm [69]. For the new setup an RSI was built in the so-called reflection mode and measured the reflected light of the resonator (Fig. 6.1). Such setup of the interferometer is also called a Gires-Tournois interferometer. Measuring the reflected light is especially essential when the mirror substrate is not transparent in the spectral region of interest. The MIR light is guided by a gold mirror to the interferometer. The partial reflector (PR) is a 3 mm thick zinc selenide (ZnSe) substrate, coated with a gold layer with a thickness of 5 nm. The sample is mounted on a translation stage to adjust the distance between the two mirrors. The reflected light with the resonance peaks is measured with the FTIR spectrometer. The interference signal only appears when the two mirror surfaces are exactly parallel to each other. For this alignment the beam of a He-Ne laser is coupled into the optical path. An interference pattern generated by the sample and the partial reflector is now observed. The tilt of the sample is carefully changed now until the interference fringes are circular. That means the two laser beams are collinear and the sample is exactly parallel to the partial reflector. For a single GDD measurement, a few spectra are acquired at different thickness of the air-spacer. 10 spectra are typically enough to get a reliable result. The spectra are evaluated using the algorithm recently developed by Trubetskov et al. [69].

### 6.1.2 White light interferometer (WLI)

A WLI is a Michelson interferometer with a broadband incoherent light source. When both arms of the interferometer have the exact same length, interference fringes are visible at the output, where the two beams overlap. By increasing and decreasing the path length of one arm, the interference vanishes because of the short coherence length of the light source. Different methods and algorithms exist to measure and calculate the group delay from WLI measurements [44, 70, 73, 74]. In the new setup the light at the output is measured with a spectrometer. The signal for each wavelength of the spectrometer versus the path length is an interferogram. For each wavelength an envelope of the interferogram is calculated and the position of the maximum in respect to the delay is determined. For the case of an empty WLI with no dispersion, that's when the end mirrors are metal mirrors, the maxima of the interferograms appear all at the same path length. When one end mirror is exchanged for a dispersive mirror, the maxima of the interferograms can have a relative delay. That means that the penetration depth changes for different wavelength. The time delay between the maxima

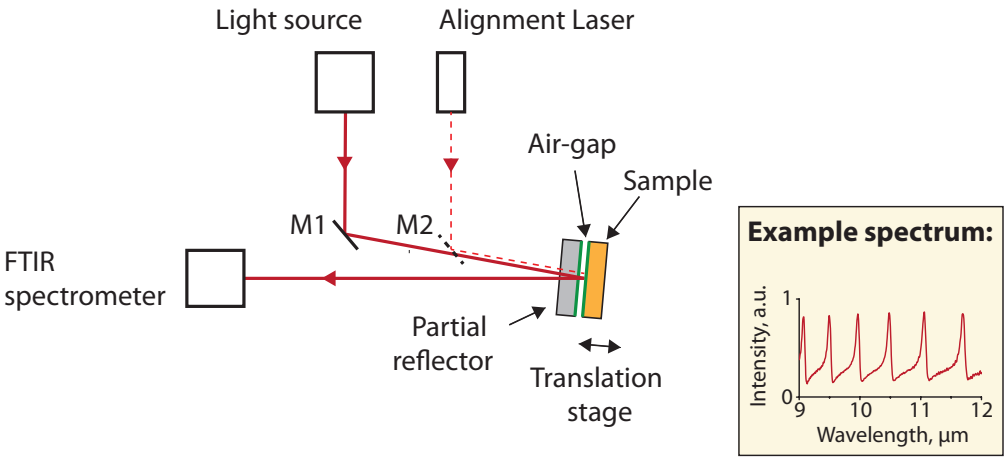


**Figure 6.1:** Optical setup of the resonant scanning interferometer (RSI): Light is guided under a small angle into the Gires-Tournois interferometer. The distance between the partial reflector and the sample can be changed by the translation stage. The alignment laser is needed to adjust the sample to be parallel to the partial reflector. The insert shows an example of a single measurement. The GD is calculated from the distance of the resonance peaks.

is exactly the group delay GD caused by the sample.

The WLI setup is shown in Fig. 6.2. The light source and the FTIR spectrometer are the same as used for the RSI setup described in section 2.1. The beam from the light source is split into two parts with a KBr thin-film beam splitter. As illustrated in Fig. 6.2, the compensation plate is put directly onto the beam-splitter. The compensation plate is needed in order to have the same amount of dispersion in both arms of the interferometer. One end mirror of the interferometer is mounted onto a motorized translation stage. For a GDD measurement, the stage is put into a position out of the interference maximum, to be able to record one whole interferogram with the maximum in the middle. Then the stage starts moving and the spectrometer acquires spectra continuously. Typically 8,000 spectra with a resolution of $10\,\mathrm{cm}^{-1}$ are taken. Since the resolution of the FTIR spectrometer is defined in the frequency space, it depends on the wavelength. For example the resolution of 10 cm-1 corresponds to a wavelength resolution of 0.1 µm at 10 µm or 25 nm at a wavelength of 2 µm. For the evaluation of the data acquired by the WLI, it was necessary to develop new algorithms, to get the most precise measurement results (see appendix B). The algorithm is written using Matlab, and it is based on the publication of Amotchkina et al. [46].

### Accuracy

The spectral resolution of the WLI is in principle defined by the spectral resolution of the spectrometer. For each spectral point an interferogram is acquired, which is one data point in the GD plot. The GD value is derived from the position of the interferogram in time. Here

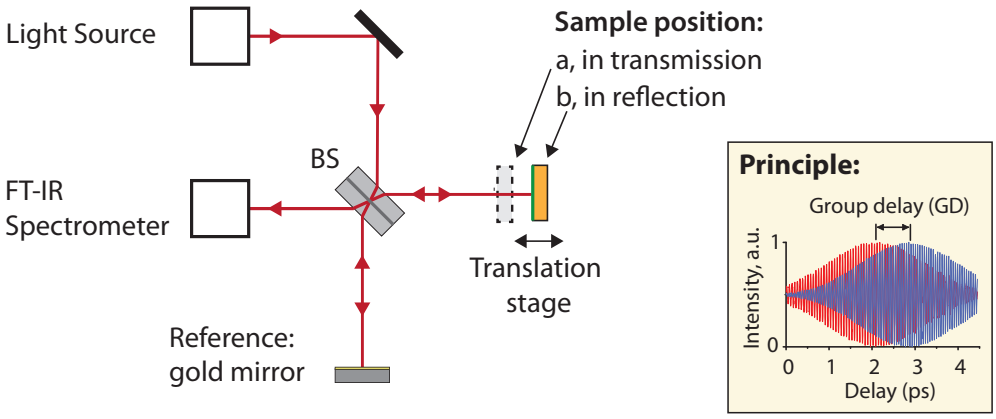


**Figure 6.2:** Optical setup of the white light interferometer (WLI): Light is split into two arms by a thin film beam splitter. The compensation plate is directly put onto the beam splitter. The end mirrors are gold mirrors. If a sample is measured in reflection, it replaces a gold mirror and is used as an end mirror. For transmission measurements the sample is placed in the optical path of one arm. In the small box, the working principle of a WLI is shown. The relative delay between two interferograms is the group delay (GD).

the accuracy is strongly dependent of the spatial precision of the translation stage, because the stage position determines the delay in time. In the algorithm for the GDD evaluation, this uncertainty is reduced by calibrating the movement with one reference interferogram. Since an interferogram consists of oscillations with exactly the period of one wavelength, it can be used to calibrate the translation of the stage. Therefor the remaining error in the absolute GD is minimal. More influence on the accuracy has the determination of the position of the maximum for each interferogram. An envelope of an interferogram has to be found and thus fitted for instance with an Gauss-function. The uncertainty in the time axis of this fit is a source of deviation in the GD result. This uncertainty created noisy results for the GD and GDD curves. Averaging has to be applied to smooth the curves, but this unfortunately reduces the spectral resolution.

### 6.1.3 GD and GDD measurements

In the following three paragraphs measurements from both devices, RSI and WLI are presented to demonstrate the capabilities of the devices. Two multilayer mirrors are measured with both devices and the data is plotted into one graph. The measurements are compared with each other and with theoretical values. At last the dispersion of a zinc selenide substrate in transmission measured with the WLI.

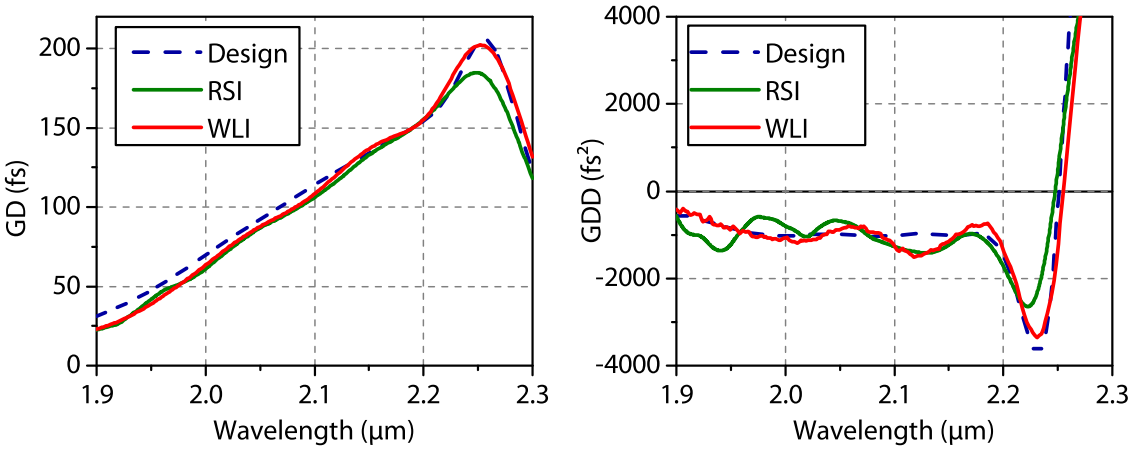


**Figure 6.3:** High dispersive mirror designed for GDD $= -1{,}000\,\mathrm{fs}^2$ in the range of 2.0 to 2.15 µm. The oscillations are an indication for layer-thickness deviation during the coating process.

### Dispersive mirror for near infrared light

The coating design for the dispersive mirror was optimized to have a flat GDD from 2.0 to 2.15 µm (Fig. 6.3, dashed line). The dispersive mirror is produced in a reactive magnetron sputter process (Helios from Leybold Optics) using tantalum pentoxide and silicon dioxide as layer materials. The measurement demonstrates that the two presented devices allow measurements in the near infrared spectral range. The measurement of the RSI and the WLI agree with each other in the region of interest from 2.0 to 2.15 µm and provide an average GDD value of $-1{,}000\,\mathrm{fs}^2$ (Fig. 6.3 right). Both measurements show small oscillations in this range, which are a typical indication of small layer-thickness deviations during the coating process. The thickness-errors are typically below 0.5 % for our sputter process, since the coating process is very stable and well understood. The layer thicknesses are controlled by time and calibrated by an optical broadband monitor. Outside of the region of interest the WLI produced more reliable GDD data than the RSI, since the the reflectance of the mirror decreases outside the designed range and therefore the intensity and the sharpness of the resonant peaks decrease.

### Multilayer mirror for MIR radiation

A mirror for wavelengths from 8.5 to 12 µm was produced, using an electron beam process using germanium and zinc sulfide as layer material. The mirror is described in detail in section 6.3.1. The design is a simple quarter-wave stack (QWS) with 9 layers. The first and the last layer are Ge and the coating stack is described by the formula [Ge ZnS]4 Ge. The substrate material is also germanium. In Fig. 6.4 the measurements and the theoretical values are shown.

The measured values of the GD and GDD for the range of high reflectance from 8.5 to 12 µm coincide well with the theoretical values for both devices. Like in the previous section,

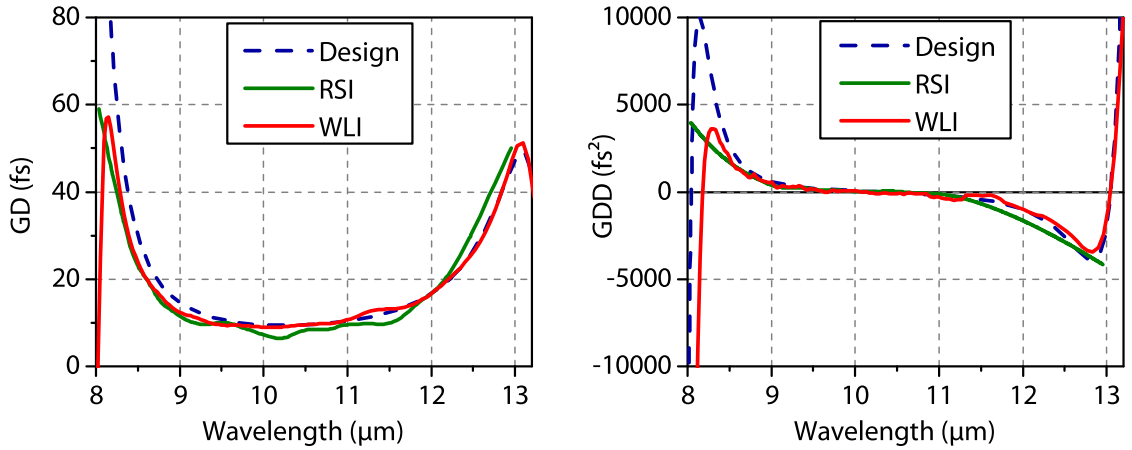


**Figure 6.4:** Mirror for MIR light. The mirror is a QWS centered at 10.5 µm and is produced by electron beam deposition. It shows the typical shape of GD and GDD of a QWS. The characteristic is flat around the central wavelength, and the values increase when locking to shorter and longer wavelengths.

the WLI produced more reasonable values outside of the reflectance range. Also the thickness errors were estimated for this e-beam coating run. Since the spectral characteristics and the GDD of a QWS are very robust versus thickness deviations, only small deviations of the GDD measurement can be seen in the region of interest between 8.5 to 12 µm. But the peak in GDD at about 8.3 µm is obviously reduced. An error analysis of the coating design reproduced this lowered peak and indicates a random thickness-error of about 1.5 %. As expected, the value is higher as for the sputter process, but it gives reason for further optimization and stabilization of the e-beam coating process.

### Dispersion of a zinc selenide substrate

In the following is shown, that the WLI is also capable to measure the GDD in transmission of bulk material for the whole working range from 1.9 to 20 µm. For better comparability with other substrate materials the group velocity dispersion (GVD) is shown, which is the GDD per unit length. The GVD of a 3 mm thick Zinc selenide substrate was measured by putting the substrate in one optical path of WLI. The end mirrors of the WLI were both gold mirrors. This kind of measurement can't be realized by RSI, because the principle of an RSI is a Fabry-Perot interferometer with a cavity length of a few tens of micrometers. The literature values of the wavelength dependent refractive indices $n(\lambda)$ of ZnSe from 0.5 to 18.2 µm were taken from [75]. With these values the group velocity $v_g$ and the group velocity dispersion GVD

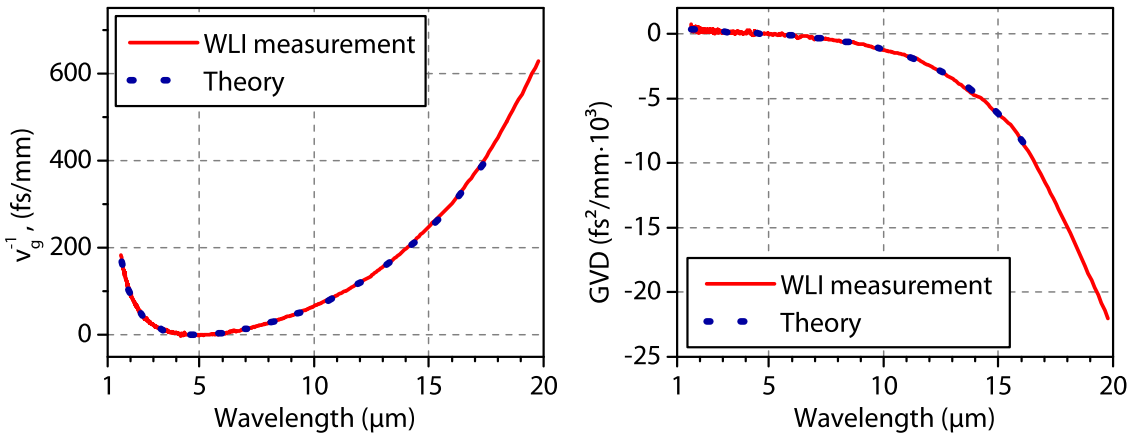


**Figure 6.5:** Shows the inverse group velocity $v_g^{-1}$ (left) end the GVD of ZnSe (right). The measurement is conducted using the WLI. The theoretical values are calculated from wavelength dependent refractive indices.

were calculated using their definitions:

$$v_g = \left(\frac{\partial k}{\partial \omega}\right)^{-1} = \frac{\partial}{\partial \omega}\left(\frac{\omega}{c} n(\omega)\right)^{-1} \tag{6.1}$$

$$\mathrm{GVD} = \frac{\partial}{\partial \omega} v_g^{-1} = \frac{\partial^2 k}{\partial \omega^2} \tag{6.2}$$

Here $k$ is the wavenumber and $\omega$ is the angular frequency. The calculated values and the measurements are plotted in Fig. 6.5. The measured data was taken from 1.9 to 20 μm in one single measurement scan and is in excellent agreement with the literature values.

## Summary of GDD measurement devices for MIR coatings

Two devices are demonstrated that allow the measurement of the GD and GDD of optics for ultrashort laser pulses covering the NIR and the MIR up to a wavelength of 20 μm for the first time, to my knowledge. The RSI allows fast measurements, due to a simple alignment procedure and the need of only a few spectra at different air-spacer thicknesses. The WLI produces more robust and reliable data, however the alignment of the Michelson interferometer is more challenging, and a measurement scan takes more time. GDD measurements of two interference coatings and the GVD of a ZnSe substrate show excellent agreement with theoretical values. The devices pave the way for the development of novel optical components needed for ultrashort laser sources for the mid-infrared spectral range.

## 6.2 Coating Process for MIR interference coatings

In this section the deposition process for interference coating for the MIR spectral range from 2 µm to about 11.5 µm is described. The choice of coating materials is crucial for the the mid-infrared range. Germanium (Ge) is used as coating material with a high refractive index ($n = 4.1$) and zinc sulfide (ZnS) as low-index material ($n = 2.3$), since this combination has a very high contrast in refractive index, which is desirable for broadband mirrors. For instance the bandwidth of a quarter-wave with these materials has a relative bandwidth of nearly 40 % of its central wavelength (For explanation, see Fig. 2.2 on page 10). The combination of germanium and zinc sulfide are also widely used for mid-infrared interference coatings [76–79].

An automated electron beam process was developed for both coating materials using electron beam evaporation (see section 3.1).

### 6.2.1 Process for zinc sulfide

Zinc sulfide has an reflective index of about 2.2 at 2 µm and is used as a low index material with germanium. It can also be used as a high index material in combination with fluoride materials, which have a refractive index of around 1.5. Zinc sulfide with grains of 1.5 to 5 mm and a purity of 99.99 % was employed. The process temperature is set to a rather low value of 80 °C, because the zinc sulfide layers thicknesses become more sensitive with increasing process temperatures. The reason for this is, that zinc sulfide totally dissociates during evaporation, and the condensation coefficient of zinc rapidly decreases with increasing substrate temperatures [80]. Therefore the also the deposition rate decreases significantly at higher temperatures and more material accumulates on the chamber-walls. The effect was observed by coating zinc sulfide single layers onto a germanium and a fused silica substrate in one coating run. Since the fused silica substrate absorbs more infrared radiation of the heaters, its temperature is higher than of the germanium substrate and thus the layer was about 3 % thinner on the germanium substrate, which mostly transmits the heat radiation and stays cooler. The substrate temperatures were measured with a thermal camera right after the coating run, after opening the vacuum chamber. The germanium substrate had a temperature of 75 °C and was 15 °C colder than the fused silica substrate having about 90 °C.

The search for a good process to evaporate zinc sulfide, required many attempts. Only a few process details for zinc sulfide were found in the literature [31, 77, 78, 80–83]. For the initial tests, zinc sulfide was taken from our storage, and it was tried to evaporate it with e-beam. Zinc sulfide grains were filled in a small crucible with a diameter of 32 mm. But as soon as the material was hit by the electron beam, the single grains were jumping away. The electron beam was moved manually around the crucible, but all grains jumped until the crucible was empty. In conclusion, it was not possible to coat this material with e-beam.

Therefore another method had to be found. Thermal evaporation using a so-called boat is also a common evaporation method for zinc sulfide. For this, coating material is filled in

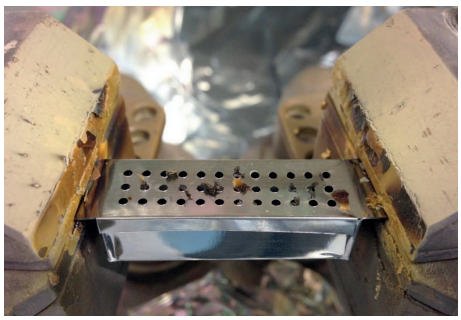

**Figure 6.6:** This is a molybdenum boat with cover and a volume of 4 $cm^3$ to evaporate zinc sulfide. The cover prevents the grains to jump out of the boat. For thicker multilayer coatings, a significant larger boat, as the one shown, with a volume of 40 $cm^3$ was used.

a boat, which is metal container with a certain electrical resistance. A high electric current flows through the boat and heats it up until the coating material evaporates. For zinc sulfide a special boat with a cover was used to avoid that the grains jump out of it. The coating chamber had to be retooled to install the required electric contacts for the boat. Since the chamber is rather small, no empty feedthroughs were available. Thus the installed plasma source had to be removed in order to install the thermal evaporator. A coating process with this plasma source is shortly described in appendix A. In Fig. 6.6, the photograph of a boat with cover is seen. The holes in the cover are small enough to prevent the grains to jump out of the boat, while the coating material can escape.

First tests of depositing single layers with thermal evaporation were successful. But the volume of the boats of 4 $cm^3$ hold only zinc sulfide grains to coat a layer of only 430 nm, and the mirror planned to coat had zinc sulfide layers with a total thickness of 4 µm. Thus a larger boat was ordered with a volume of 40 $cm^3$. With this configuration, our first multilayer mirror for Mid-IR was coated.

When new zinc sulfide granulate was ordered, one could see a significant difference in optical appearance to the old material, even it was from the same supplier. It seems likely, that the old material suffered from some kind of aging effect, for example it absorbed water, which could explain the heavy jumping of the grains during e-beam evaporation. Therefore a new attempt was conducted to evaporate zinc sulfide with e-beam, since it has advantages over thermal evaporation. At first with the right crucible much more material can be deposited with e-beam. Secondly there is the opportunity to also use the plasma source for future experiments. The new try with e-beam and the new coating material was now successful. Still, jumping of the grains was observed, but less strong. At the end, a so called ring-rill crucible is used, which is shown in Fig. 6.7. It has a volume of 250 $cm^3$ and thus over six times more than the largest used boat. The ring-rill crucible slowly rotates with only 0.1 rounds per minute, while the e-beam sweeps only one small radial stripe of zinc sulfide. A current of the e-beam 20 mA yields a deposition rate of about 1.0 nm/s.

**Figure 6.7:** Ring-rill crucible for e-beam evaporation filled with zinc sulfide (left). After depositing a dispersive mirror with a total thickness of zinc sulfide of 20 µm (right). Here the protection cover is still installed, which prevents the zinc sulfide from being contaminated by germanium during its deposition. Some small grains can be seen on the covers, which jumped out of the crucible, but they are only a few if the many hours of evaporation are considered. Also interesting to note is, that the material lost its yellowish color, which is most likely caused by additional loss of Sulfur (S) during the evaporation.

It was found, that zinc sulfide single layers have adhesion problems on most of the employed types of substrate materials. Thicker layers of about more than about 500 nm didn't pass a simple tape test, were the adhesion of the coating is tested by trying to pull it off with an adhesive tape. The solution for this problem was found to coat a thin germanium layer on the substrate before the zinc sulfide. All of the later multilayer coating are made with germanium as the first layer and show excellent adhesion. But for the determination of the refractive index, in the next section, no germanium layer was used.

Since the coating plant is equipped with an in-situ broad band optical monitor, it was possible to measure the vacuum shift of the zinc sulfide layers. For this a spectrum of the sample is measured in vacuum after the coating process, and another one is taken of the same sample after venting the chamber. After one hour in atmosphere, the spectrum shifted only about 1 %. This indicates a dense and optical stable layer structure.

### 6.2.2 Process for germanium

Germanium is used as high-index material with its high refractive index of 4.1 at a wavelength of 5 µm. As for zinc sulfide, only a few process-details are published [31, 77, 78, 84]. In this work, germanium is only used in combination of zinc sulfide, and therefore the temperature is also set to 80 °C. The raw germanium are grains with the size of 1 to 3 mm and a purity of 99.999 %. Also a large amount of germanium is needed to realize MIR-dispersive mirrors. Therefore a copper crucible with five pockets is used. Each pocket can hold germanium with a

| | $A_0$ | $A_1$ | $A_2$ | $A_3$ | $A_4$ |
|---|---|---|---|---|---|
| Germanium | 18.50 | −2.014 | −11.31 | | |
| Zinc sulfide | 5.312 | −0.359 | −3.884 | 0.508 | 461.9 |

**Table 6.1:** Sellmeier-coefficients for the wavelength in µm for the coating materials derived from single layer transmission measurements.

volume of about 38 $cm^3$. Germanium is filled directly in the copper pocket. It was found, that germanium seems not to react with copper, since the molten germanium block can easily be removed from the pocket; it doesn't stick to the copper. The pocket is filled up with material within several time-consuming steps. Germanium granulate is filled until about one third of the pocket. Then it is molten under vacuum until no grains are left and a solid block of germanium is created. This is repeated until the pocket is full with germanium. If one fills the whole pocket with granulate at once, molten germanium is built at first only at the surface and seals the grains underneath. The residual contaminations like water on the grains evaporate and blow up the molten germanium.

For a coating process, the germanium block made like described above, builds a nice melt at a current of 260 mA and this yields in a deposition rate of about 0.5 nm/s.

### 6.2.3 Determination of the refractive index of the layer materials

With the process parameters mentioned above, single layers of zinc sulfide and germanium are deposited on potassium bromide (KBr) substrates, which have a low reflective index of 1.5 at a wavelength of 10 µm, and they are highly transparent from 0.4 to 20 µm. The transmittance of the coated substrates are measured using the FTIR spectrometer (description in section 3.4). The single layer spectra were evaluated using the software OptiChar (Optilayer GmbH). The Sellmeier model (see equation 2.9) for the dispersion of the refractive index was used to fit the measured spectra. The measurements and the model-data are given in Fig. 6.8 and the according Sellmeier-coefficients are listed in table 6.1. Germanium requires three coefficients of the equation to sufficiently describe the dispersion. Zinc sulfide requires five coefficients, to map the turning point in the middle of the spectrum. The existence of this turning point can also be seen in [85, 86]. According to our data, the refractive index of germanium is 4.12 at 5 µm wavelength, and for zinc sulfide 2.23.

## 6.3 Dispersive mirror coatings

In the following, the results for two dispersive multilayer coatings are shown. The first mirror is a quarter-wave stack (QWS) consisting of nine layers, and is designed as cavity mirror with low dispersion. The second mirror is a dispersive mirror with a total physical thickness of 30 µm which is designed to compensate the dispersion introduced by 1 mm of zinc selenide.

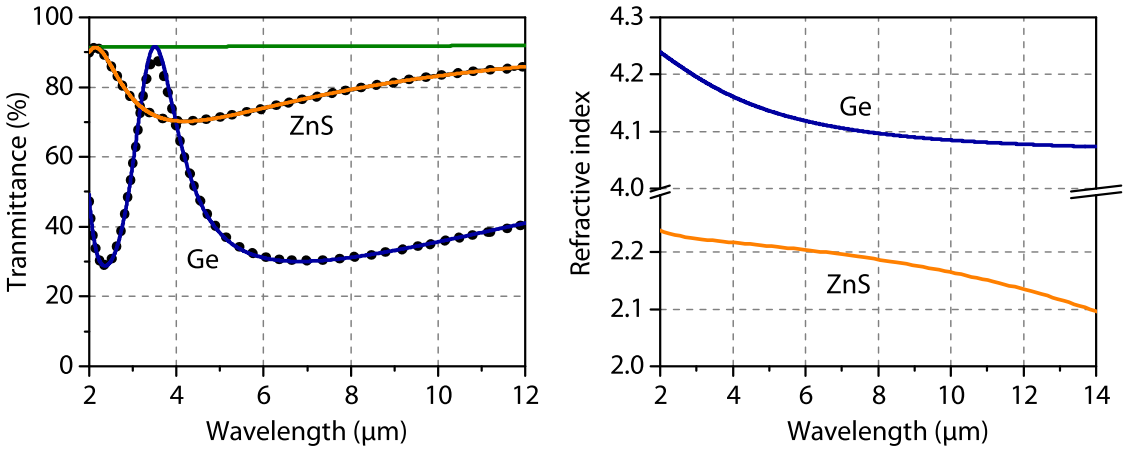


**Figure 6.8:** Spectra of germanium and zinc sulfide single layers (left). The data (dots) is fitted with the Sellmeier model (line). In green, the transmission of the uncoated substrate is plotted. The resulting wavelength dependent refractive index is sown on the right diagram.

### 6.3.1 Low dispersive broadband cavity mirror

The substrate material for the QWS was optical grade germanium with a diameter of 1 inch, a thickness of 0.25 inch and a radius of curvature (ROC) of −2 m. Also a substrate with plane surface was coated, on which the following measurements are conducted. The first layer for all mirrors was chosen to be germanium, because it was found that zinc sulfide has adhesion problems on most types of substrates. Therefore all multilayer stacks described below start with germanium as the first layer, because it improves the adhesion. The QWS is also the very first mirror produced with the process described above. The zinc sulfide was evaporated using thermal evaporation. And it's important to note, that the FTIR spectrometer (see section 3.4) was not yet available to characterize the coating materials before the coating. Thus the measurements seen in Fig. 6.9 were conducted later. The GDD measurement was already shown in the previous section 6.1.3 to demonstrate the capability of the GDD measuring devices, and it is published in [68], since it is the first measurement of its kind in the MIR spectral range to my knowledge. The design consists of nine layers with the following QWS design: [Ge ZnS]4 Ge. The central wavelength was targeted to be 9 µm and the transmittance is designed to be 0.8 % to allow light to be coupled out of the cavity. Thus the reflectance should be 99.2 %. Since the contrast in the refractive indices of the coating material is very high, nine layer are enough to reach this reflectance and the high bandwidth to support laser pulses with the duration of about 100 fs FWHM. The total physical thickness of the coating stack is 8.3 µm. The transmittance and reflectance measurements are conducted with an FTIR spectrophotometer (see section 3.4)

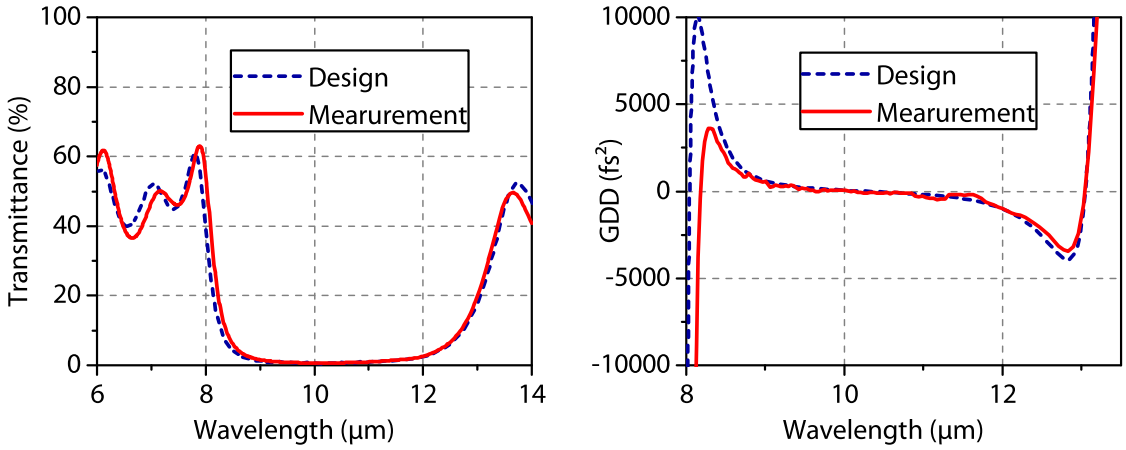


**Figure 6.9:** Transmittance of the QWS centered at 10 µm and coated on a germanium substrate (left).. The thickness of layer number 7 was reduced because of a problem during the coating process. This explains the non-typical characteristics of spectrum for a QWS from 6 to 8 µm. The lowered transmittance peak near 14 µm is caused by absorption of the Ge substrate. GDD measurement (right)

### 6.3.2 Highly dispersive broadband mirror

The next coating is a broadband dispersive mirror with an average GDD of +1,500 $fs^2$ for the bandwidth of 9 to 11.5 µm. It is designed to compensate the dispersion of 1 mm zinc selenide. For this first approach, the third order dispersion (TOD) of zinc selenide was neglected, resulting in a constant GDD target value of +1,500 $fs^2$. The dispersion measurement of a zinc selenide substrate can be seen in above in Fig. 6.5. The coating design of the dispersive mirror is given in 6.10.

Again, the first layer is germanium to improve the adhesion. The design has 36 layers and has a total physical thickness of 30.7 µm. This enormous thickness exceeds the thickness of

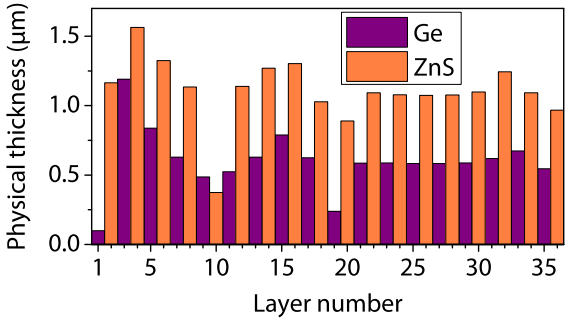


**Figure 6.10:** Layer thicknesses of the dispersive mirror. The first layer is germanium to improve the adhesion of the following zinc sulfide layer.

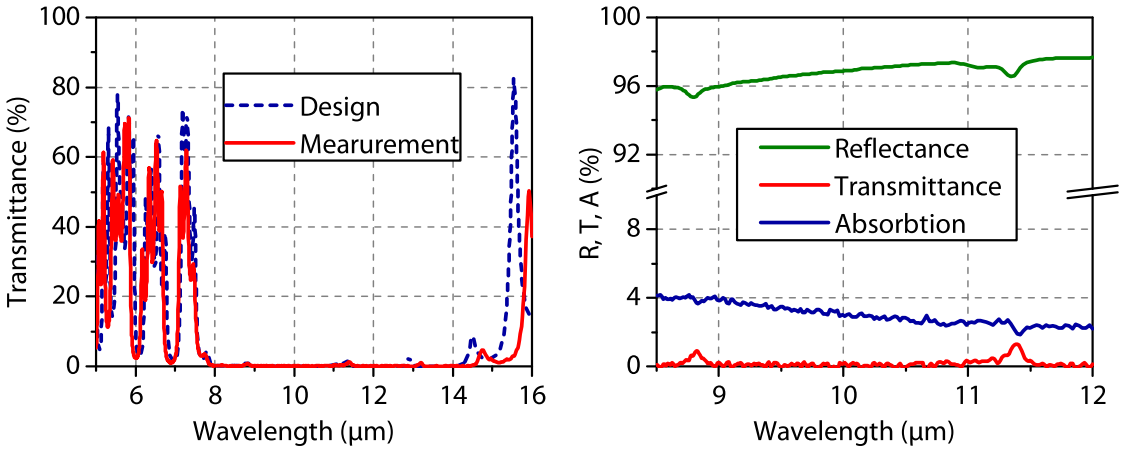


**Figure 6.11:** The transmittance is compared to the design (left). The Reflectance measurement reveals absorption (right). The absorption is calculated by $A = 100\,\% - T - R$, assuming, that there is no scattering.

conventional dispersive mirrors for near infrared pulses of more than a factor of two [3]. Both materials are evaporated with the process described above, and all of the four available quartz crystals in the crystal changer were prepared. A new crystal has a resonance frequency of about 5.9 MHz. During the process the crystal is coated and the frequency decreases. Below 5.5 MHz the response becomes non-linear and thickness errors increase. Thus the crystal is changed after depositing around 8 µm of coating material. A germanium, a zinc selenide and fused silica substrate were coated with the fully automated process. Since this was the first kind of a coating of this thickness, the crystals and the germanium pockets were change manually. All four crystals were used up and the total process time was 11.5 hours. After the coating process, the adhesion of the coating was tested with a tape as described above. The coating was not removed by the tape and therefore the test proved good adhesion.

The transmittance and Reflectance was measured on the manufactured mirrors. The measurement showed, that the mirror is spectral shifted to longer wavelengths by 4 %. This shift is a manufacturing tolerance and is caused by not yet correct tooling factors of the layer thickness measuring quartz-crystals. The shift is added to all following theoretical design curves to allow better comparison with the measurements. The broadband transmittance measurement (Fig. 6.11, left) agrees well with the design for shorter wavelength. There is a spectral shift between the design and the measurement at longer wavelength >14 µm, which is caused by deviating refractive indices at these wavelength. Also the absolute reflectance of the mirror was measured (Fig. 6.11, right). The absorption of around 3 % was not expected, since previous reflectance measurements on the quarter wave stack shown above, did not indicate absorption.

Reverse engineering was conducted on the measurements shown in Fig. 6.11 to estimate the extinction coefficient, which could explain the absorption. The result is, that either zinc sulfide or germanium has an extinction coefficient of about $k = 1 \times 10^{-2}$. This value could

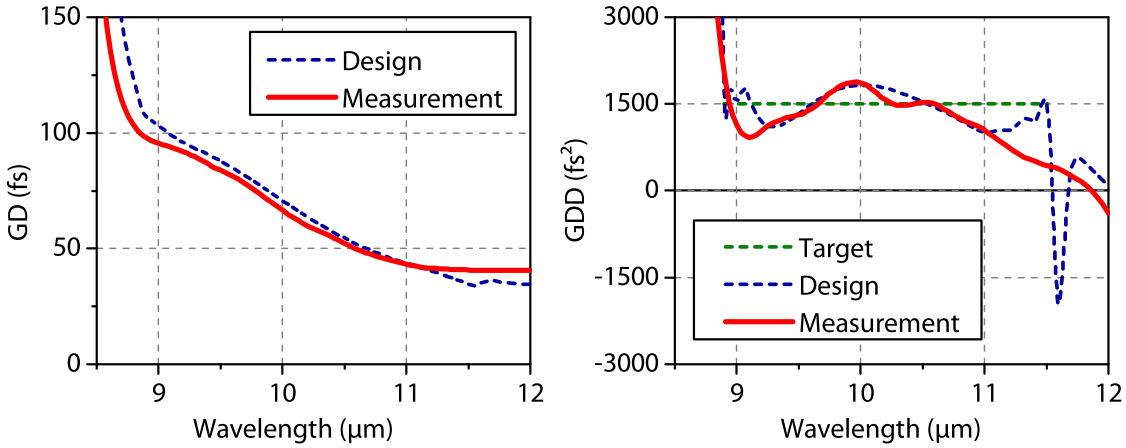


**Figure 6.12:** GD (left) and GDD measurement (right) of the MIR dispersive mirror. The measurement agrees well with the design.

also be caused by both materials in sum. The origin of the absorption is not clear, since the bulk materials of germanium (see Fig. 3.3 on page 17) and zinc sulfide [67] don't indicate this high amount. Most reviewed publications for germanium and zinc sulfide don't mention absorption. Perez et al. [87] mentions a low absorption of $k < 1 \times 10^{-3}$ for germanium, which would explain only absorption of <0.3 %. Only Lemarquis et al. [76] published an extinction coefficient of $k = 1 \times 10^{-2}$ for germanium and $k = 1 \times 10^{-3}$ for zinc sulfide [88]. Thus the observed absorption is likely induced by germanium. It has to be investigated, if the absorption can be reduced for instance by increasing the process temperature.

## Summary of MIR dispersive mirrors

For the first time, dispersive mirrors for the mid-infrared spectral range were demonstrated. For their manufacturing, an e-beam coating process was developed using the two coating materials germanium and zinc sulfide. A new white-light interferometer for dispersion measurements was developed, to get insight of the GDD introduced by the coatings, which characterization is indispensable for ultrafast applications. The first ever reported dispersive mirror for the wavelength range of 9 to 11.5 µm with an average GDD of +1,500 $fs^2$ is presented. With the new coating process and the characterization techniques for the multilayer coatings, the potential of realizing any kinds of mid-infrared dispersive mirrors is given. These new possibilities pave the way for advancing the development of femtosecond mid-infrared lasers, by manufacturing customized dispersive mirrors for controlled beam manipulations and a precise dispersion management.

# Chapter 7

# Ion beam sputtered coatings for energetic few-cycle pulses

The key component which often prevents the further power-scaling of state of the art ultrafast laser systems, is often a dielectric coating. Every interference coating absorbs light even if only in the lower ppm (parts per million) range. The absorbed energy transfers into heat, this deforms the optic and subsequently distorts the laser beam, which prevents the laser from a stable operation. To reduce the heating of the optics, the further reduction of intrinsic absorption losses of coatings is mandatory. In the high energy femtosecond regime, a second absorption effect comes into place. The two photon absorption (2PA) becomes dominant at high energies. Here the absorption is depends on the bandgap of the coating material [26–28]. 2PA is the major damage mechanism for this regime. The 2PA can be reduced within a limited range by using material with a higher band gap, which corresponds to a lower refractive index. The only approach to significantly reduce the absorption in optical coatings is to reduce the energy density of the incident radiation by increasing the beam diameter. This demands the development of large scale low loss multilayer optics, which require a the right coating process.

Recently, large scale low loss mirrors became much attention by scientist around the world in connection with the first ever detected gravitational wave on September 14, 2015 [89]. The two used detectors for this are Michelson-kind interferometers with orthogonal arms having a length of 4 km each [90]. The large end-mirrors act as test masses having a weight of 40 kg. The diameter of the fused silica substrates is 350 mm and were coated by the Laboratoire des Matériaux Avancés (LMA) in France, using a home-built ion beam sputtering machine. The high-reflective coating has a residual transmittance of 3 ppm, scattering losses lower than 10 ppm and remarkable ultra-low absorption of an average value of 0.24 ppm within a diameter of 150 mm [91]. For this applications, the ultra-low absorption is of highest priority, since the induced thermal noise, which generates fluctuations of the mirror surface [92], prevents the detection of gravitational waves, which change the arm-length of the interferometer just in the order of $10^{-18}$ m, which a fraction of the diameter of a proton.

In the following the a ion beam sputtering (IBS) process is demonstrated, which considerably advances both approaches mentioned above, the reduction of the intrinsic absorption and the increase of coating area. At the end a ultra-low loss coating and a state of the dispersive coating

is shown, which can be deposited onto substrates with large dimensions.

## 7.1 IBS coating plant and its infrastructure

Ion beam sputtering (IBS) more or less combines the advantages of the two methods described above. It uses plasma sputtering for dense and precise layers combined with the advantageous geometry of thermal evaporation, where the substrates are coated upside-down and are separated from the coating source, which leads to less contamination of the coatings. This is the main reason for the development of the IBS process, the manufacturing of low loss coatings [40]. A tender for a IBS coating machine was carried out, and in the end the system was acquired from Cutting Edge Coatings GmbH.

A sketch with all important components is shown in Fig. 7.1. The vacuum is generated by a cryopump [93] and can reach levels of the lower $10 \times 10^{-8}$ mbar region. Cryopumps are known to be the only pumps not contaminating the process chamber, since they have no moving parts inside the chamber and they have no open connection to the environment. The coating chamber is also equipped with a load-lock system, which allows to load and unload substrates without breaking the vacuum. The core-component of the machine is the Kaufman-type ion source [94]. Within the source a plasma of Argon or Xenon is generated using radio-frequency radiation. The ions are extracted from the source with a three-grid ion optic. The first grid facing the plasma has a positive potential screens the negative potential of the accelerator-grid. The third grid is on ground potential and decelerates the ions, but allows tighter focusing of the ion-beam towards the target. The beam-diameter is about 8 cm at the target. The two coating-materials are mounted side by side as indicated an insert box of Fig. 7.1. The so called zone-target moves laterally in order to switch from one material to the other. Due to this movement, the two materials can be continuously mixed, any refractive index between the two material can be obtained. Thus, so-called rugate-filters [95] can be manufactured, which have a continuous variation of the refractive indices, in contrast to discrete layers of conventional coatings. For example, the laser induced damage threshold may be increased [96, 97] by rugate-designs.

The laboratory for the IBS machine is designed from scratch (Fig. 7.2). Empty laboratories were teared down to enable the building of the new rooms containing a Class ISO 5 clean room. The layout is planned to precisely fit the IBS coating plant and also the ultrasonic cleaning equipment. As well the footprint is optimized to enable the most convenient handling of precision optics throughout the laboratory, which will help to get state of the art laser optics with the lowest possible particle contamination. In Fig. 7.2, the usual path of a laser optic is tagged by numbers. (1) The supplied substrates are inspected and loaded into fixtures on a table with a filter-fan-unit (FFU) on top. (2) The substrates are loaded into the first ultrasonic basin. (3) In the last step of cleaning, the substrates are inspected and either loaded directly into the coating fixtures, or in a box for later use. (4) The covered substrates are put into the material gate for the clean room. (5) The substrates are loaded into fixtures for coating, or

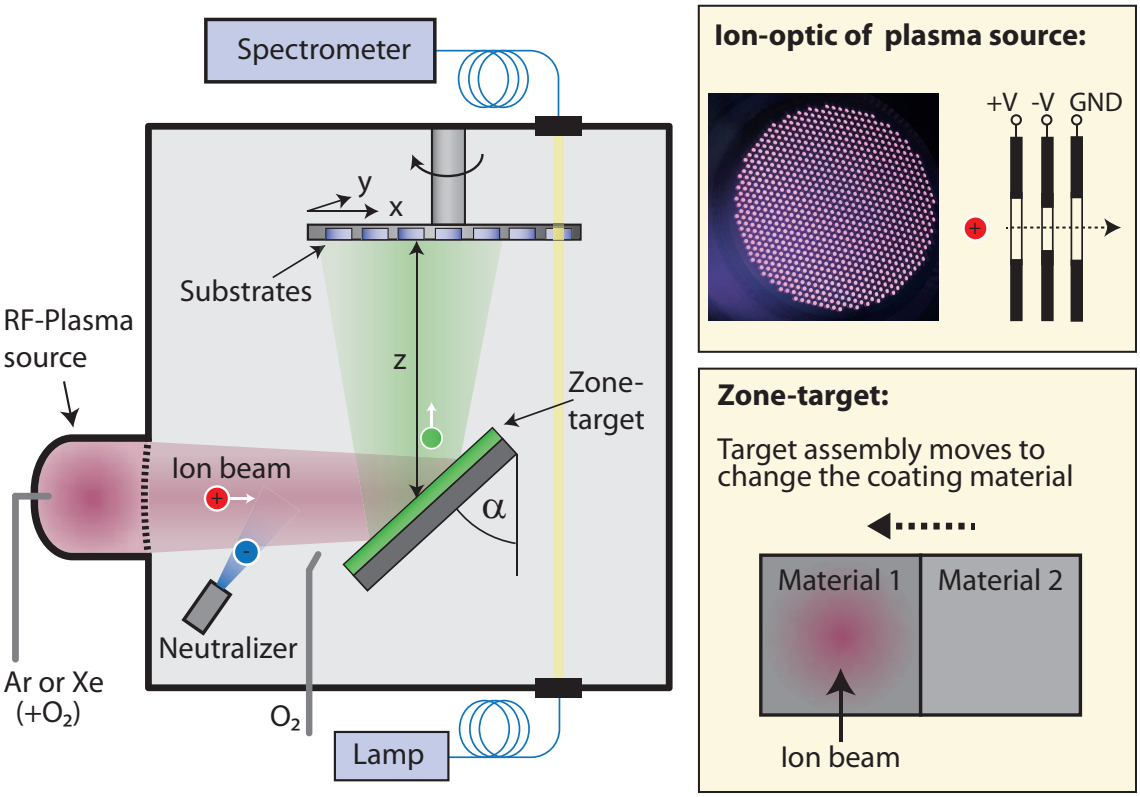


**Figure 7.1:** IBS coating chamber with all important components: The plasma source is on the left. The plasma is extracted with an ion-optic assembled of three grids (see insert). The photo shows the grid with plasma behind. The accelerated and slightly focused beam of ions hit the coating material (target) and sputters it towards the substrates. A insert shows the method used to change the coating material. A so called zone-target is used. The two coating materials are mounted side-by-side. The material is changed by horizontally move the zone-target. Thus also material mixtures can be realized, by stopping the zone-target at a intermediate position, were the ion-beam sputters both materials.

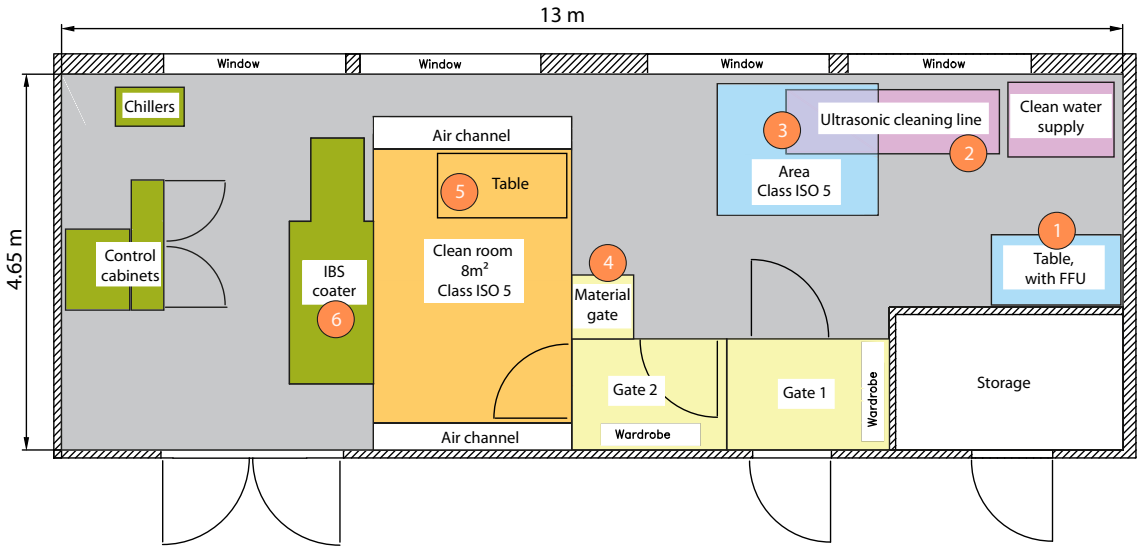


**Figure 7.2:** Overview of the newly built coating laboratory for IBS coatings. It was designed from scratch especially for the development of state of the art laser optics. The core of the lab is the 8 $m^2$ clean room with the IBS coating machine directly connected to. The machine is loaded and operated within the clean room, while all machinery is suited in the gray room. The path of a substrate from cleaning to coating. The way of an optic from inspection to coating is indicated by the numbers.

directly loaded into the coating chamber (5).

## 7.2 Process development

In order to meet our demands, the IBS machine had to be optimized to develop its full potential. Below, the thickness control and the coating homogeneity is described.

### 7.2.1 Layer thickness control

The machine is designed to only use a BBOM for layer thickness monitoring (see section 3.2). To realize dispersive mirrors with a high number of layers, calibrated time monitoring (see also section 3.2) had to implemented, but some properties of the machine prevented this. Modifications of the control-software had to be done in collaboration with the supplier of the machine in order to meet the requirements for calibrate time control. At first the current of the Ion beam was changing with time, resulting in changing deposition rates. The RF-power was set to a fixed value and the current measured in the first grid was slowly drifting. Therefor a control loop is embedded that keeps the current stable within 1 mA, while regulating the RF-power.
Another problem is, that the ion source shows a discharging effect. Here a temporary shortcut

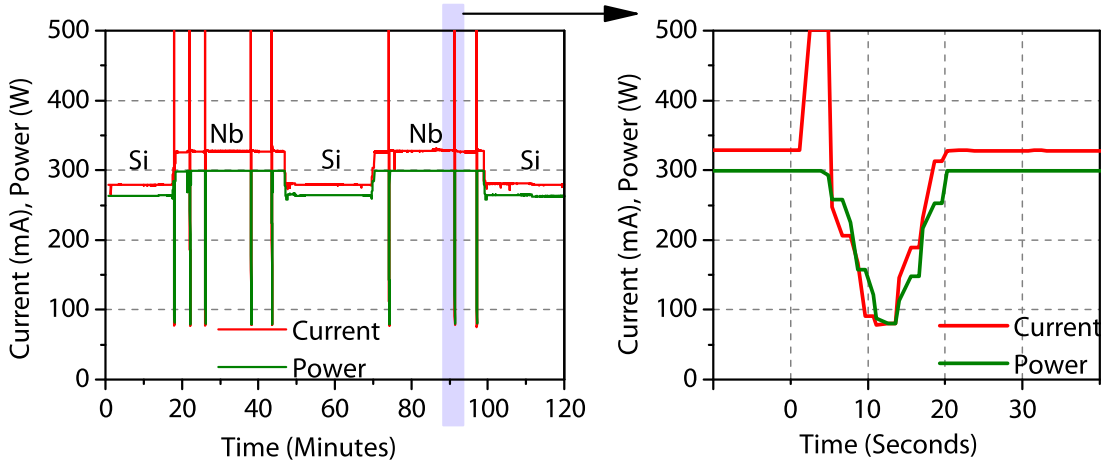


**Figure 7.3:** This is a typical section of a coating sequence (left). The two materials are sputtered with different values for RF-power and current. The needle-shaped distortions are shortcuts in the grid-system, causing a outage of the ion-beam of several seconds. During this state, the deposition rate is zero or significantly reduced. The right graph is a zoom-in to such an event.

in grid-system takes place. A localized spark can be observed by eye when looking through the window of the chamber. Probably the shortcut happens between the first two grids facing to the plasma. The difference of potential is here usually about 2 kV. With a new grid system and clean chamber, this event occurs about 2 times per hour, but it rapidly increases within days to higher values. A shortcut is most likely induced by particles which get between the grid. The shortcut immediately leads to an outage of the sputtering ion beam, and therefore to an interruption of the deposition. The current of one grid reaches its limit of 500 mA. The effect is illustrated in Fig. 7.3.

The left graph shows a typical section of a coating process, represented by the RF-power of the ion source and the current of one grid. The spikes are shortcuts in the grid-system, causing a outage of the ion-beam of several seconds. On the right graph a cut out of such an event is shown. The time from the shortcut and until the beam is up again takes about 20 seconds. During this time the deposition rate is zero and ramps up gain with an unknown characteristic. This issue makes a precise thickness-control by time monitoring impossible. The down-time is estimated to be 14 seconds and the control-software of the machine was changed to take this value into account. With this new parameter a complex dispersive mirror presented below was successfully deposited by calibrated time monitoring.

A close-up picture of a grid system is shown in Fig. 7.4. It was in use already for many coating runs. In the middle grid, which has a smaller diameter, the inner surface became contaminated. It is some accumulation of most likely coating material which is sputtered back from the target into the grid. It sits only loose and the bigger crumbles can be removed for instance by turning an Allen key within the hole. The very left hole in Fig. 7.4 is cleaned as

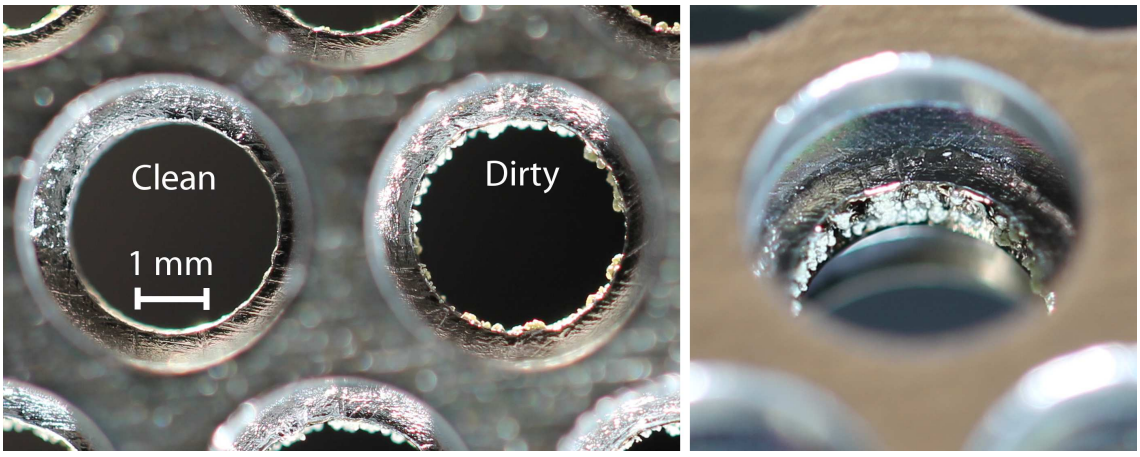


**Figure 7.4:** Close-up Photographs of a 3-grid-system dismounted from the ion source. For better understanding of the grids, a sectional drawing of the system is shown in an inset-box of Fig. 7.1. Left: Shows a photo taken from the plasma side of the grid-system. A cleaned (left) and a contaminated (right) inlet is seen. Material accumulates only at the grid in the middle. This contamination is barely seen by eye. Right: This photo is taken under an angle from the side facing to the target. The material accumulations are clearly visible. The whole grid consists of more than 800 of these inlets.

described. The right hole still has the contamination. Since this material is very loose, it very likely induces such shortcuts. The grid shown in the picture generated more than 20 discharges per hour, meaning more than 4 minutes without deposition. And the thickness errors caused by these frequent events can hardly be compensated, even when the estimated down-time is taken into account in the control-software, as described before. After replacing the grid to a new one, the discharges were reduced to 2 per hour, which is tolerable level. But of course it would be the best to totally avoid the discharges.

### 7.2.2 Refractive indices of the coating materials

The refractive indices for the IBS process were not determined by the analysis of single layer spectra, because the results of using them for the deposition of dispersive mirrors are not precise enough. The values are derived from multiple in situ spectra, measured with the broad band monitor. Here, a multilayer coating is deposited using the BBOM for layer thickness monitoring. The BBOM takes a spectra after every deposited layer. The spectra of about the first 10 layers are loaded into the thin-film design software. If the dispersion data of the layer materials are not yet known good enough, there is a deviation between the measurement and the calculated values. A algorithm now minimizes the differences between the design and the measurements by changing the dispersion values for the coating materials. This process is repeated iterative for the next layers and even the next coating runs until no further optimization

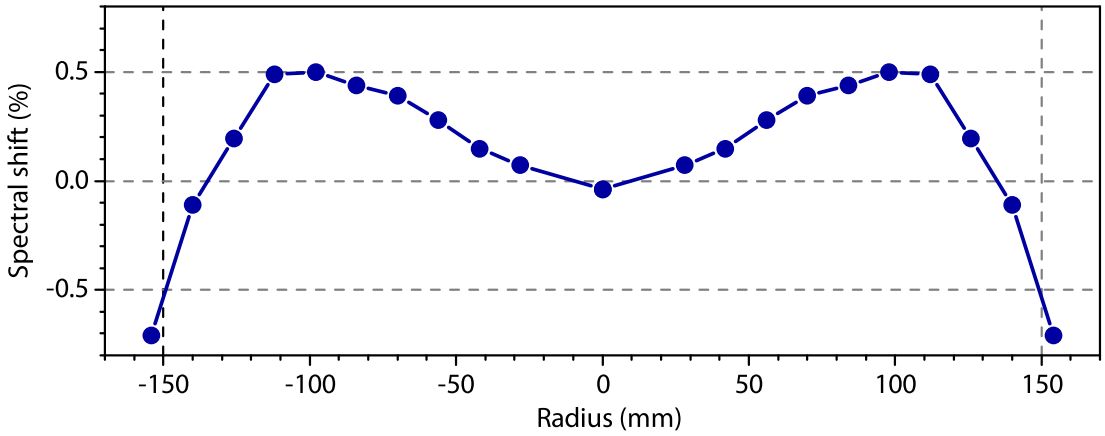


**Figure 7.5:** Variation of the spectral shift in dependence of the radius of the coated area. The homogeneity within the diameter of 300 mm is better than 1 %. Remark: Only the radial positions from 0 to 154 mm were evaluated. Because of the radial symmetry caused by the permanent rotation of the fixture, the data points were mirrored into the negative range, to illustrate the homogeneity of the whole coating area.

of the dispersion data is necessary. With this method the Sellmeier-coefficients were derived which enabled the precise deposition of the broadband dispersive mirror shown below.

### 7.2.3 Homogeneity

Besides the need of growing layers with precise thicknesses, it is also important to sustain this precision in the horizontal plane, to enable the homogenous coating of large substrates with delicate multilayer coatings. In the Navigator IBS machine, the substrate fixture has a radial symmetry and it rotates in the chamber. Due to the rotation, the substrates, which are on the same radius on the fixture, have the same thickness of deposited layers. By moving the axis of the rotating substrate-fixture in 3-dimensions within the sputter-beam, the homogenous area can be enhanced. For this machine a position was found which enables the coating of an area with an diameter of 300 mm, where the thickness variation is within 1 %. Fig. 7.5 shows the evaluation of a coating run made with tantalum and silicon.

## 7.3 IBS dispersive coatings

As a demonstration of the optimized process, a complex dispersive mirror design was successfully reproduced, which is commonly employed in our laboratories. The octave spanning double-angle mirror is used for pulse compression mainly after pulse broadening using a neon filled hollow core fiber. It is routinely produced with our magnetron sputtering machine using the same material combination of silicon an niobium. The double angle mirror is already

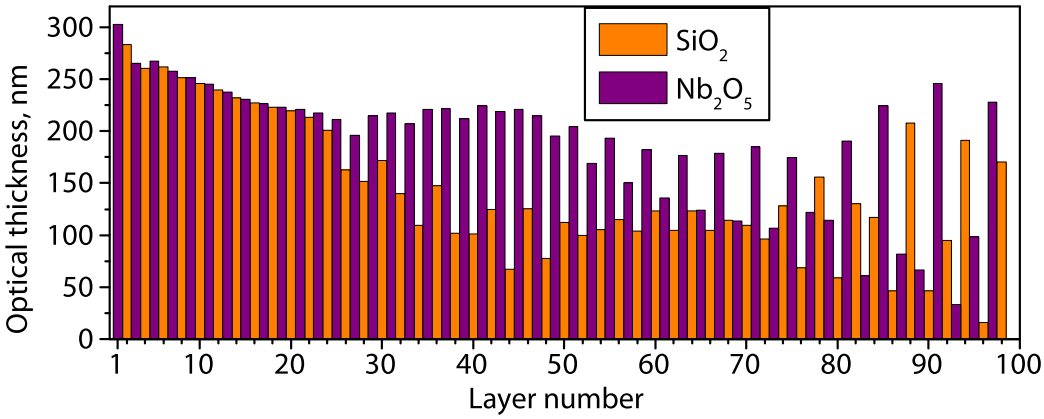


**Figure 7.6:** Coating design of the double angle broadband dispersive mirror, consisting of 98 layers. Layer number one is the closest to the substrate.

| Parameter | Unit | Niobium | Silicon |
|---|---|---|---|
| Substrate z-position | [mm] | -65 | -43 |
| Target angle | [°] | 50 | 55 |
| Deposition rate | [nm/s] | 0.094 | 0.155 |
| Oxygen (chamber) | [sccm] | 85 | 90 |
| Argon (source) | [sccm] | 40 | 40 |
| RF-power | [W] | 285 | 240 |
| Grid, positive voltage | [V] | 1650 | 1400 |
| Grid, negative voltage | [V] | -600 | -600 |
| Neutralizer, current | [mA] | 500 | 500 |
| Neutralizer, Argon | [sccm] | 6 | 6 |

**Table 7.1:** Parameters for the niobium process with argon as sputter gas.

introduced in section 5.2, were it is also used as a reference-design for the wedge dispersive mirror. Exactly the same coating design as shown in Fig. 5.2 on page 35 was taken and refined to adopt to the refractive indices of the IBS process. The process parameters used for this coating are given in table 7.1.

## 7.4 Ultra low loss coatings

The total optical losses (TOL) of a highly reflecting dielectric coating includes all linear losses which forbid a mirror to reflect 100 % of the incident light with wavelength $\lambda_0$. The TOL is the sum of the residual transmittance of the coating, the absorption and the scattering of radiation.

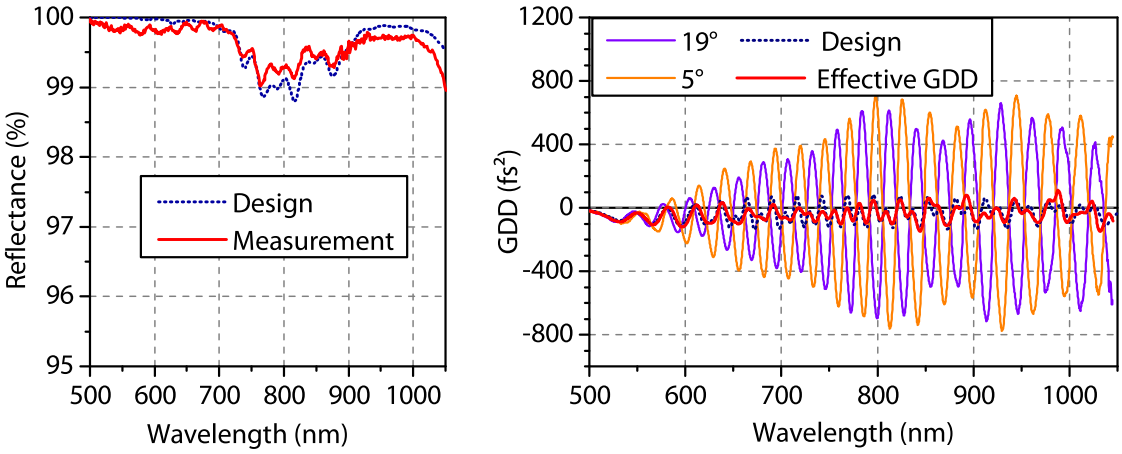


**Figure 7.7:** Measurement of Reflectance and GDD of a double angle broadband dispersive mirror. The Reflectance (left) is more than 99 % in average and agrees with the design within manufacturing and reflectance-measurement accuracy. Thus there is no indication for absorption. The GDD-measurement is also in good agreement with the design (right). The effective GDD for one mirror is $-40\,\mathrm{fs}^2$ on average.

$$\text{Total optical losses} = T + A + S \tag{7.1}$$

$T$ : Transmittance

$A$ : Absorption

$S$ : Scattering

Non-linear loss-channels like two photon absorption are neglected here. For this work the TOL is measured using the cavity ring down technique (see section 3.4).

To develop the process for ultra low loss mirrors, a simple coating design, a quarter wave stack was chosen. This design is very robust against layer thickness errors and can be easily monitored by BBOM (see section 3.2). The reflectance is determined by the number of layers and the refractive indices of the layer materials. Tantalum pentoxide and silicon dioxide are used for this work, since all published low loss coatings are made with these materials [98–102]. As an outlook, the coating absorption can be pushed below 1 ppm by using Titanium-doped Tantalum pentoxide, as it was used for the mirrors employed for the gravitational wave detectors [92, 103, 104]. For the ultra-low loss coating, the central wavelength of 1,030 nm was chosen. The design has 41 layers and a theoretical reflectance of R=99.99995 % which implies a theoretical transmittance loss of T=0.5 ppm. To find the best coating process, two different processes were developed, using argon in one, and xenon in the other one. The atomic mass of argon is 40 u, but it is 131 u for xenon. And since sputtering is a kinematic process, many process parameters change. For instance the refractive index of tantalum pen-

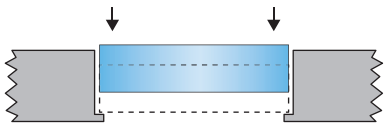

**Figure 7.8:** The inlet of the fixture must be very clean and prepared with care to avoid the contamination of the surface during the insertion of the super polished substrate.

toxide is about 0.1 smaller when using argon. Therefore 47 layers were needed for a low loss mirror made with argon to keep the transmittance losses below 0.5 ppm.

In the low loss regime, the losses generated by scattered light becomes dominant, . In this regime, the scattered light is mainly caused by the surface roughness of the substrates. For this reason so-called super polished substrates are used. The manufacturer of our substrates is the company Gooch and Housego. The substrates have an extremely low surface roughness of $<1$ Å (specified by the company), are very clean and boxed in a clean room environment, and are only unpacked in our clean room to ensure the cleanness. When the substrates are removed from their box right before the coating process, no particles or defects are visible by eye using a cold light source or a microscope. Therefore they don't need to be cleaned and are directly loaded into the fixtures for coating.

The fixtures have to be prepared with care. The inlet for the substrate must be very clean and free of particles, otherwise the substrates will be contaminated with particles at the edges and all over the surface when inserted in the fixtures (Fig.7.8).

To keep the fixture as clean as possible, the shaft and the border of the inlet are polished with fine sandpaper, after being sandblasting. Now the holder is cleaned in a ultrasonic bath filled with filtered distilled water, and then dried and baked out in an oven for 2 hours at 200 °C. Using this method, The particle contamination is reduced to a minimum. Maybe an alternative concept for fixing the substrates has to be considered, were the substrate is fixed with less risk of being contaminated.

After the coating process, the coated low loss mirrors are unloaded from the chamber and again examined with the same light source. Small and randomly distributed particles are visible. An example of a typical spot on a coated mirror are given in Fig. 7.9. These particles can't be removed by wiping with an acetone soaked tissue. They must be embedded in the coating, meaning that they whether come from the loading process or from the coating process itself.

To roughly determine the negative influence to the total losses of one of these particles, a rough estimation is given. Our cavity ring down setup (see 3.4), to measure the total losses, has a beam diameter of about 1 mm on the sample. The assumption is, that a particle on the surface illuminated by the laser beam totally absorbs or scatters the incident light within its cross-section. The actual area covered by the circularly shaped measurement beam is about 0.785 $mm^2$. The shape of the beam is approximated to be of a flat-top shape. A typical particle, also with circular shape and with the diameter of 2 µm like shown in Fig. 7.9, has an area of

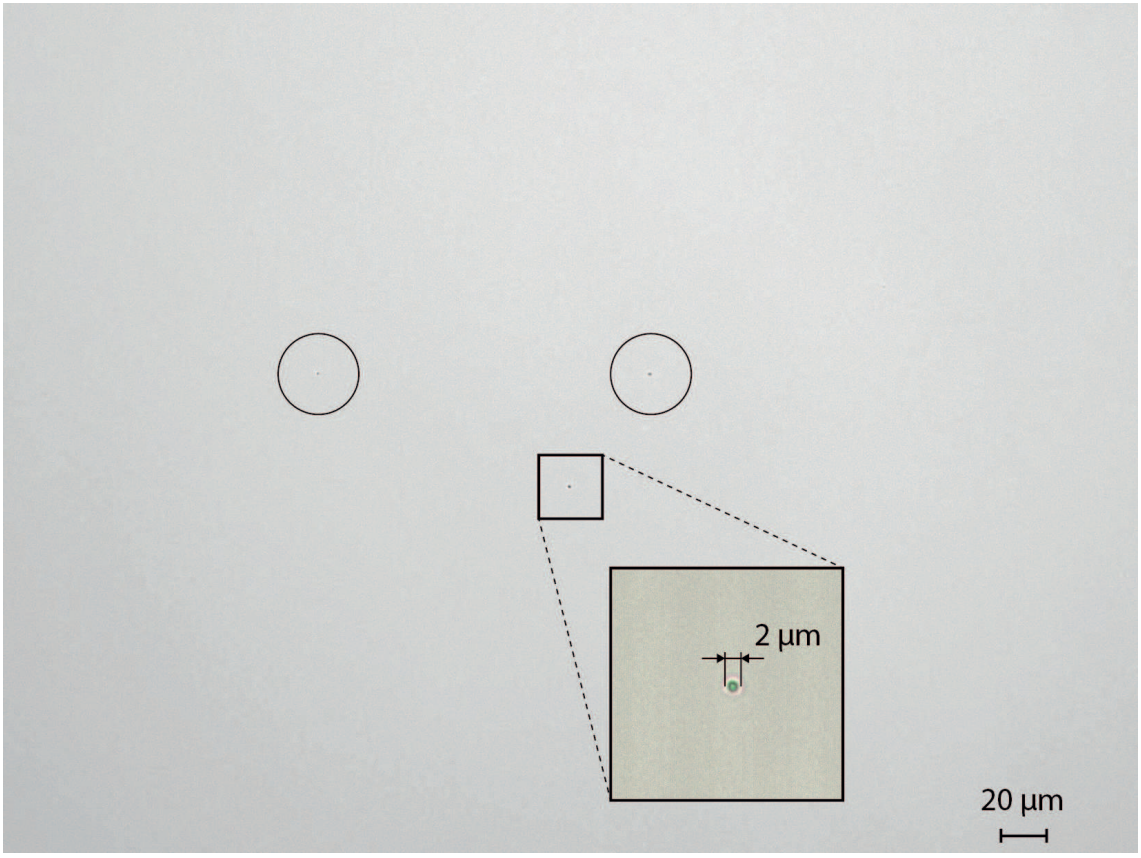


**Figure 7.9:** Microscope picture of a low loss mirror containing three particles in this area marked with a circle. The size on the surface covered is 500 µm × 400 µm, which is the largest area one can observe with our microscope. It represents a typical spot in the center of a low loss mirror. This area in contaminated by three particles, which is about the upper limit for all manufactured low loss mirrors. Therefore there are spots in the surrounding without any particles visible with this magnification. The photo of the detail of one particle was made with a higher magnification.

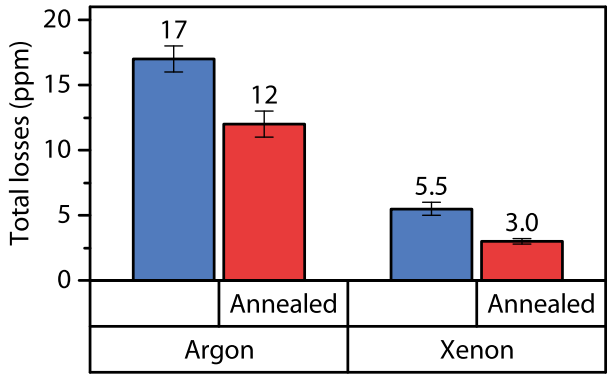


**Figure 7.10:** Comparison of two different low loss mirrors coated with argon and xenon as sputter gas. One value is given for the mirror just after coating, and another value is given after annealing the mirror for 12 hours at 350°. The best result of 3.0 ppm is obtained with xenon and post-annealing.

$3.14\,\mu m^2$ and thus leads to a loss of $\frac{3.14}{0.785 \times 10^6} = 4 \times 10^{-6} = \mathbf{4\,ppm}$. This estimation illustrates the importance of the cleanliness of low loss mirrors during the measurement.

The avoidance of particle contamination in the manufacturing chain of utmost importance. Of course this chain of cleanliness should be continued to the total loss measurement, or later until the mirror reaches its final destination in a laser setup. Since our cavity ring down setup is not operated in clean room conditions, special precautions are taken. When the reference cavity is measured. The hermetic box of the setup is closed. In the beginning, the signal is heavily fluctuating, because of dust-particles crossing the cavity. It can take up to 8 hours, until these particles settle at the bottom and a stable signal is reached. Now the reference result is taken, the lid is opened and the sample is inserted in the v-cavity configuration. The box is closed and it can take again up to 8 hours until a stable signal is obtained.

As indicated before, two different processes were pursued. One with argon and one with xenon as sputtering gas. The total optical losses of the manufactured samples are measured. Then the samples are annealed at 350° for 8 hours. Then the losses are measured again. The results are given in Fig. 7.10

The results clearly reveal that xenon is the sputter gas which produces the lowest losses. Also annealing reduces the losses significantly. The lowest value of 3.0 ppm for the total optical losses was measured at a sample, which was coated with the xenon process and annealed afterward. To proof this result, the measurement was repeated for three times, with the time consuming method described before. Therefore the error bar is the smallest of all values. The process parameters for the process are given in table 7.2.

| Parameter | Unit | Tantalum | Silicon |
|---|---|---|---|
| Substrate z-position | [mm] | -62 | -38 |
| Target angle | [°] | 55 | 55 |
| Deposition rate | [nm/s] | 0.18 | 0.17 |
| Oxygen (chamber) | [sccm] | 90 | 90 |
| Xenon (source) | [sccm] | 15 | 15 |
| RF-power | [W] | 240 | 240 |
| Grid, positive voltage | [V] | 1800 | 1400 |
| Grid, negative voltage | [V] | -600 | -600 |
| Neutralizer, current | [mA] | 450 | 450 |
| Neutralizer, Argon | [sccm] | 6 | 6 |

**Table 7.2:** Parameters for the low-loss tantalum process with xenon as sputter gas.

## Summary of IBS coatings

The fundamentals for the next generation of large and ultra-low loss dispersive mirrors are established. A new ion-beam sputtering machine was acquired and integrated in a newly constructed clean room environment, both designed for high precision and particle free optical coatings. A coating process, which enables the manufacturing of mirrors up to a diameter of 300 mm and coated with a complex state of the art octave spanning dispersive design was demonstrated. Also ultra-low loss coatings are shown, with total losses as low as 3.0 ppm. Both developments pave the way for new dispersive mirrors, which enable the realization of lasers, enhancement cavities and beam distribution systems with unprecedented optical powers.

# Chapter 8

# Summary and Outlook

Below, the major topics of this work are summarized and a short outlook is given.

In chapter 4, two low-dispersive multilayer optics were investigated, which have a nearly zero dispersion, and are thus designed to not change the temporal profile of a reflected pulse. At first a turning mirror for near-UV radiation, with a high reflectance of more than 98 %, outperforms metallic mirrors by far. With this mirror, the ultrashort pulse in a UV-pump-probe spectrometer can be steered with unprecedented efficiency. The second low-dispersive optic is a ultra-broadband polarizer, with an extraordinary bandwidth which supports sub-12 fs pulses. The stress of the coating and the resulting deformation of the substrate are compensated by a specially adapted antireflection coating on the second side of the substrate, keeping the spatial beam-profile unchanged for both, the reflected and the transmitted pulses. This ultra-broadband polarizer enables novel laser systems, wherein energetic few-femtosecond pulses are separated, combined or attenuated.

In chapter 5, the novel wedge dispersive mirror is presented. It's design, production and characterization is shown. For one application, wedge dispersive mirrors were manufactured, which compress an energetic octave spanning near-infrared laser pulse down to a duration of 3.8 fs. The mirrors exploit a newly discovered averaging effect of oscillations in the group delay dispersion by introducing a wedged layer. The new wedge dispersive mirrors combine the advantages of the two existing approaches of oscillation-free dispersive mirrors. Since the wedged layer can be realized by a standard thin-film coating process, the new mirrors are simpler to produce than mirrors basing on the conventional single mirror approach. Furthermore the wedge dispersive mirrors are much easier to implement in optical setups than double angle mirrors, since the angle of incidence has a wide working range.

In chapter 6, for the first time, dispersive mirrors for the mid-infrared spectral range were demonstrated. For their manufacturing, an e-beam coating process was developed using the two coating materials germanium and zinc sulfide. A new white-light interferometer for dispersion measurements was developed, to get insight of the GDD introduced by the coatings, which characterization is indispensable for ultrafast applications. The first ever reported dispersive mirror for the wavelength range of 9 to 11.5 μm with an average GDD of +1,500 $fs^2$ is presented. With the new coating process and the characterization techniques for the multilayer coatings, the potential of realizing any kinds of mid-infrared dispersive mirrors is given. These new possibilities enable the the development of advanced femtosecond mid-infrared lasers, by

manufacturing customized dispersive mirrors for controlled beam manipulations and a precise dispersion management.

In chapter 7, the fundamentals for the next generation of large and ultra-low loss dispersive mirrors are established. A new ion-beam sputtering machine was acquired and integrated in a newly constructed clean room environment, both designed for high precision and particle free optical coatings. A coating process, which enables the manufacturing of mirrors up to a diameter of 300 mm, and coated with a complex state of the art octave spanning dispersive design is demonstrated. Also ultra-low loss coatings are shown, with total losses as low as 3.0 ppm. Both developments pave the way for new dispersive mirrors, which enable the realization of lasers, enhancement cavities and beam distribution systems for unprecedented optical powers.

In the scope of this thesis, the properties of current dispersive mirrors were significantly advanced in many aspects. For instance the applicable wavelength range of the current mirror technology is enhanced in both endings, to shorter and longer wavelengths. Dispersive mirrors for femtosecond pulses are demonstrated with the lowest ever reported wavelength limit of 250 nm in the near-UV range, and another dispersive mirror is shown with the highest ever reported wavelength limit of 11,500 nm in the mid-infrared spectral region. To cover this extreme spectral range, several different coating materials were used, and thus also many of the most advanced physical vapor deposition processes were employed.

# List of Publications

Within the scope of my thesis, the following articles were published in peer-reviewed journals, or are recently accepted. Moreover the results of two projects were presented on conferences.

## Journal articles

- **F. Habel** and V. Pervak, "Dispersive mirror for the mid-infrared spectral range of 9 to 11.5 μm," accepted, Appl. Optics.
  Contribution: I developed the coating process and the mirror, characterized it and prepared the manuscript.

- **F. Habel**, M. Trubetskov, and V. Pervak, "Group delay dispersion measurements in the mid-infrared spectral range of 2-20 μm," Opt. Express 24, 16705–16710 (2016).
  Contribution: I developed the measurement setups and the software for the white-light interferometer, made the measurements and prepared the manuscript.

- **F. Habel**, V. Shirvanyan, M. Trubetskov, C. Burger, A. Sommer, M. F. Kling, M. Schultze, and V. Pervak, "Octave spanning wedge dispersive mirrors with low dispersion oscillations," Opt. Express 24, 9218–9223 (2016).
  Contribution: I had the idea of the wedge dispersive mirror, developed the mirror and characterized it, except of the FROG and beam-profile measurements. I prepared the manuscript.

- **F. Habel**, W. Schneider, and V. Pervak, "Broadband thin-film polarizer for 12 fs applications," Opt. Express 23, 21624–21628 (2015).
  Contribution: I produced the polarizer, characterized it and prepared the manuscript.

## Conference contributions

- **F. Habel** and V. Pervak, "Ultrafast interference coatings for the MIR spectral range," in Optical Interference Coatings 2016, Tucson, USA.
  Contribution: I developed the coating process and presented the results in a talk and a poster.

- B. Baudisch, **F. Habel**, V. Pervak, and E. Riedle, "On the Edge: Characterizing Broadband Dielectric Mirrors from UV to NIR Using a Pump-Probe Technique," in 20$^{th}$ International

Conference on Ultrafast Phenomena 2016, USA.
Contribution: I designed, produced and measured the dispersion of the UV-mirror using our white-light interferometer.

# Appendix A

# Plasma assisted e-beam coatings

In the early stages of this thesis, a process was developed, together with my colleague Elena Fedulova, which enables the deposition of complex dispersive coatings onto large substrates, using an e-beam process with ion assisted deposition (IAD). For this the advanced plasma source (APS) from Leybold Optics GmbH was used. In principle up to four substrates with a diameter of 300 mm can be coated in one run. The coating machine is described in section 3.1 and a sketch is given in Fig. 3.1. At an IAD process, during the e-beam deposition, the growing layer is irradiated by energetic ions (here argon). The so produced layers are very dense and have comparable properties as sputtered layers. In Fig. A.1 a demonstration for the potential of the process is given. The design has 42 layers and is has an average GDD of $-60\,fs^2$ for the wavelength range of 650 to 900 nm. The thickness was purely controlled by BBOM (see 3.2 and the coating materials are titan dioxide $TiO_2$ and silicon dioxide $SiO_2$. The result seen in Fig. A.1 is very promising. The measured oscillations of the GDD are larger than designed, but are still $-60\,fs^2$ in average. With some optimizations for the dispersion data of the coating material, and by using the calibrated time monitoring technique, the result can be improved. The current process parameters are given in table A.1.

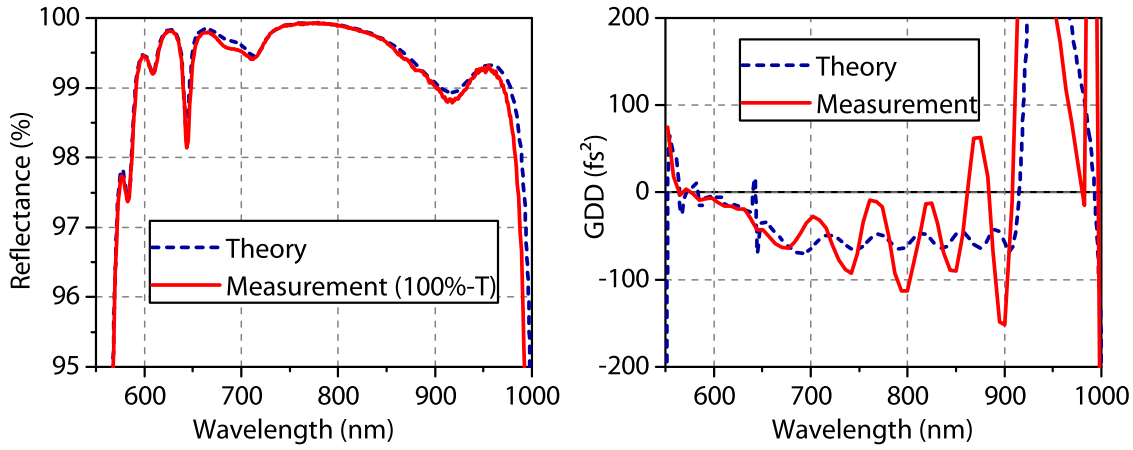


**Figure A.1:** Measurements compared with theoretical values of a dispersive mirrors produced with ion assisted deposition (IAD). Left: Transmission measurement converted in reflectance by R=100 %-T. Right: GDD measurement.

| **Parameters** | **Value** | |
|---|---|---|
| Temperature | 200 | °C |
| Base pressure | $<8 \times 10^{-6}$ | mbar |
| Rate $TiO_2$ | 0.35 | nm/s |
| Rate $SiO_2$ | 0.50 | nm/s |
| **Plasma source** | | |
| Discharge current | 50 | A |
| Bias voltage | 120 | V |
| Coil current | 1.2 | A |
| Argon flow | 4 | sccm |
| Oxygen flow $TiO_2$ | 18 | sccm |
| Oxygen flow $SiO_2$ | 4 | sccm |

**Table A.1:** Parameters for the IAD process

# Appendix B

# Software for white light interferometers

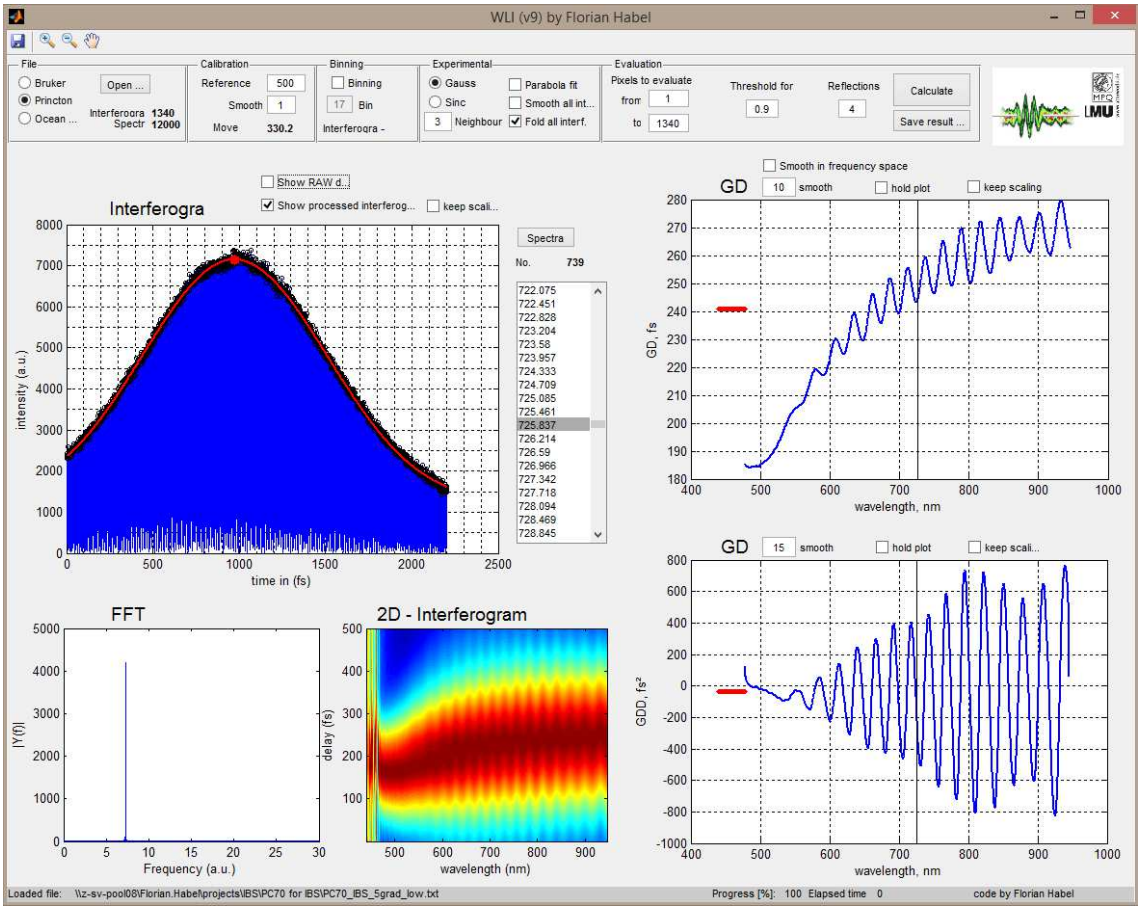


**Figure B.1:** Screen-shot of the WLI evaluation software developed using Matlab. All important settings are in the top row and explained in the text. The hole data set is represented in the 2D-interferogram.

For the evaluation of the data acquired by the mid-infrared white-light interferometer shown in section 6.1, it was necessary to develop new algorithms, to get the most precise measurement results. A screen-shot of the Matlab based software is given in Fig. B.1. In the following the settings available in the user interface from top-left to right are explained:

- **File**: Data of three different spectrometers can be evaluated. "Bruker" is for the FTIR spectromter, "Princton" for the UV-VIS-NIR spectrometer and "Ocean" is experimental for an Ocean optics device. When a file is opened, the number of interferograms and spectra are displayed.

- **Calibration**: The reference wavelength is chosen which is used, to calibrate the displacement of the stage. Especially for FTIR data, smoothing has to be set to about 3. Starting from 1, it should be increased until the displayed "move" is stable. With every change of these values, the reference interferogram is shown in the plot "Interferogram".

- **Binning**: The new solid algorithm does not require binning, but it can be activate if wished. Binning adds up the selected number of interferograms, thus the spectral resolution decreased, but also the noise level and the calculation time.

- **Experimental**: Important settings to test and fine-tune the evaluation. The envelopes of the interferograms can be fitted using either a Gauss- or a Sinc-function. The letter is physically the right one, but is slower and not better than the Gauss. To actually determine the envelope, the maximum of every oscillation of one interferogram must be found. These point are plotted in black circles. To find them, each data-point is compared with the number of neighbors selected. If the other ones are lower, the current one is a maximum. The maximum can be determined with higher precision, if a parabola-fit is calculated for each maximal point and its neighbors. This seems to the best option, but it is very time consuming and it does not give better results than without it. For one interferogram, actually two envelopes exist, one for the positive and one negative values. To simplify the calculation the absolute values are taken, meaning the flip of the negative to positive values. This is set by "Fold all interf."

- **Evaluation**: Here some general settings are made. One can select only the wavelength range (Pixels) of interest for evaluation, in order to reduce the calculation time. The "Threshold" is the merit-function of the envelope fit, which must be topped to be a valid fit and to be plotted in the GD and GDD graphs. The number of reflections on the sample is very important. The evaluated GD is divided by this number. A wrong value directly falsifies a result.

# Appendix C

# Data archiving

All experimental data and all figures presented in this thesis are stored on the data archive server of the laboratory for Attosecond physics located at the Max Planck Institute of Quantum Optic in Garching: `\afs\rzg\mpq\lap\publication_archive\`

The files are all related to the figure in the text by the distinct file name having the prefix "`Fig x.x`", where `x.x` is the number of the figure in this thesis. Every single Figure of this thesis is stored in the subfolder "`\Figures`" in the `eps` format.

The RAW data is organized in subfolders having the name of the containing chapter. The RAW ASCII files are given as well as the Origin-file (OriginPro 9.1.0G), where the data was evaluated and the figures were created. Additionally, the coating designs are stored in a OptiLayer project file (OptiLayer 64 for windows, Version 11.61).

The source code for the data evaluation of white light interferometers (see screenshot in appendix B) is stored in the subfolder "`\Source code MATLB for WLI evaluation`". The code is written with MATLAB R2013a.

# Bibliography


[1] V. Pervak, "Recent development and new ideas in the field of dispersive multilayer optics," *Applied Optics*, vol. 50, pp. C55–61, mar 2011.

[2] V. Pervak, *Optical Thin Films and Coatings*. Elsevier, 2013.

[3] V. Pervak, V. Fedorov, Y. A. Pervak, and M. Trubetskov, "Empirical study of the group delay dispersion achievable with multilayer mirrors," *Optics Express*, vol. 21, p. 18311, jul 2013.

[4] R. Szipocs, K. Ferencz, C. Spielmann, and F. Krausz, "Chirped multilayer coatings for broadband dispersion control in femtosecond lasers," *Optics Letters*, vol. 19, pp. 201–203, feb 1994.

[5] T. Brabec and F. Krausz, "Intense few-cycle laser fields: Frontiers of nonlinear optics," *Reviews of Modern Physics*, vol. 72, pp. 545–591, apr 2000.

[6] A. H. Zewail, "Femtochemistry: Atomic-Scale Dynamics of the Chemical Bond," *J. Phys. Chem. A*, vol. 2000, no. 104, pp. 5660–5694, 2000.

[7] F. Krausz, "The birth of attosecond physics and its coming of age," *Physica Scripta*, vol. 91, no. 6, p. 063011, 2016.

[8] F. Krausz, "Attosecond physics," *Reviews of Modern Physics*, vol. 81, pp. 163–234, feb 2009.

[9] M. Hentschel, R. Kienberger, C. Spielmann, G. A. Reider, N. Milosevic, T. Brabec, P. Corkum, U. Heinzmann, M. Drescher, and F. Krausz, "Attosecond metrology," *Nature*, vol. 414, pp. 509–513, nov 2001.

[10] S. Neppl, R. Ernstorfer, A. L. Cavalieri, C. Lemell, G. Wachter, E. Magerl, E. M. Bothschafter, M. Jobst, M. Hofstetter, U. Kleineberg, J. V. Barth, D. Menzel, J. Burgdörfer, P. Feulner, F. Krausz, and R. Kienberger, "Direct observation of electron propagation and dielectric screening on the atomic length scale," *Nature*, vol. 517, no. 7534, pp. 342–346, 2015.

[11] G. Steinmeyer, D. H. Sutter, L. Gallmann, N. Matuschek, and U.Keller, "Frontiers in ultrashort pulse generation: pushing the limits in linear and nonlinear optics," *Science*, vol. 286, pp. 1507–1512, nov 1999.

[12] F. X. Kärtner, N. Matuschek, T. Schibli, U. Keller, H. A. Haus, C. Heine, R. Morf, V. Scheuer, M. Tilsch, and T. Tschudi, "Design and fabrication of double-chirped mirrors," *Optics Letters*, vol. 22, no. 11, pp. 831–833, 1997.

[13] V. Pervak, I. Ahmad, M. K. Trubetskov, A. V. Tikhonravov, and F. Krausz, "Double-angle multilayer mirrors with smooth dispersion characteristics.," *Optics Express*, vol. 17, no. 10, pp. 7943–7951, 2009.

[14] S.-H. Chia, G. Cirmi, S. Fang, G. M. Rossi, O. D. Mücke, and F. X. Kärtner, "Two-octave-spanning dispersion-controlled precision optics for sub-optical-cycle waveform synthesizers," *Optica*, vol. 1, p. 315, nov 2014.

[15] M. T. Hassan, T. T. Luu, A. Moulet, O. Raskazovskaya, P. Zhokhov, M. Garg, N. Karpowicz, a. M. Zheltikov, V. Pervak, F. Krausz, and E. Goulielmakis, "Optical attosecond pulses and tracking the nonlinear response of bound electrons," *Nature*, vol. 530, no. 7588, pp. 66–70, 2016.

[16] N. Matuschek, X. K. Franz, and U. Keller, "Theory of double-chirped mirrors," *IEEE Journal of Selected Topics in Quantum Electronics*, vol. 4, no. 2, pp. 197–208, 1998.

[17] P. Baum, M. Breuer, E. Riedle, and G. Steinmeyer, "Brewster-angled chirped mirrors for broadband pulse compression without dispersion oscillations," *Optics Letters*, vol. 31, no. 14, p. 2220, 2006.

[18] W. Schneider, A. Ryabov, C. Lombosi, T. Metzger, Z. Major, J. A. Fülöp, and P. Baum, "800-fs, 330-$\mu$J pulses from a 100-W regenerative Yb:YAG thin-disk amplifier at 300 kHz and THz generation in LiNbO3," *Optics letters*, vol. 39, pp. 6604–7, dec 2014.

[19] H. Fattahi, H. G. Barros, M. Gorjan, T. Nubbemeyer, B. Alsaif, C. Y. Teisset, M. Schultze, S. Prinz, M. Haefner, M. Ueffing, A. Alismail, L. Vámos, A. Schwarz, O. Pronin, J. Brons, X. T. Geng, G. Arisholm, M. Ciappina, V. S. Yakovlev, D.-E. Kim, A. M. Azzeer, N. Karpowicz, D. Sutter, Z. Major, T. Metzger, and F. Krausz, "Third-generation femtosecond technology," *Optica*, vol. 1, no. 1, pp. 45–63, 2014.

[20] E. R. Crosson, K. N. Ricci, B. A. Richman, F. C. Chilese, T. G. Owano, R. A. Provencal, M. W. Todd, J. Glasser, A. A. Kachanov, B. A. Paldus, T. G. Spence, and R. N. Zare, "Stable isotope ratios using cavity ring-down spectroscopy: Determination of 13C/12C for carbon dioxide in human breath," *Analytical Chemistry*, vol. 74, no. 9, pp. 2003–2007, 2002.

[21] A. Schliesser, N. Picqué, and T. W. Hänsch, "Mid-infrared frequency combs," *Nature Photonics*, vol. 6, pp. 440–449, jun 2012.

[22] M. W. Todd, R. A. Provencal, T. G. Owano, B. A. Paldus, A. Kachanov, K. L. Vodopyanov, M. Hunter, S. L. Coy, J. I. Steinfeld, and J. T. Arnold, "Application of mid-infrared cavity-ringdown spectroscopy to trace explosives vapor detection using a broadly tunable (6-8 μm) optical parametric oscillator," *Applied Physics B: Lasers and Optics*, vol. 75, no. 2-3, pp. 367–376, 2002.

[23] H. Pires, M. Baudisch, D. Sanchez, M. Hemmer, and J. Biegert, "Ultrashort pulse generation in the mid-IR," *Progress in Quantum Electronics*, aug 2015.

[24] I. Pupeza, D. Sánchez, J. Zhang, N. Lilienfein, M. Seidel, N. Karpowicz, T. Paasch-Colberg, I. Znakovskaya, M. Pescher, W. Schweinberger, V. Pervak, E. Fill, O. Pronin, Z. Wei, F. Krausz, A. Apolonski, and J. Biegert, "High-power sub-two-cycle mid-infrared pulses at 100 MHz repetition rate," *Nature Photonics*, vol. 9, pp. 721–724, sep 2015.

[25] I. Pupeza, T. Eidam, J. Rauschenberger, B. Bernhardt, A. Ozawa, E. Fill, A. Apolonski, T. Udem, J. Limpert, Z. A. Alahmed, A. M. Azzeer, A. Tünnermann, T. W. Hänsch, and F. Krausz, "Power scaling of a high-repetition-rate enhancement cavity," *Optics letters*, vol. 35, pp. 2052–4, jun 2010.

[26] I. B. Angelov, A. von Conta, S. a. Trushin, Z. Major, S. Karsch, F. Krausz, and V. Pervak, "Investigation of the laser-induced damage of dispersive coatings," *Laser-Induced Damage in Optical Materials*, vol. 8190, pp. 81900B–1–7, 2011.

[27] L. Gallais, B. Mangote, M. Zerrad, M. Commandré, A. Melninkaitis, J. Mirauskas, M. Jeskevic, and V. Sirutkaitis, "Laser-induced damage of hafnia coatings as a function of pulse duration in the femtosecond to nanosecond range," *Applied optics*, vol. 50, pp. C178–C187, 2011.

[28] B. Mangote, L. Gallais, M. Commandré, M. Mende, L. Jensen, H. Ehlers, M. Jupé, D. Ristau, A. Melninkaitis, J. Mirauskas, V. Sirutkaitis, S. Kičas, T. Tolenis, and R. Drazdys, "Femtosecond laser damage resistance of oxide and mixture oxide optical coatings," *Optics Letters*, vol. 37, no. 9, p. 1478, 2012.

[29] F. Träger, *Springer Handbook of Lasers and Optics*. Springer International Publishing, 2012.

[30] J.-C. Diels and W. Rudolph, *Ultrashort laser pulse phenomena*. Elsevier/Academic Press, second edi ed., 2006.

[31] H. A. Macleod, *Thin-Film Optical Filters*. CRC Press, 4th ed., 2010.

[32] N. Kaiser and H. K. Pulker, *Optical Interference Coatings*, vol. 32. Springer International Publishing, 2003.

[33] A. V. Tikhonravov, M. K. Trubetskov, and G. W. Debell, "Application of the needle optimization technique to the design of optical coatings.," *Applied optics*, vol. 35, pp. 5493–508, oct 1996.

[34] A. V. Tikhonravov, M. K. Trubetskov, and G. W. DeBell, "Optical coating design approaches based on the needle optimization technique," *Applied Optics*, vol. 46, p. 704, feb 2007.

[35] A. Thelen, *Design of Optical Interference Coatings*. McGraw-Hill Paperbacks, McGraw-Hill, 1989.

[36] M. Scherer, "Reactive alternating current magnetron sputtering of dielectric layers," *Journal of Vacuum Science & Technology A: Vacuum, Surfaces, and Films*, vol. 10, no. 1992, p. 1772, 1992.

[37] M. Scherer, H. Hagedorn, W. Lehnert, and J. Pistner, "Innovative production of thin film laser components," *Advances in Optical Thin Films II*, vol. 5963, pp. 596319–596319–10, 2005.

[38] M. Scherer, J. Pistner, and W. Lehnert, "UV- and VIS Filter Coatings by Plasma Assisted Reactive Magnetron Sputtering (PARMS)," *Optical Interference Coatings*, p. MA7, 2010.

[39] R. J. Crase, "Optical Thin-Film Coating Methods Features - Oct 2008 - Photonics Spectra," 2008.

[40] D. Ristau and T. Gross, "Ion beam sputter coatings for laser technology," *Advances in Optical Thin Films II*, vol. 5963, no. 1, p. 596313, 2005.

[41] J. R. Sites, "Ion bean sputter deposition of optical coatings," *Optical Engineering*, vol. 22, p. 224447, aug 1983.

[42] K. Starke, T. Grosz, M. Lappschies, and D. Ristau, "Rapid prototyping of optical thin film filters," in *Optical and Infrared Thin Films* (M. L. Fulton, ed.), p. 83, International Society for Optics and Photonics, oct 2000.

[43] D. Ristau, H. Ehlers, T. Gross, and M. Lappschies, "Optical broadband monitoring of conventional and ion processes," *Applied Optics*, vol. 45, p. 1495, mar 2006.

[44] W. H. Knox, N. M. Pearson, K. D. Li, and C. A. Hirlimann, "Interferometric measurements of femtosecond group delay in optical components," *Optics Letters*, vol. 13, pp. 574–576, jul 1988.

[45] D. Grupe, *Measuring group delay dispersion in the UV-VIS-IR range by white-light interferometry*. PhD thesis, Ludwig-Maximilians-University, 2008.

[46] T. Amotchkina, A. V. Tikhonravov, M. K. Trubetskov, D. Grupe, A. Apolonski, and V. Pervak, "Measurement of group delay of dispersive mirrors with white-light interferometer.," *Applied optics*, vol. 48, pp. 949–56, feb 2009.

[47] D. Z. Anderson, J. C. Frisch, and C. S. Masser, "Mirror reflectometer based on optical cavity decay time," *Applied Optics*, vol. 23, p. 1238, apr 1984.

[48] A. O'Keefe and D. A. G. Deacon, "Cavity ring-down optical spectrometer for absorption measurements using pulsed laser sources," *Review of Scientific Instruments*, vol. 59, no. 12, pp. 2544–2551, 1988.

[49] O. Razskazovskaya, M. T. Hassan, T. Luu, E. Goulielmakis, and V. Pervak, "Efficient broadband highly dispersive HfO_2/SiO_2 multilayer mirror for pulse compression in near ultraviolet," *Optics Express*, vol. 24, no. 12, p. 13628, 2016.

[50] U. Megerle, I. Pugliesi, C. Schriever, C. F. Sailer, and E. Riedle, "Sub-50 fs broadband absorption spectroscopy with tunable excitation: putting the analysis of ultrafast molecular dynamics on solid ground," *Applied Physics B*, vol. 96, pp. 215–231, aug 2009.

[51] B. Baudisch, F. Habel, V. Pervak, and E. Riedle, "On the Edge: Characterizing Broadband Dielectric Mirrors from UV to NIR Using a Pump-Probe Technique," in *20th International Conference on Ultrafast Phenomena*, (Santa Fe, USA), 2016.

[52] M. Lorenc, M. Ziolek, R. Naskrecki, J. Karolczak, J. Kubicki, and A. Maciejewski, "Artifacts in femtosecond transient absorption spectroscopy," *Applied Physics B: Lasers and Optics*, vol. 74, pp. 19–27, jan 2002.

[53] F. Habel, W. Schneider, and V. Pervak, "Broadband thin-film polarizer for 12 fs applications," *Optics Express*, vol. 23, pp. 21624–21628, aug 2015.

[54] A. V. Tikhonravov and M. K. Trubetskov, "Modern design tools and a new paradigm in optical coating design.," *Applied optics*, vol. 51, pp. 7319–32, oct 2012.

[55] T. Amotchkina, M. K. Trubetskov, Y. Pervak, L. Veisz, and V. Pervak, "Stress compensation with antireflection coatings for ultrafast laser applications: from theory to practice," *Optics Express*, vol. 22, p. 30387, nov 2014.

[56] F. Habel, V. Shirvanyan, M. Trubetskov, C. Burger, A. Sommer, M. F. Kling, M. Schultze, and V. Pervak, "Octave spanning wedge dispersive mirrors with low dispersion oscillations," *Optics Express*, vol. 24, pp. 9218–9223, may 2016.

[57] V. Pervak, A. Tikhonravov, M. Trubetskov, S. Naumov, F. Krausz, and A. Apolonski, "1.5-octave chirped mirror for pulse compression down to sub-3 fs," *Applied Physics B*, vol. 87, pp. 5–12, oct 2006.

[58] G. Steinmeyer, "Femtosecond dispersion compensation with multilayer coatings: toward the optical octave," *Applied Optics*, vol. 45, no. 7, pp. 1484–1490, 2006.

[59] G. Tempea, V. Yakovlev, B. Bacovic, F. Krausz, and K. Ferencz, "Tilted-front-interface chirped mirrors," *Journal of the Optical Society of America B*, vol. 18, no. 11, p. 1747, 2001.

[60] N. Matuschek, L. Gallmann, D. Sutter, G. Steinmeyer, and U. Keller, "Back-side-coated chirped mirrors with ultra-smooth broadband dispersion characteristics," *Applied Physics B: Lasers and Optics*, vol. 71, pp. 509–522, oct 2000.

[61] G. Steinmeyer, "Brewster-angled chirped mirrors for high-fidelity dispersion compensation and bandwidths exceeding one optical octave," *Optics Express*, vol. 11, p. 2385, sep 2003.

[62] V. Laude and P. Tournois, "Chirped-mirror pairs for ultra-broadband dispersion control," in *Technical Digest. Summaries of papers presented at the Conference on Lasers and Electro-Optics. Postconference Edition. CLEO '99.*, pp. 187–188, Opt. Soc. America, 1999.

[63] F. X. Kärtner, U. Morgner, R. Ell, T. Schibli, J. G. Fujimoto, E. P. Ippen, V. Scheuer, G. Angelow, and T. Tschudi, "Ultrabroadband double-chirped mirror pairs for generation of octave spectra," *Journal of the Optical Society of America B*, vol. 18, no. 6, p. 882, 2001.

[64] V. Pervak, I. Ahmad, S. A. Trushin, Z. Major, A. Apolonski, S. Karsch, and F. Krausz, "Chirped-pulse amplification of laser pulses with dispersive mirrors," *Optics Express*, vol. 17, pp. 19204–12, oct 2009.

[65] G. Sansone, G. Steinmeyer, C. Vozzi, S. Stagira, S. De Silvestri, K. Starke, D. Ristau, B. Schenkel, J. Biegert, A. Gosteva, U. Keller, and M. Nisoli, "Mirror dispersion control of a hollow fiber supercontinuum," *Applied Physics B: Lasers and Optics*, vol. 78, pp. 551–555, mar 2004.

[66] R. Trebino, K. W. DeLong, D. N. Fittinghoff, J. N. Sweetser, M. A. Krumbugel, B. A. Richman, and D. J. Kane, "Measuring ultrashort laser pulses in the time-frequency domain using frequency-resolved optical gating," *Review of Scientific Instruments*, vol. 68, p. 3277, sep 1997.

[67] D. C. Harris, M. Baronowski, L. Henneman, L. LaCroix, C. Wilson, S. Kurzius, B. Burns, K. Kitagawa, J. Gembarovic, S. M. Goodrich, C. Staats, and J. J. Mecholsky, "Thermal, structural, and optical properties of Cleartran multispectral zinc sulfide," *Optical Engineering*, vol. 47, p. 114001, nov 2008.

[68] F. Habel, M. Trubetskov, and V. Pervak, "Group delay dispersion measurements in the mid-infrared spectral range of 2-20 μm," *Optics Express*, vol. 24, pp. 16705–16710, jul 2016.

[69] M. K. Trubetskov, M. von Pechmann, I. B. Angelov, K. L. Vodopyanov, F. Krausz, and V. Pervak, "Measurements of the group delay and the group delay dispersion with resonance scanning interferometer," *Optics express*, vol. 21, pp. 6658–69, mar 2013.

[70] A. P. Kovács, K. Osvay, Z. Bor, and R. Szipöcs, "Group-delay measurement on laser mirrors by spectrally resolved white-light interferometry," *Optics Letters*, vol. 20, pp. 788–790, apr 1995.

[71] W. H. Knox, "Dispersion measurements for femtosecond-pulse generation and applications," *Applied Physics B Laser and Optics*, vol. 58, pp. 225–235, mar 1994.

[72] K. Osvay, G. Kurdi, J. Hebling, A. P. Kovacs, Z. Bor, and R. Szipocs, "Measurement of the group delay of laser mirrors by a Fabry-Perot interferometer," *Optics Letters*, vol. 20, p. 2339, nov 1995.

[73] K. Naganuma, K. Mogi, and H. Yamada, "Group-delay measurement using the Fourier transform of an interferometric cross correlation generated by white light," *Optics Letters*, vol. 15, p. 393, apr 1990.

[74] S. Diddams and J.-C. Diels, "Dispersion measurements with white-light interferometry," *Journal of the Optical Society of America B*, vol. 13, p. 1120, jun 1996.

[75] J. Connolly, B. DiBenedetto, and R. Donadio, "Specifications Of Raytran Material," in *Techincal Symposium East* (R. E. Fischer, ed.), pp. 141–144, International Society for Optics and Photonics, sep 1979.

[76] F. Lemarquis, G. Marchand, C. Amra, C. Buil, B. Cousin, and G. Otrio, "Infrared optical filters for the Infrared Atmospheric Sounding Interferometer meteorological space instrument," *Applied Optics*, vol. 38, p. 4182, jul 1999.

[77] J. A. Aguilera, J. Aguilera, P. Baumeister, A. Bloom, D. Coursen, J. a. Dobrowolski, F. T. Goldstein, D. E. Gustafson, and R. a. Kemp, "Antireflection coatings for germanium IR optics: a comparison of numerical design methods.," *Applied optics*, vol. 27, no. 14, pp. 2832–40, 1988.

[78] G. J. Hawkins, R. Hunneman, R. Sherwood, and B. M. Barrett, "Interference Filters and Coatings for Mid-Infrared Astronomy (8-30$\mu$m)," in *Astronomical Telescopes and Instrumentation* (E. Atad-Ettedgui and S. D'Odorico, eds.), pp. 43–55, International Society for Optics and Photonics, feb 2003.

[79] H. R. Dobler, "Infrared coatings," *Applied Optics*, vol. 28, p. 2698, jul 1989.

[80] E. Ritter, "Influence of Substrate Temperature on the Condensation of Vacuum Evaporated Films of MgF2 and ZnS," *Journal of Vacuum Science and Technology*, vol. 6, pp. 733–736, jul 1969.

[81] J. T. Cox and G. Hass, "Antireflection Coatings for Germanium and Silicon in the Infrared*," *Journal of the Optical Society of America*, vol. 48, pp. 677–680, oct 1958.

[82] M. Sánchez-Agudo, I. Génova, H. J. B. Orr, G. Harris, and G. Pérez, "ZnS films for infrared optical coatings: Improvement of adhesion to Ge substrates," in *Optical Systems Design* (N. Kaiser, M. Lequime, and H. A. Macleod, eds.), pp. 71011K–71011K–9, International Society for Optics and Photonics, sep 2008.

[83] E. Ritter, "Optical film materials and their applications.," *Applied optics*, vol. 15, pp. 2318–27, oct 1976.

[84] A. Ghosh, P. Kant, P. Bandyopadhyay, P. Chandra, and O. Nijhawan, "Antireflection coating on germanium for dual channel (3–5 and 7.5–10.6 $\mu$m) thermal imagers," *Infrared Physics & Technology*, vol. 40, no. 1, pp. 49–53, 1999.

[85] M. Debenham, "Refractive indices of zinc sulfide in the 0.405–13-$\mu$m wavelength range," *Applied Optics*, vol. 23, pp. 2238–2239, jul 1984.

[86] C. A. Klein, "Room-temperature dispersion equations for cubic zinc sulfide," *Applied Optics*, vol. 25, pp. 1873–1875, jun 1986.

[87] G. Pérez, A. Bernal-Oliva, E. Márquez, J. González-Leal, C. Morant, I. Génova, J. Trigo, and J. Sanz, "Optical and structural characterisation of single and multilayer germanium/silicon monoxide systems," *Thin Solid Films*, vol. 485, pp. 274–283, aug 2005.

[88] F. Lemarquis, G. Marchand, and C. Amra, "Design and Manufacture of Low-Absorption ZnS-YF(3) Antireflection Coatings in the 3.5-16-num Spectral Range.," *Applied optics*, vol. 37, no. 19, pp. 4239–44, 1998.

[89] B. P. Abbott et al., "Observation of Gravitational Waves from a Binary Black Hole Merger," *Physical Review Letters*, vol. 116, p. 061102, feb 2016.

[90] J. Aasi et al., "Advanced LIGO," *Classical and Quantum Gravity*, vol. 32, no. 7, p. 074001, 2015.

[91] L. Pinard, C. Michel, B. Sassolas, L. Balzarini, J. Degallaix, J. Dolique, R. Flaminio, D. Forest, M. Granata, B. Lagrange, N. Straniero, J. Teillon, and G. Cagnoli, "The Mirrors Used in the LIGO Interferometers for the First-time Detection of Gravitational Waves," in *Optical Interference Coatings 2016*, (Tucson, USA), p. MB.3, OSA, 2016.

[92] M. Granata, E. Saracco, N. Morgado, A. Cajgfinger, G. Cagnoli, J. Degallaix, V. Dolique, D. Forest, J. Franc, C. Michel, L. Pinard, and R. Flaminio, "Mechanical loss in state-of-the-art amorphous optical coatings," *Physical Review D - Particles, Fields, Gravitation and Cosmology*, vol. 012007, pp. 1–31, 2016.

[93] P. D. Bentley, "The modern cryopump," *Vacuum*, vol. 30, no. 4-5, pp. 145–158, 1980.

[94] H. R. Kaufman, J. J. Cuomo, and J. M. E. Harper, "Technology and applications of broad-beam ion sources used in sputtering. Part I. Ion source technology," *Journal of Vacuum Science and Technology*, vol. 21, p. 725, sep 1982.

[95] B. G. Bovard, "Rugate filter theory: an overview," *Applied Optics*, vol. 32, no. 28, p. 5427, 1993.

[96] M. Jupé, M. Lappschies, L. Jensen, K. Starke, and D. Ristau, "Laser-induced damage in gradual index layers and Rugate filters," in *Laser-Induced Damage in Optical Materials* (G. J. Exarhos, A. H. Guenther, K. L. Lewis, D. Ristau, M. J. Soileau, and C. J. Stolz, eds.), p. 640311, International Society for Optics and Photonics, oct 2006.

[97] Z. Qiao, P. Ma, H. Liu, Y. Pu, and Z. Liu, "Laser-induced damage of rugate and quarter-wave stacks high reflectors deposited by ion-beam sputtering," *Optical Engineering*, vol. 52, p. 086103, aug 2013.

[98] G. M. Harry et al., "Titania-doped tantala/silica coatings for gravitational-wave detection," *Classical and Quantum Gravity*, vol. 24, pp. 405–415, jan 2007.

[99] G. Rempe, R. J. Thompson, H. J. Kimble, and R. Lalezari, "Measurement of ultralow losses in an optical interferometer," *Optics Letters*, vol. 17, p. 363, mar 1992.

[100] H. Sekiguchi, N. Uehara, A. Ueda, T. Mitake, K. Nakamura, K. Ueda, N. Kitajima, and I. Kataoka, "Ultralow-loss mirror of the parts-in-10^6 level at 1064 nm," *Optics Letters*, vol. 20, p. 530, mar 1995.

[101] A. Ueda, N. Uehara, K. Uchisawa, K.-i. Ueda, H. Sekiguchi, T. Mitake, K. Nakamura, N. Kitajima, and I. Kataoka, "Ultra-High Quality Cavity with 1.5 ppm Loss at 1064 nm," *Optical Review*, vol. 3, no. 5, pp. 369–372, 1996.

[102] F. Beauville et al., "Low loss coatings for the VIRGO large mirrors," sep 2003.

[103] L. Pinard, B. Sassolas, R. Flaminio, D. Forest, a. Lacoudre, C. Michel, J. L. Montorio, and N. Morgado, "Toward a new generation of low-loss mirrors for the advanced gravitational waves interferometers.," *Optics letters*, vol. 36, no. 8, pp. 1407–9, 2011.

[104] E. Hirose, K. Craig, H. Ishitsuka, I. W. Martin, N. Mio, S. Moriwaki, P. G. Murray, M. Ohashi, S. Rowan, Y. Sakakibara, T. Suzuki, K. Waseda, K. Watanabe, and K. Yamamoto, "Mechanical loss of a multilayer tantala/silica coating on a sapphire disk at cryogenic temperatures: Toward the KAGRA gravitational wave detector," *Physical Review D - Particles, Fields, Gravitation and Cosmology*, vol. 90, no. 10, pp. 2–7, 2014.

# Acknowledgments

I am very grateful to Ferenc Krausz for enabling me to work in his group of highly professional scientists, and for being my doctoral adviser. I feel very honored to do research with all these outstanding peoples in excellent equipped laboratories. Thank you Ferenc for Your personal and financial support, which was the foundation of this work. I am also very thankful to Detlev Ristau from Laser Zentrum Hannover for reviewing this thesis, and for traveling to Munich for by defense! As well I am deeply grateful to my supervisor Vladimir Pervak for giving me the chance to work in his international renowned coating-group. Thank you for the always constructive and great 24/7 support during any time of this thesis!

Many thanks also goes to the rest of the coating team: Thank you Elena Fedulova for being my always cheerful colleague. We've done great work together. Thank You Michael Trubetskov for all your ultrafast assistance in software and theoretical questions. Thank You Tatiana Amotchkina for involving me in your challenging projects. Many thanks goes also to Olga Razskazovskaya and Ivan Angelov, who helped me a lot in the beginning of this work. Of course I want to say thank You to Sigi and Bernd, our coating-technicians, who always provided the cleanest possible substrates.

Many thanks goes also to Vage Shirvanyan, who helped conducted the FROG and the beam profile measurements with the wedge dispersive mirrors. Thank You Annkatrin Sommer for helping we with the evaluation of the FROG traces. Thank you Martin Schultze for the beam time and your review of the paper. I'm also thankful to Christian Burger, who succsesfully conducted the first frustrating measurements with the wedge mirror. Thank You Matthias Kling for the support and for reviewing the paper. Also many thanks goes to my current and former office mates Matthias Kübel, Waldemar Schneider, Ernst Fill and Hirofumi Yanagisawa for providing the very important pleasant office environment, and for the interesting and fruitful discussions, like they randomly occur in an office.

Thanks goes also to the rest of the group for being a fantastic community, like (alphabetical order!) Alexander Apolonski, Peter Baum, Jonathan Brons, Bo-Han Chen, Soo Hoon Chew, Dominik Ehberger, Hanieh Fattahi, Killian Fritsch, Klaus Franke, Harald Fuest, Alexander Guggenmos (Thanks for the discussions!), Nils Haag, Marinius Huber, Christina Hofer, Maximilian Högner, Simon Holzberger, Ka Fai Mak, Daniel Kreier, Stefan Lahme, Tobias Ostermayr, Kellie Pearce, Oleg Pronin, Ioachim Pupeza, Philipp Rupp, Andrey Ryabov, Tobia Saule, Wolfgang Schweinberger and Marcus Seidel (Thank You two for Your excellent collaboration!), Christoph Skrobol, Steffen Volgmann, Matthew Walbran and Mihaela Zigman. I hope I didn't forget any one.

Thank you Kai, Slawik and Stefan from Cutting Edge Coatings GmbH for the support with

the IBS machine and for the collegial cooperation!

I am also grateful to Eberhard Riedle and Bastian Baudisch for offering their fruitful collaboration!

Last but not least I also thank my whole family and especially my beloved wife Christiane and my two awesome kids for their patience and mental support. Moritz and Felix, I'm so looking forward to the moment when you'll be able to read this!

# Curriculum vitae


| | |
|---|---|
| Name: | Florian Habel |
| Email: | f.habel@icloud.com |
| Nationality: | German |
| Date of birth: | 11th July 1980 |
| Place of birth: | Bad Reichenhall |
| Personal status: | Married, two children |


### Present

| | |
|---|---|
| 2013 - present | **Doctoral candidate**, chair of laser physics (Prof. Dr. Krausz), Ludwig-Maximilians-Universität Munich |

### Professional experience

| | |
|---|---|
| 2013 - 2015 | **Technical engineer** for the production of dispersive mirrors, Ultrafast Innovations GmbH (part time: 50 %) |
| 2010 - 2013 | **Development engineer** for interference coatings, Laser Components GmbH |
| 1999 - 2000 | **Industrial plant electrician**, Saline Bad Reichenhall |

### Education

| | |
|---|---|
| 2004 - 2010 | **Diploma in physics**, Title: *Optische Erzeugung und Generation von hochfrequenten akustischen Oberflächenwellen.* University of Konstanz |
| 2002 - 2004 | **University-entrance diploma** (Abitur) Upper vocational school, Traunstein |
| 1995 - 1999 | **Apprenticeship, Industrial plant electrician** Saline Bad Reichenhall |
| 1986 - 1995 | **Certificate of Secondary education** (Hauptschulabschluss) Primary and secondary school, Piding |